REGIONAL CHARACTERIZATION OF LARGE LANDSLIDES IN SOUTHWEST YUKON, WITH EMPHASIS ON THE ROLE OF NEOTECTONICS

by

KEITH ALAN EVERARD
B.A.Sc., The University of British Columbia, 1989

A THESIS SUBMITTED IN PARTIAL FULFILLMENT
OF THE REQUIREMENTS FOR THE DEGREE OF
MASTER OF APPLIED SCIENCE

in

THE FACULTY OF GRADUATE STUDIES

(Department of Geological Sciences)
(Geological Engineering Programme)

We accept this thesis as conforming
to the required standard

THE UNIVERSITY OF BRITISH COLUMBIA

December 1994

In presenting this thesis in partial fulfilment of the requirements for an advanced degree at the University of British Columbia, I agree that the Library shall make it freely available for reference and study. I further agree that permission for extensive copying of this thesis for scholarly purposes may be granted by the head of my department or by his or her representatives. It is understood that copying or publication of this thesis for financial gain shall not be allowed without my written permission.

Department of GEOLOGICAL SCIENCES

The University of British Columbia
Vancouver, Canada

Date DECEMBER 28, 1994

DE-6 (2/88)

ABSTRACT

Neotectonics may be defined as any recent movement or deformation at or near the earth's surface, and the associated geological processes or mechanisms thereof (Vita-Finzi 1986). A regional study of large landslides was undertaken in southwest Yukon, with the aim of assessing the relationship between large landslides and neotectonic processes, with particular emphasis on the role of seismicity.

Landslides were inventoried in an area covering 18,800 km^2 in southwest Yukon and 4,400 km^2 in adjacent south-eastern Alaska. Their spatial distribution was found to correlate with certain lithological units, regional faults, and often dense clusters of low-level earthquakes. Seismicity is especially intense in the Cement Creek area, where the relative temporal distribution of landslides departs from the regional slope exhaustion model and more closely resembles a steady-state distribution. A recent (1983) landslide in this area was attributed to a modest M5.4 earthquake (Power 1988).

Field reconnaissance in Cement Creek valley was undertaken to assess the possible role of neotectonic processes, and to gather data for a program of numerical modelling. Rupture surfaces of the landslides were generally coincident with bedding surfaces in the tightly folded volcanic rocks. Geomorphic evidence suggests an incremental displacement failure mechanism.

The available methods of dynamic numerical modelling are reviewed. Program UDEC is found to be an appropriate analytical package for the modelling program. Limited verification tests of UDEC were performed.

Strong motion data from a magnitude 4.6 earthquake were input successively to a representative slope model. The program was able to simulate geomorphic features related to slope deformation at Cement Creek, as well as confirming seismicity as a possible landslide triggering mechanism.

TABLE OF CONTENTS

LIST OF FIGURES

LIST OF TABLES

LIST OF PLATES

ACKNOWLEDGMENTS

This research was made possible by the contributions and efforts of many people and organizations.

Foremost, I wish thank Dr. K. Wayne Savigny for providing support and guidance throughout this endeavour, and for helping me to find the middle ground. The members of my committee, Dr. R.M. Bustin, Dr. J.J. Clague, Dr. R. Ellis, and especially Dr. Peter Byrne provided thoughtful and insightful suggestions.

My sincerest thanks to my family for their unfailing support. Many supportive friends are owed my gratitude, but especially Bruce James, Bob James, H. Stiff, B. Gaertner, and P. Marcus. B. Cranston provided much humour (and hockey) amidst the pathos.

Support in kind in Yukon was generously provided by S. Morison at Indian and Northern Affairs Canada, and Ray Brennemen and his staff at Kluane National Park Headquarters. K. Hennebury and S. Alexander provided able assistance in the field.

Thanks as well to Dr. R. Horner for interesting discussions, and Dr. D. Weichert for generously supplying valuable data. J. Amor at the UBC Geophysics Department performed critical electronic data transfer long before FTP was a fashionable acronym.

CHAPTER 1

Introduction

1.1 Background

The evaluation of terrain hazards becomes increasingly important with the expansion of urban development and transportation networks into mountainous areas. Among the most prevalent of these hazards are landslides which account for significant losses in life and property annually.

An inventory of slope movements in Fraser Valley (southwestern British Columbia) by Savigny *(in press)* revealed more than 30 Holocene (post-glacial) landslides with volumes up to 550 million cubic metres. Many of these landslides are concurrent with local and regional faults, a correlation also noted in southwestern British Columbia by Piteau (1977). It was proposed that, among other factors, neotectonic processes may have contributed to these slope movements.

Seismicity along the fault systems in Fraser Valley is currently quiescent, and the relationship between landslide processes and neotectonic activity in Fraser Valley is enigmatic. In a study of the interrelationship between large ancient landslides and seismicity in Fraser Valley, Naumann (1990) concluded that slope pore pressures had a potentially greater effect on slope stability than paleoseismicity. However, positive correlations between comparatively recent earthquakes and large landslides in the Canadian Cordillera are documented by Mathews *et al.* (1978), Mathews (1979), and Evans *et al.* (1987). For this reason a parallel study was undertaken to assess the effect of neotectonic activity on landslide processes.

1.2 Research Synopsis

The aim of this research is to assess the relationship between large landslides and neotectonic processes, with particular emphasis on seismicity. Within this context, neotectonics may be defined as any recent movement or deformation at or near the earth's surface, and the associated geological processes or mechanisms thereof. There is no generally accepted time-scale implied in the definition of neotectonics (Vita-Finzi, 1986), and hence here it shall be arbitrarily taken as the period that has elapsed since the final retreat of continental ice from the landscape.

The study area chosen is in southwest Yukon Territory, encompassing portions of eastern St. Elias Mountains, western Yukon Plateau, and the intervening valley system. Terrain in this region is not only physiographically similar to the mountains of southwest British Columbia, but it has undergone similar patterns of Late Cenozoic continental glaciation. The southwest Yukon is dissected by several seismically active regional faults and has a comparatively greater degree of tectonic activity. Moreover, Holocene displacements have been reported along contiguous structures in southeastern Alaska (Richter *et al.*, 1971; Plafker *et al.*, 1977). The importance of neotectonism in the assessment of terrain hazards in this region is underscored by Clague (1979, 1982).

Regional landslide data were derived primarily from aerial photograph interpretation with limited field verification. The landslide population is assessed in terms of the factors that contribute to slope instability. Although some degree of interrelationship exists between them, care must be taken to separate the role of the contributing factors from the mechanisms that trigger instability, such as seismicity.

Seismicity is a temporally transient neotectonic process that is to some extent spatially constrained. Its effect on regional landslide patterns should be manifest as an overprint that may have a distinct spatial bias and temporal signature. Once areas have been defined where seismicity is a suspect mechanism, localized studies may be undertaken to assess the specific effect.

1.3 Thesis Structure

This thesis is arranged in two distinct but related parts.

Part I is comprised of Chapters 1 through 4. The introductory comments are contained in Chapter 1. In Chapter 2 the regional geological and physiographic setting of southwest Yukon are cast. Chapter 3 contains a presentation of aerial photograph inventories in southwest Yukon and adjacent southeastern Alaska. These are followed by an analysis of the factors that contribute to regional slope instability patterns. Chapter 4 focuses on Cement Creek, an area where neotectonic effects are considered an important factor contributing to landsliding. Numerical study of the effects of seismicity on slope stability are recommended as a complement to Part I.

Part II is comprised of Chapters 5 and 6, embodying the results of Part I and applying them specifically to numerical analyses. Chapter 5 provides an overview of the available numerical methods for dynamic analysis of rock slopes, including the chosen method, program UDEC. This is followed by a verification of UDEC. Chapter 6 contains the results of the UDEC analyses. Chapter 7 contains the conclusions of the research.

CHAPTER 2

Regional Setting

2.1 Location

The study area encompasses approximately 18,800 km^2 in southwestern Yukon (Fig. 2.1), and includes portions of Kluane National Park and Kluane Wildlife Preserve. Extensions of the study into contiguous corridors of eastern Alaska cover an additional 4400 km^2. The population centres include Haines Junction, Destruction Bay, and Burwash Landing. Haines Road and Alaska Highway, important transportation links between Yukon and Alaska, are located in Shakwak Valley.

2.2 Physiography and Climate

The principal physiographic divisions in the study area are Shakwak Valley, St. Elias Mountains, and Yukon Plateau (Muller, 1967; Rampton, 1981) (Fig. 2.2).

Shakwak Valley is a broad trough extending from Dezadeash Lake northwest to Alaska, separating St. Elias Mountains from Yukon Plateau. The valley floor descends from 900 m in the southeast to 600 m in the northwest, and varies between four and ten kilometres in width. Gently undulating valley bottom topography is characterized by glacial landforms, and hosts several rivers and large lakes. Drainage is good to moderately poor, with no stream extending along the length of the valley.

St. Elias Mountains in Yukon comprise a vast region of rugged terrain that includes Kluane, Donjek, Alsek, and Icefield ranges, and Duke Depression (Rampton, 1981; Fig. 2.2).

The Kluane Ranges rise abruptly to the southwest of Shakwak Valley, offering relief exceeding 1600 m and a virtually continuous escarpment of 950+ m on the valley frontage that is breached only by major drainages. They are separated from Icefield Ranges to the west by Duke Depression and Donjek Ranges, and to the south by Alsek Ranges. Characteristically steep, angular peaks are separated by serrated ridges, and commonly attain heights of 2000 m or more, with some exceeding 2500 m. Alpine glaciers mantling the peaks are more abundant to the west. Duke Depression (Muller, 1967) is a system of upland plateaux and valleys 200 m to 500 m higher than Shakwak Valley, that extends northwest from Burwash Uplands near Kluane Lake to White River near the Alaskan border (Rampton, 1981). The region is dissected by several antecedent braided river valleys that are fed by glaciers descending from the icefields to the west. Between these valleys, well incised, high gradient rectangular drainages often follow structural trends. Further west, Icefield Ranges form the core of St. Elias Mountains. They rise to well over 3000 metres beneath a thick carapace of ice, and include the Mt. Logan massif, the highest point in Canada at 6050 m.

In sharp contrast with St. Elias Mountains, topography of Yukon Plateau rising to the northeast of Shakwak Valley (Bostock, 1948) is characteristically subdued. Rounded or flat-topped peaks of Ruby, Dezadeash, and Nisling ranges comprising its western edge are connected by broad ridges, typically attaining heights of 1500 m to 1750 m, with a few rising to 2200 m. Non-continuous frontage along Shakwak Valley is typically less than 900 m, giving way to low, rounded, domal hills to the northwest. Reticulate drainage dissecting this region occupies broad, well incised, low gradient, stream valleys.

The climate regime in the study area is designated *dry continental* (Wahl *et al.*, 1987). St. Elias Mountains to the west form a major orographic barrier to inland movement of warm, moist Pacific air masses; mean annual precipitation in St. Elias Mountains is transitional from up to 3500 mm near the coast to less than 500 mm in eastern Icefield Ranges and Kluane Ranges, and to less than 400 mm in Shakwak Valley (Wahl *et al.*, 1987). Summers are characteristically

brief and cool, and the winters long and cold. The mean monthly temperatures for Burwash Landing and Haines Junction in Shakwak Valley are shown on Figure 2.3.

2.3 Glaciation and Quaternary History

Southwest Yukon and eastern Alaska have been extensively glaciated in Late Tertiary and Quaternary time. Tillites interbedded with Neogene volcanic rocks were identified in areas of Alaska adjacent to the study area (Denton *et al.*, 1969). In Shakwak Valley, three major glacial advances of Wisconsinan and Illinoian age have been identified (Denton *et al.*, 1967; Muller, 1967). These advances correlate at least partially with advances further northwest near the Yukon-Alaska border (Rampton, 1971), and in eastern Alaska (Denton, 1974). An approximate chronology of late Pleistocene and younger advances for the Kluane Lake area was compiled by Rampton (1981) (Table 2.1).

Table 2.1. *Quaternary glacial chronology of the Kluane Lake area.*

Neoglaciation	< 2,800 b.p.
Slims Nonglacial	2,800 - 12,500 b.p.
Kluane Glaciation	12,500 - 29,500 b.p.
Boutellier Nonglacial Icefield Glaciation	29,600 - 100,000 b.p.
Silver Nonglacial Shakwak Glaciation	> 100,000 b.p.

A reconstruction of the Kluane glaciation proposed by Denton (1974) involves ice lobes from Kaskawulsh, Dusty, and Lowell glaciers coalescing in Shakwak Trench and merging with northwest flowing ice from Donjek Valley. Surficial features in Shakwak Valley infer a maximum ice height of at least 1830 metres during this period (Denton *et al.*, 1967), with the

height decreasing somewhat to the northwest (Rampton, 1979*a*). The ice was constrained by Kluane and Ruby ranges before exiting Shakwak Valley and merging with a smaller lobe from White River Valley. The maximum glacial advance was attained at the northwest end of Shakwak Valley around 14,000 b.p., followed by a rapid recession.

2.4 Regional Geology

2.4.1 Tectonic Setting

The boundary between the northeastern Pacific Plate and the North American Plate is the principal tectonic feature of southeastern Alaska. Movement along the plate boundary is transitional from primarily dextral-transcurrent slip on Queen Charlotte-Fairweather Fault to convergence on Chugach-St. Elias and Pamplona Fault Zones (Perez *et al.*, 1980). Northwestward motion of the northeastern Pacific Plate relative to the North American Plate is estimated at 59 to 63 mm/year in the Holocene (Chase, 1978; Minister *et al.*, 1978 *in* Perez *et al.*, 1980). Strain is accommodated by oblique subduction offshore in Transition Fault Zone, folding and thrusting in Chugach-St. Elias Fault System (Plafker, 1987), and dextral offset on Totschunda Fault (Lisowski *et al.*, 1987). Evidence of Holocene strain in Yukon is limited (Souther *et al.*, 1975; Clague, 1979).

Two distinct, sub parallel zones of seismicity are recognized in this region (Horner, 1983; Wetmiller *et al.*, 1989). Situated along the southeastern Alaskan coast, Fairweather-Yakutat Zone includes Queen Charlotte-Fairweather and Chugach-St. Elias Faults, and, Transition and Pamplona Fault Zones. One hundred and twenty five kilometres inland, Denali-Shakwak Zone, which includes Denali Fault System, Duke River Fault, and Totschunda Fault, passes through southwestern Yukon and southern Alaska (Fig. 2.4). Denali-Shakwak Zone is less active than Fairweather-Yakutat Zone in terms of both magnitude and total number of recorded earthquakes (Horner, 1991 *pers. comm.*).

The principal faults and terranes in southwest Yukon are shown on Figure 2.4. Segments of Denali Fault in Yukon and eastern Alaska underwent several hundred kilometres of dextral transcurrent displacement between latest Cretaceous and Eocene time, with less than 40 km of subsequent offset (Lanphere, 1978; Plafker, 1989). Surficial and stratigraphic features in Yukon (Clague, 1979) and eastern Alaska (Richter *et al.*, 1971; Plafker, 1977) suggest Pleistocene or Holocene offsets have occurred, but Quaternary dislocations are confirmed only to the west of Nabesna River, some 70 kilometres into Alaska.

Duke River Fault (Muller, 1967) separates predominantly Paleozoic rocks of Alexander terrane from Permo-Triassic rocks of Wrangellia terrane. Major displacements are post-Late Triassic and pre-Miocene aged (Campbell *et al.*, 1978), although possibly related faults in western Yukon exhibit Miocene or later offset (Muller, 1967; Souther *et al.*, 1975); the magnitude of the displacements are unknown. Quaternary movement on Duke River Fault has not been noted (Campbell *et al.*, 1978). Structure and stratigraphy west of Kluane Lake near Steele Creek indicate northeast directed thrusting on a steeply southwest dipping plane (Muller, 1967), although transcurrent offset has also been suggested (Read, 1976; Campbell *et al.*, 1978).

In eastern Alaska, Totschunda Fault extends over 180 kilometres northwest from near the Yukon border to where it merges with Denali Fault. Vertical and invariably dextral horizontal offsets in Wisconsin aged glacial deposits on Totschunda Fault indicate significant Quaternary movement (Richter *et al.*, 1971). Estimates of Late Cenozoic transcurrent displacement were refined by Plafker *et al.* (1977) to four kilometres or less with an age not older than Late Miocene.

2.4.2 Geology Southwest of Denali Fault

Pre-Cenozoic rocks of Wrangellia (Fig. 2.4) described by Read *et al.* (1975) and Read (1976) consist of a thick succession of Pennsylvanian to Permian volcanics beneath Permian clastic sediments and carbonates. These in turn are overlain by Upper Triassic to possibly early

Jurassic subaerial and submarine basic volcanics and Middle Triassic to Jura-Cretaceous(?) shallow marine sediments. These sequences are intruded by Cretaceous and Tertiary plutons, and predominantly basic Permo-Triassic through Tertiary sills and dykes (Dodds, 1982*a, b, c*). Where present, cover consists of Jura-Cretaceous flysch (Dezadeash Formation of Eisbacher 1976), Lower Tertiary clastic sediments (Amphitheatre Formation), and Neogene (Wrangell) volcanic rocks (Dodds, 1982*a, b, c*). Contiguous strata in the eastern Alaska Ranges are described by Richter *et al.* (1973) and Richter (1976).

Permo-Triassic strata of Wrangellia are typically folded about northwest trending axes and are highly dissected by faulting. Folding and faulting are most intense in the areas immediately west and south of Kluane Lake where Duke River Fault and Denali Fault converge. Tertiary cover is folded about northwest trending axes and is locally dislocated by faults, although not to the extent of the underlying strata.

Rocks of Alexander terrane (Fig. 2.4) described by Read *et al.* (1975) and Campbell *et al.* (1978) are predominantly comprised of generally low-grade metamorphosed, pre-Ordovician through Triassic volcanics, volcaniclastics, sediments and carbonates. They are intruded by Pennsylvanian through Permian and Jurassic through Cretaceous dioritic bodies, Tertiary plutons, sills, and dykes, as well as basic sills and dykes of lower Paleozoic(?) through Tertiary ages (Dodds, 1982*a, b, c*). Basement rocks are locally overlain by Upper Cretaceous and Lower Tertiary (Amphitheatre Formation) clastic sediments, and Neogene (Wrangell) volcanic rocks (Dodds, 1982*a, b, c*).

These assemblages have undergone at least two pre-Cenozoic deformation episodes with attendant folding and faulting. A third post-Miocene episode created predominantly strike-slip faulting and prominent west-southwest and west-northwest trending folds. Deformation is most intense to the east near Duke River Fault and the trace of Denali Fault (Read, 1976; Campbell *et al.*, 1978).

2.4.3 Geology Northeast of Denali Fault

Rocks northeast of Denali Fault described by Kindle (1953), Muller (1967), and Tempelman-Kluit (1974) are comprised primarily of Paleozoic metamorphic terrane and Jurassic through Early Tertiary igneous rocks (Fig. 2.4).

Paleozoic and lower Mesozoic oceanic rocks of Windy-McKinley terrane ('Unit 3' of Muller 1967) consist of metamorphosed marine sediments, mafic volcanics, ultramafics and [metamorphosed] limestone bodies (Wheeler *et al.*, 1987). Contiguous sections in the eastern Alaska Ranges are described by Richter (1976).

Nisling terrane is locally comprised of two packages of rocks; to the east are Cambrian through Devonian "partly metamorphosed carbonaceous and siliceous offshelf sediments" and to the southeast is a Cambrian "metamorphosed passive continental margin assemblage" (Wheeler *et al.*, 1987). The rocks consist of quartzite, biotite-muscovite schist, marble lenses and locally phyllite, greenstone, and amphibolite (Wheeler *et al.*, 1987). They are in part equivalent to "Aishihik Assemblage" of Erdmer (1991), "Nasina Quartzite" and "Biotite Schist" of Tempelman-Kluit (1976), and "Unit 1" of Muller (1967).

Gravina-Nutzotin Belt (Berg *et al.*, 1972) in Yukon is comprised of Jura-Cretaceous flysch (*Dezadeash Formation* of Eisbacher, 1976), minor non-marine strata, and on Figure 2.4 includes Paleozoic metamorphic rocks ("Kluane Assemblage" and, in part, "Aishihik Assemblage" of Erdmer, 1991). Igneous terrain includes mid-Jurassic, Cretaceous, and early Tertiary granitic bodies (Muller, 1967; Tempelman-Kluit, 1975). Original structures are poorly preserved in the metamorphic terranes; tightly spaced west-northwest and north trending folds are preserved in the flysch sequences (Eisbacher, 1976).

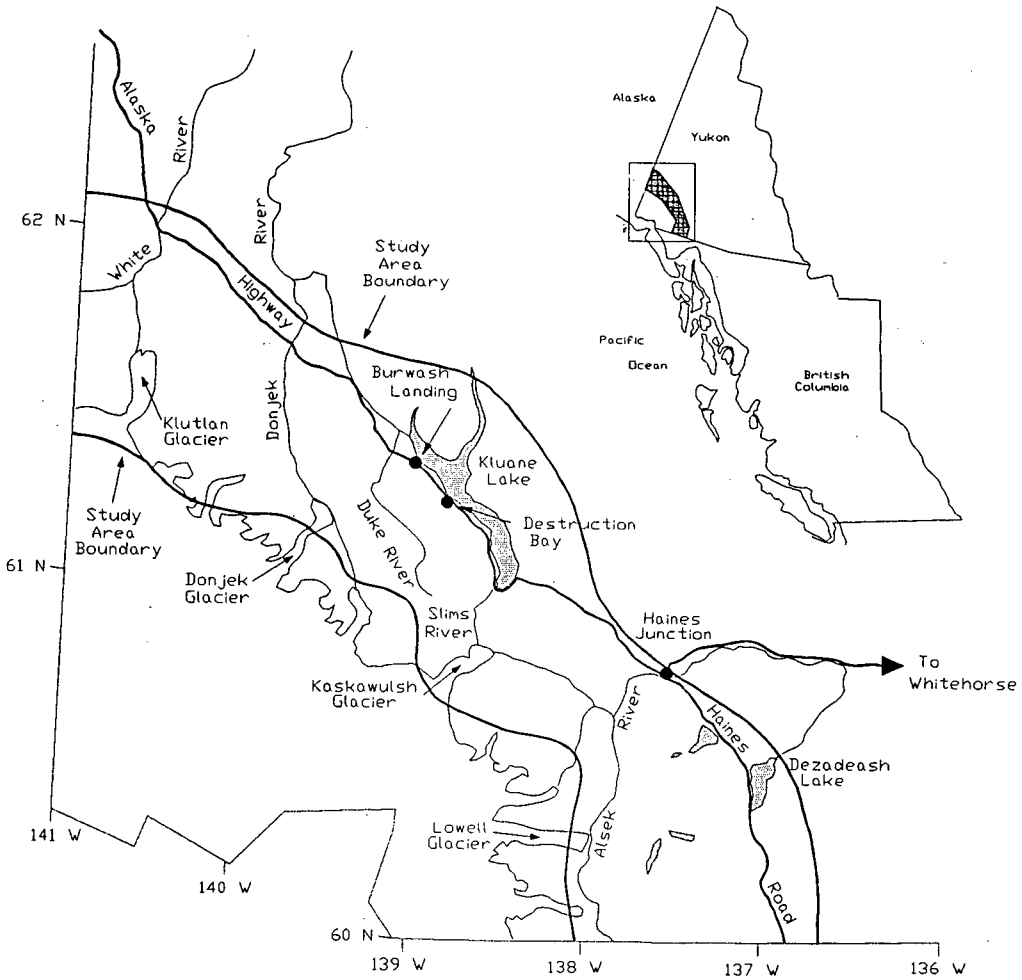

Figure 2.1. *Location and general features of the Yukon study area. Regional location is shown shaded on the inset.*

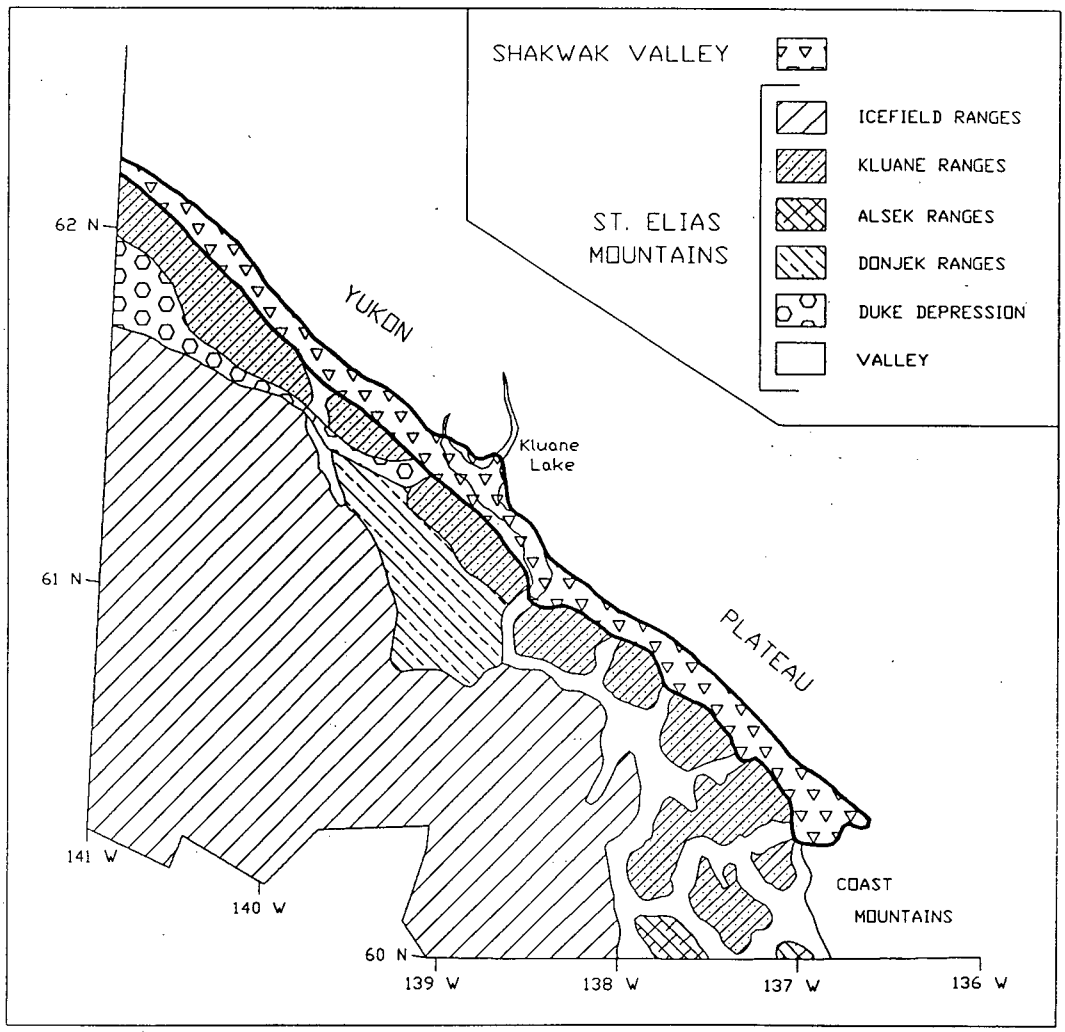

Figure 2.2. *Physiographic divisions and elements of the southwest Yukon study area (adapted, after Rampton, 1981).*

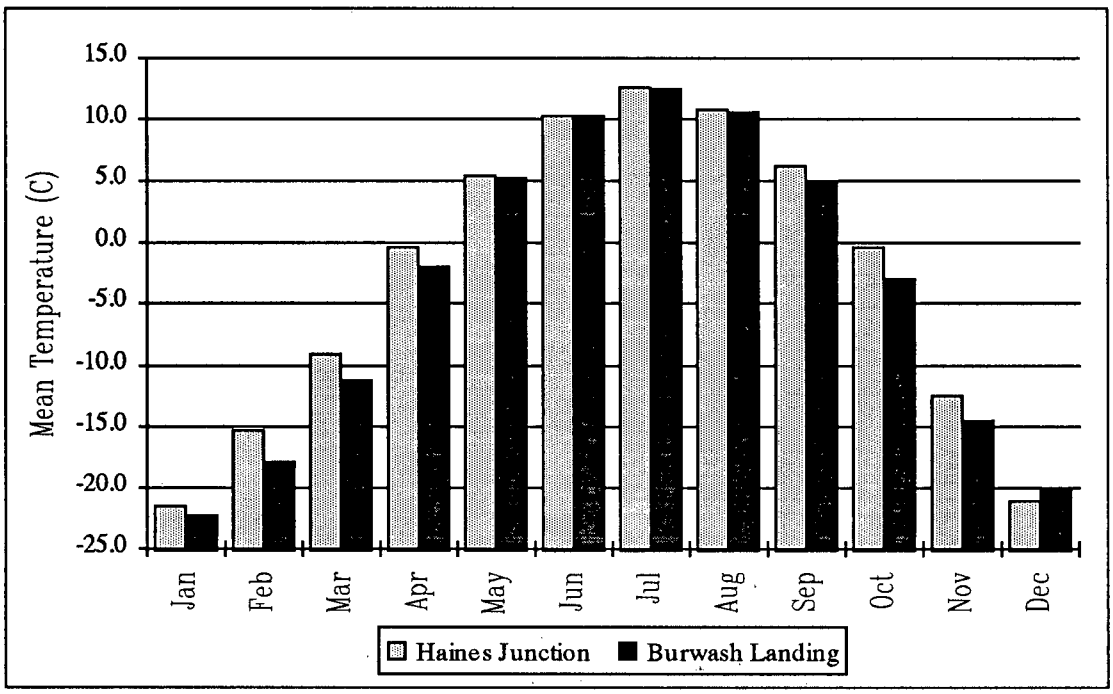

Figure 2.3. *Monthly mean temperatures for Haines Junction, Yukon (1960-1985) and Burwash Landing, Yukon (1966-1990).*

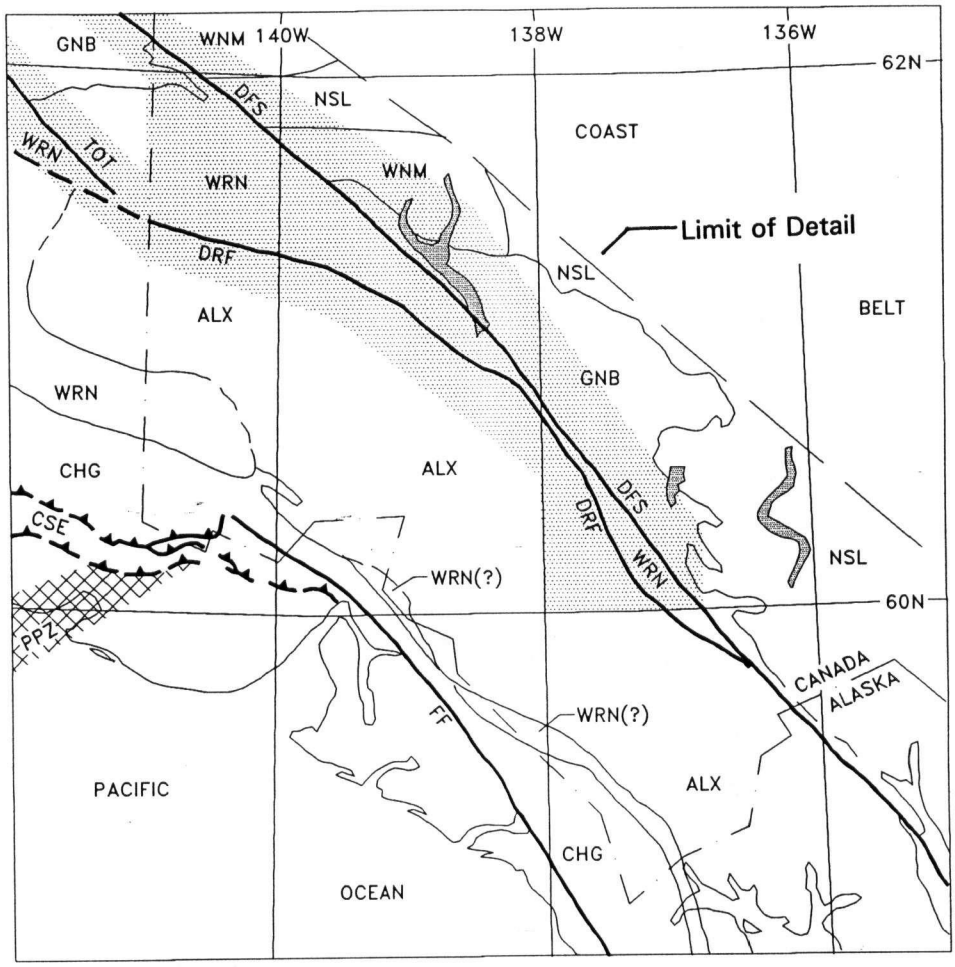

DFS - Denali Fault System
DRF - Duke River Fault
TOT - Totschunda Fault
FF - Fairweather Fault
PPZ - Pamplona Zone (hatched)
ALX - Alexander
WNM - Windy-McKinley
GNB - Gravina-Nutzotin Belt
CSE - Chugach-St. Elias Zone
WRN - Wrangellia
NSL - Nisling
CHG - Chugach

Figure 2.4. *Tectonic features of southwest Yukon and adjacent Alaska. The study area is shown (lightly shaded) in relation to regional faults and terranes in southwest Yukon; major lakes have darker shading (modified; after Dodds, 1982a, b, c; Wheeler et al., 1987; & Horner, 1983).*

CHAPTER 3

Landslide Inventories and Regional Assessment

3.1 Introduction

A brief description of the inventory method and its limitations in Section 3.2 is followed by presentation of the Yukon and Alaska inventories in Sections 3.3 and 3.4. An assessment of the landslide distribution is given in Section 3.5, and the factors controlling the distribution are discussed in Section 3.6. An overview of steady-state and exhaustion regional landslide distribution models in given in Section 3.7.

3.2 Inventory Method

The landslide and lineament inventories were prepared with data collected from small scale (*ca.* 1:70,000) black and white aerial photographs. The airphoto set was analyzed a minimum of three times to improve the consistency and accuracy of the interpretations. Preliminary results were calibrated by comparison with available records of landslide occurrences in the inventory area. Field visits in 1990 and 1991 at a number of the sites verified the airphoto interpretations.

The morphological features used to identify landslides in aerial photographs include scarps, ground cracks, rupture surface scars, debris trains or lobes, slope ponding, bulges or depressions in slope profile, offset or dammed drainages, tonal variations, and contrasting vegetative patterns (Mollard, 1977; Rib *et al.*, 1978). Topographic lineaments are commonly

expressed as linear or sub-linear ridges or depressions, distinct patterns of drainage or vegetation, tonal variations, or alignments of topographic features (Ray, 1972; Mollard, 1988).

Landslide and lineament locations were transcribed to 1:250,000 scale compilation maps. Plan areas of the landslides were taken from the compilation maps with an analog planimeter. Summary information for each of these sites in Appendix 1 includes the following; (a) an informal site name, usually based upon a local geographic feature; (b) the type of movement, based upon the classification of Varnes (1978); (c) the site location, both as a latitude-longitude pair, and as a coordinate pair corresponding to the alpha-numeric grid on the border of Figures 3.1 and 3.2; (d) the predominant bedrock division at the site, taken from compilation maps by Dodds (1982*a, b, c*) and Kindle (1953) and; (e) observations and comments specific to each site in the last column. Because most of the landslides are complex movements, the type given (point (b) above) corresponds to the predominant mode: wherever the mode is uncertain it is annotated with a question mark (?). The term "landslide zone" refers to areas of widespread, often coalescing landslides where individual movements cannot be discerned.

3.2.1 Inventory Limitations

Significant effort was made to ensure the inventory is accurate and complete. Notwithstanding these efforts, the inventory has several limitations. First, the diagnostic morphology of most of the landslides in this region is modified by exogenic processes. Modification can be substantial with increasing age, making recognition of older landslides difficult, and as a consequence the number of ancient landslides may be under-represented in the total population. Secondly, small landslides (those with volumes less than approximately 1×10^6 m^3) were ignored because they are difficult to identify consistently on small-scale aerial photographs. Such landslides are ubiquitous in the study area, and contribute significantly to mass wasting in this region. Their importance as a regional slope forming process cannot be discounted, especially in those areas where large-scale slope movements are absent.

3.3 Yukon Landslide Inventory

3.3.1 Previous Studies

Several landslides in the study area are shown on maps of bedrock geology (Dodds, 1982*a, b, c*) and surficial geology (Rampton, 1979*a, b, c*; 1981). A suite of landslides on Mount Wallace (Sheep Mountain) at the south end of Kluane Lake was investigated by Clague (1981). His study concluded that extreme relief, geological structure, seismicity, and intense precipitation were the probable causes of instability. A regional synthesis of natural hazards by Clague (1982) included the locations of a number of landslides in St. Elias Mountains and Shakwak Valley. Power (1988) studied a recent landslide in Tertiary volcanic sequences at Cement Creek, and concluded that geological structure, groundwater conditions, and seismicity contributed to that event. A terrain hazard inventory of the Kluane Regional Planning Area prepared by Thurber Consultants (1989) notes several landslides in the northeastern study area. No regional study of large landslides in southwest Yukon had been undertaken prior to this study.

3.3.2 Results

The distribution of landslides and lineaments is shown on Figures 3.1 and 3.2. 98 landslides covering approximately 230 km^2 (1.2% of the study area) were identified. The temporal distribution of the landslides has not been determined. However, the age of one landslide (Sheep Mountain Rock Avalanche) has a radiocarbon age between 500 and 1950 b.p. (Clague, 1981), and another (Cement Creek #1), occurred in the spring of 1983 (Power, 1988). Based upon their appearance and with assumed rapid physical modification, the majority are considered Middle-to-Late Holocene in age. However, the span of ages is believed be from earliest post-glacial (*ca.* 12,500 b.p.) to very recent.

3.4 Alaska Landslide Inventory

3.4.1 Previous Studies

Landslides in the Eastern Alaska Ranges along Totschunda Fault and the westernmost segment of Denali Fault are noted by Richter *et al.* (1971). Additional landslides in this region are shown on a geological map of the Nabesna Quadrangle compiled by Richter (1976). An aerial photograph reconnaissance of Totschunda and Denali Faults in Eastern Alaska Ranges by Plafker (unpublished data) identifies a number of landslides.

3.4.2 Results

The distribution of landslides and lineaments in the eastern Alaska study area is shown on Figure 3.3. 14 landslides covering an area of approximately 40 km^2 (1.0% of the Alaskan study area) were identified along Totschunda Fault corridor; no landslides were identified on the Alaskan segment of Denali Fault. The temporal distribution of the landslides has not been determined, but the majority are believed to be of Middle-to-Late Holocene age.

3.5 Assessment of the Regional Landslide Distribution

The assessment of the regional landslide distribution is in two sections. First, a brief overview of the fundamental aspects and limitations of regional assessment are given, and secondly, the gross slope stability patterns are described.

3.5.1 Fundamental Considerations

The scope and methods of assessing slope stability at regional scale differ from those used in localized studies. Local (site specific) studies usually emphasize post-failure analysis,

and tend to concentrate on site description, the geometry and mechanics of the landslide, the engineering properties of the earth materials, and other aspects of local significance (*i.e.* Hendron *et al.*, 1985; Evans *et al.*, 1989; Cruden *et al.*, 1992). In contrast, regional studies generally focus on the identification and mapping of a landslide population, usually by remote sensing, followed by the application of comparative analyses to the population (*i.e.* Piteau, 1977; Nilsen *et al.*, 1977; Hansen *et al.*, 1991; Savigny *in press*). The aim is usually to identify the underlying factors affecting the population, with the possibility of extrapolating the results to adjacent areas, or to other regions with similar geological, tectonic, or geomorphic styles or processes. By their nature, regional studies emphasize the qualitative aspects of slope stability because the large number of intrinsic and extrinsic factors affecting a landslide population often cannot be practically quantified at regional scale. Indeed, from the regional perspective, the effect of local variations in rock mass strength and behaviour on slope stability average out (Piteau, 1977), and the overall slope stability pattern reflects the relative stability of entire rock sequences, geological features, or physiographic divisions.

The many factors that affect slope stability are summarized by Coates (1977) and Piteau (1977), and may be grouped into three broad categories. First are the properties of the earth materials, such as their structural and lithological character, as well as their arrangement and orientation in space. Secondly are the aspects of the geomorphic setting and environment such as topography, total relief, slope form and orientation, and hydrology. The final category of factors are the external factors, also termed triggering mechanisms, that include peak climatic events or climatic change, seismicity and neotectonism, and anthropogenic modification. The trigger mechanisms are considered to be independent of the earth material properties and the geomorphic setting (Coates, 1977).

At any time, and under a prescribed set of ambient geological and geomorphic conditions, the stability (or instability) of a slope reflects the balance between geological processes that create relief, and erosional processes that diminish relief. It is assumed that slopes

have a tendency to evolve toward an equilibrium state under the influence of the ambient conditions. Landsliding is one possible response to disequilibrium between the opposing processes. In slopes at or near limiting equilibrium, movement is initiated when the local critical stability threshold is exceeded by stresses imposed by the external triggering mechanisms (Coates *et al.*, 1977; Palmquist *et al.*, 1980). An important corollary to this model is that the character, magnitude, or frequency of these processes may change with time, and for this reason, the concept of slope equilibrium (or disequilibrium) is relative only to the temporal interval it is defined for.

3.5.2 Spatial Distribution and Density

The spatial distribution of landslides in Yukon is shown on Figures 3.1 and 3.2, and in Alaska on Figure 3.3. In Yukon the majority of the landslides are situated in St. Elias Mountains; comparatively few occur in Shakwak Valley or to the east in Yukon Plateau. Several distinct clusters of landslides are apparent on Figures 3.1 and 3.2; one to the west of Donjek River (~ H5, Fig. 3.1), and the other between Kathleen and Mush Lakes (~ G7, Fig. 3.2). Smaller clusters also occur in the Grizzly Creek area (~ C12, Fig. 3.1), the south end of Kluane Lake (~ B16, Fig. 3.1), and at Chalcedony Mountain (~ K2, Fig. 3.2). The remaining landslides are sporadically scattered throughout the study area. The majority of landslides in the Alaskan study area are proximal to Totschunda Fault and faults related to it (Fig. 3.3).

The population density of large landslides (total landslide population divided by the total area of the study region) for this inventory and other regional studies in mountainous terrain are compared in Table 3.1. The densities represent the average spatial frequency of landsliding. As noted in Section 3.1.1, the data in Table 3.1 are biased toward comparatively recent landslides. This effect was also noted by Whitehouse *et al.* (1983) for data from New Zealand, and probably applies to the data of Savigny (*in press*) as well. Therefore, rather than representing a uniform

sample of landslides throughout Holocene time, the densities are considered more representative of Late Holocene landslides.

Table 3.1. *Comparison of landslide population densities.*

Location	Area (km^2)	Density (km^{-2})	Source
Southwest Yukon, Canada	18,800	1/192	Everard (*this study*)
Central South Island, N.Z.	10,000	1/238	Whitehouse *et al.* (1983)
Southwest B.C., Canada	4900	1/140*	Savigny (*in press*)
Eastern Alaska, USA	4400	1/314*	Everard (*this study*)

* Reflects population density in a corridor specifically adjacent to a regional fault.

In general, population densities are on the order of one per several hundred square kilometres in all four regions. The results obtained in Yukon and New Zealand are similar, but exhibit some disparity when compared with the densities from Alaska and British Columbia. A comparatively high population density derived from the data of Savigny (*in press*) suggests that rocks near major faults are more susceptible to instability. Indeed, while landslides and landslide deposits occupy one percent of the eastern Alaska study area, the corresponding coverage in southwestern British Columbia is nearly four percent (Savigny, *in press*), suggesting the latter rocks are especially susceptible to instability. However, this contrasts with a rather lower density from data in eastern Alaska. The differences are attributed to the sharpness of relief and climate, both of which are more conducive to instability in southwest British Columbia.

3.6 Factors Affecting the Landslide Distribution

3.6.1 Climate and Climatic Change

The principal climatic factors that affect slope stability, either as peak events of comparatively short duration or as gradients in ambient climatic conditions over extended periods of time, are the precipitation and temperature regimes.

The mean annual temperature in the study area is dependent on elevation, and varies from approximately -3C in Shakwak Valley to below -10C in St. Elias Mountains (Wahl *et al.*, 1987). The mean annual temperature is -3C and -4C at Haines Junction and Burwash Landing respectively (Environment Canada, 1993), and decreases with increasing altitude to between -10C and -15C at 2500 m (Wahl *et al.*, 1987).

The primary effect of this temperature regime is to encourage the formation of ground ice and permafrost. Permafrost is continuous from the latitude of Kluane Lake and north, except for isolated pockets of discontinuous permafrost in lowland areas and at higher elevations in St. Elias Mountains (Heginbottom *et al.*, 1992). South and east of Kluane Lake the permafrost regime in upland areas degrades to discontinuous and becomes sporadic near the British Columbia border. Lowland and valley bottom areas in the vicinity of Dezadeash Lake have only isolated pockets of permafrost (Heginbottom *et al.*, 1992). The presence of permafrost in hill slopes inhibits deep penetration of atmospheric water, and tends to enhance active layer slope-movement processes and surficial denudation. This is well evinced by the presence of solifluction lobes, skin flows, and surficial landsliding throughout the study area.

Frost-wedging on slopes may occur in near surface pore spaces during the April-May and September-October shoulder seasons when the mean temperature is near freezing. Data discussed by Piteau (1977) accentuates a positive correlation between rockfalls on steep slopes

and the frequency of freeze-thaw cycles, but this process affects a relatively thin near surface zone and is not considered a controlling factor in deep-seated slope movements.

The mean annual precipitation in Shakwak Valley at Burwash Landing and Haines Junction is 289.9 mm and 305.8 mm respectively (Environment Canada, 1993), and generally increases to the west (Wahl *et al.*, 1987) as noted in Section 2.2. Precipitation data for Burwash Landing and Haines Junction are presented on Figures 3.4, and 3.5; detailed data for the eastern St. Elias Mountains are not available. Differences in the mean monthly precipitation patterns and in the rain/snow proportions of total precipitation reflect varying degrees of orographic influence at each of these locations, as well as a number of other interrelated factors (Wahl *et al.*, 1987).

In the months May through September the predominant form of precipitation is rain, and the extreme 24 hour precipitation events that have been recorded during these months comprise more than 75% of the mean monthly precipitation in most cases. Further, the expected annual 24-hour maximum total rainfall for 2, 5, and 10 year returns in Table 3.2 represent considerable portions of the mean rainfall in any month. These data suggest that high intensity rain storms are not infrequent in this region.

Table 3.2. *Expected maximum 24-hour total rainfall (mm) for various return periods.**

Return Period (years)	2	5	10	15	20	25	30	50
Burwash Landing	22.0	30.6	36.3	39.5	41.7	43.5	44.9	N/A
Haines Junction	19.0	32.0	40.6	45.4	48.8	51.5	53.6	59.5

* Source: Wahl *et al.* 1987.

In July 1988 unusually severe rainstorms preceded widespread debris torrent and shallow landslide activity in Shakwak Valley near Kluane Lake (Evans *et al.*, 1989). The association

between landslides and peak rainfall (storm) events or abnormally high antecedent rainfall in other areas is well documented (*i.e.* Evans *et al.*, 1983; Kaliser *et al.*, 1986; Polloni *et al.*, 1991). However, correlations between deep-seated slope movement and precipitation in southwest Yukon have not been reported.

In broad terms, the infiltration of atmospheric water into a slope, whether it is introduced through rainfall or rapid snow melt, has the effect of raising the piezometric surface and pore pressures within it. The amount of change in the slope hydrogeological regime depends upon the intensity and duration of moisture influx, the infiltration rate, the geological materials and their arrangement, and the saturated hydraulic conductivity of the slope (Freeze, 1982). As noted above, permafrost is continuous beneath the majority of the upland area in this study (Heginbottom *et al.*, 1992), and is believed to inhibit infiltration of atmospheric water into the subsurface. For this reason, rainfall and snow melt are not considered a significant factor controlling distribution of large landslides in these areas. In those portions of the upland area underlain by discontinuous permafrost, infiltration of atmospheric water may occur and exacerbate slope movement.

The climate in southwest Yukon has been evolving for considerable time. Burn (1994) notes that uplift in St. Elias Mountains has been virtually continuous since Oligocene time (Eisbacher *et al.*, 1977), supporting conditions amenable to glaciation and the formation of permafrost. Presumably the formation of vast ice sheets to the west as well as orographic isolation from the Pacific Ocean has had a considerable influence on the climate in this region. Evidence of paleoclimates preserved in the stratigraphic record are sporadic. Pre-Quaternary glacial activity between 2.7 and 10 Ma ago has been documented in the eastern Alaska Ranges (Denton *et al.*, 1969). Rampton (1981) discusses evidence of several Mid- to Late Pleistocene non-glacial intervals, and, more recently, a hypsithermal interval between 8700 and 2800 b.p. The warmer climates associated with the nonglacial intervals and the hypsithermal may have

caused changes in the distribution of permafrost in this region, and for the reasons discussed above, promoted slope instability.

3.6.2 Lithological Correlation

In this study, lithology refers to the mapped bedrock divisions and their spatial distribution in the study area, as compiled by Kindle (1953), Muller (1967), and Dodds (1982*a, b, c*). The correlation between landslides and the bedrock division they occur in is a convenient index for identifying rocks that are relatively more unstable than others.

An example of a lithologically controlled landslide is Bighorn Creek Rock Block-Slide/Avalanche, a large, highly mobile, bimodal rock slope movement that is characteristic of several landslides in this study. Slope failure appears to be transitional from rock-block sliding near the head of the slide to debris avalanching further down slope. Landslides with comparable mobility in other areas of the Canadian Cordillera were described by Eisbacher (1979) and Evans *et al.* (1989).

The head scarp is an arcuate scar approximately 1500 metres long and 220 metres high at the head of what was, prior to the landslide, a cirque (Fig. 3.6). It steeply dislocates bedding in Neogene volcanic rocks (Wrangell Lava), and may extend downward into underlying Ordovician sediments. Its western flank is fault bounded.

Several massive columns of virtually intact rock, one of them approximately 800 metres wide, have translated a short distance beneath the western edge of the head scarp (Plate 3.1) (Fig. 3.6). These rock blocks have not undergone significant rotation, suggesting that initial movement occurs on a basal sliding surface. This surface is believed to be either a bedding plane in the volcanic sequences or the unconformable contact with underlying Ordovician rocks.

The debris stream is confined in a narrow valley adjoining a tributary of Bighorn Creek, descending 750 m from the base of the head scarp over a horizontal distance of at least 4100 m. Its surface is hummocky and chaotic; longitudinal debris ridges on the lee side of an over-topped

bedrock ridge several kilometres from the head scarp are clearly visible. A landslide dam created at the down stream confluence was subsequently breached and eroded. The age of Bighorn Creek Rock Avalanche is unknown, although the unmodified appearance of the detachment scar and the colluvium suggest it is Late Holocene.

The extent to which the landslide distribution is affected by lithological features such as rock texture, composition, and fabric, is not addressed in this study. Figure 3.7 depicts the landslide population apportioned to each of the bedrock divisions that landslides occur in, together with the portion of the study area covered by each of these divisions. Data for individual landslides are listed in Appendix 1.

The majority of the landslides (52%, or 51 of 98) occur in stratified Neogene volcanic rocks (Wrangell Lava). Wrangell Lava overlays approximately ten percent of the Yukon study area, with the greatest accumulations occurring to the northwest (Fig. 3.8). They form discrete but sometimes extensive areas of upland terrain, typically as resistant, topographically high, scarp-edged caps covering basement rocks. Landslides seated in Wrangell Lava predominate on slopes that have been over-steepened by glacial scouring, where fold-tilted bedding planes are exposed by erosion, or where differential erosion of weak underlying rocks has undermined slope support. Because Wrangell Lava occurs as discrete packages, the landslides associated with these rocks possess a strong spatial bias, and tend to form clusters, such as those to the west of Donjek River (~H5, Fig. 3.1) and at Chalcedony Mountain (~K2, Fig. 3.2).

Thirteen percent of the landslides (13 of 98) are seated in Lower Permian metavolcanic and metasedimentary rocks of Skolai Group (Station Creek and Hasen Creek Formations respectively). These rocks are exposed over approximately five percent of the study area as fault bounded, elongate panels (Fig. 3.9). Many of these exposures are proximal to regional tectonic faults, and at outcrop scale are intensely deformed and are believed to have low rock mass strength. The remaining bedrock divisions each account for less than ten percent of the total population.

3.6.3 Geological Structure

Geological structure includes features of discontinuity and nonhomogeneity in rocks at both outcrop- and regional-scale such as faults, folds, joints, bedding planes, and lithological contacts. These features are generally considered the primary influence on rock slope stability in this area.

The most conspicuous structural features in the Yukon study area are Shakwak-Dalton segment of Denali Fault System, Duke River Fault, and Cement Creek Fault. In aerial photographs they are delineated by sub-parallel groups of topographic lineaments. Figures 3.10 and 3.11 depict the spatial relationship between landslides, lineaments, and the major faults in the Yukon study area.

A clear correlation exists between the corridors proximal to the regional faults and several of the landslides. There are several reasons for this association. First, the faults coincide with zones of sheared and metamorphosed rock that is inherently weak. An example of such a landslide is Upper Cottonwood Creek #2, an actively failing zone of friable, altered rock that is coincident with Dalton Fault. Weathering and erosion of such rocks is enhanced compared to the surrounding rocks, and as a consequence, slope support in these corridors is easily removed and slope gradients are generally over-steep. Such conditions significantly contribute to slope instability, although they are not a requisite condition for landsliding. Secondly, the degree of rock deformation is greatest near the regional faults (Read *et al.*, 1975; Read, 1976; Campbell *et al.*, 1978), suggesting that the density of minor structures also increases near them. This concurs with observations at Lower Cottonwood Creek #2 landslide where outcrop-scale features such as jointing, fracture, and minor faulting that dissect the slopes are considered the primary factors contributing to instability. The observed intense deformation is not surprising, for both Shakwak-Dalton and Duke River faults are major tectonic features that have undergone significant displacement.

An example of a landslide with close spatial association to a regional fault is Congdon Creek Rock Avalanche (CCRA), a movement first mapped by Rampton (1979*c*), and discussed briefly by Thurber Consultants (1989). The source zone of CCRA is unclear. A weathered, concave scar between approximately 1150 metres and 1600 metres elevation on the Kluane Ranges frontage is the most likely location of the source zone (Plate 3.2). It is seated in Permian metavolcanic rocks of Station Creek Formation (Skolai Group) and may coincide with steep, northeast dipping bedding and foliation (Fig. 3.12). The estimated 70×10^6 m^3 of landslide colluvium on the alluvial fan below (Thurber Consultants, 1989) appears too great to be entirely contained within this source zone. It is possible that the pre-failure slope volume was greater than can be currently estimated by extrapolation of adjacent slope profiles over the source zone. Shakwak segment of Denali Fault System passes beneath the foot of the slope (Dodds, 1982*a*).

The debris train comprises a lobate blanket on the northern slope of Congdon Creek alluvial fan and possesses a faint surficial radiating pattern. The colluvium surface is undulating and hummocky, with abundant pits and contorted debris ridges near the foot of the slope (Plate 3.2). The pits may have resulted from ablation of entrained ice. Numerous debris cones (molards) noted during a traverse along the abandoned pipeline confirm that colluvium extends at least two kilometres from the base of the suspected source zone. The position of the distal edge of the debris lobe is uncertain.

The debris train has run out nearly 2.5 km on the surface of the alluvial fan at a nominal slope angle of two to three degrees. This anomalously long run was noted by Thurber Consultants (1989). It is one of two landslides in this study exhibiting this characteristic (see Pirate Creek Rock Avalanche, Appendix 1). A statistically derived empirical formula describing landslide mobility in terms of the apparent friction coefficient, f, as a function of the landslide volume, V, was presented by Scheidegger (1973):

$$\log_{10} f = 0.62419\left(0.15666 \log_{10} V\right) \qquad [3\text{-}1]$$

(where $f=\upsilon/\kappa$ is the total relief between the top of the headscarp and the toe of the slide divided by the horizontal distance between these respective points). Using an estimated volume of 70×10^6 m^3 (Thurber Consultants, 1989), the above relation yields an apparent friction coefficient of 0.249. The estimated horizontal reach, κ, of CCRA is 3200 m. Back calculation yields the total relief, $\upsilon=3200\times0.249=795$ m. This value is nominally larger than the total relief of 765 m derived from air photo interpretation of the extents of the slide (Fig. 3.12). The discrepancy between these figures is well within the range of subjective error. These data suggest that the interpreted bounds of the slide are reasonable estimates, and that CCRA has mobility comparable to other landslides of its size. However, volume estimates used in [3.1] are very sensitive to small changes in the apparent friction angle. Calculations not based upon detailed field measurements should be interpreted appropriately. Additional formulae specific to landslides occurring in glacial and non-glacial environments are described by Evans *et al.* (1988).

Outcrop-scale features such as fractures, joints, bedding planes, and small faults are generally considered to have the greatest influence on slope stability, but because of structural complexity in the study area, their effect cannot usually be extrapolated beyond individual sites. In general terms, these structures create penetrative planes of weakness, with the effect of not only reducing rock mass strength, but also by representing potential simple or compound slip surfaces within the slope.

An outstanding example of such a slope failure is Nines Creek Rock-Block Slide (NCRS), a massive rock-block translation involving much of the eastern flank of an unnamed 2500 metre peak to the southwest of Nines Creek (Fig. 3.13). Relief from the toe to the crown of NCRS varies between 500 and 700 metres. The slide block is a coherent wedge comprised primarily of Wrangell Lava, and may include slivers of underlying Permo-Triassic and Oligocene strata at its base. It has translated approximately 375 metres vertically and 700 metres horizontally on a planar, northeast dipping surface (Plate 3.3). This surface appears to cut across bedding in the volcanic sequences, and is believed related to pervasive jointing observed in most

exposures of Wrangell Lava. It may in part be related to two northwest trending fault contacts in Permo-Triassic basement rocks that intersect the southern edge of the slide. The faults are seated in highly erodable rock coinciding with a pronounced linear trough, and may have provided a weak zone beneath the incipient failure.

The effect of penetrative discontinuities is compounded when they are tilted concurrently with folding. Weak surfaces in under-dip or dip slopes are extremely susceptible to failure, especially when they are day-lighted by erosion. This is comparatively in common topographically high Tertiary cover rocks which are often tightly folded about northwest trending axes. An example of this is Cement Creek #1 landslide (discussed in Chapter 4), where slip is localized along comparatively weak interbeds of altered breccia and volcaniclastic deposits in tilted Wrangell Lava sequences.

3.6.4 Geomorphic Setting and Slope Development

The majority of landslides are situated west of Denali Fault in St. Elias Mountains (Figs. 3.1 and 3.2). Throughout this region, tectonically driven uplift has been nearly constant since Oligocene time (Eisbacher *et al.*, 1977), accentuating relief as the base level has risen. Steep, angular mountain ranges (Sec. 2.2) are dissected by several large, antecedent river valleys and a number of tributary valleys. High gradient streams and hanging valleys suggest erosion has not kept pace with uplift.

The larger valleys possess steep-sided, often asymmetric U-shaped profiles that are the result of intense Pleistocene glacial scour, post-glacial slope movement, periglacial modification, and the underlying geology. Smaller upland stream valleys were extensively glaciated in the Late Pleistocene and often terminate in cirques or glacially sculpted upland. Their profiles tend to be somewhat more V-shaped than the larger valleys because their development has being dominated by fluvial incision since deglaciation. Slope profiles are typically straight and steep, with well

defined slope breaks, and relief sometimes exceeding 1000 m. In larger valleys, the lower slopes are generally mantled with colluvium or valley train.

Large landslides are comparatively more common in tributary and upland valleys than in trunk valleys, such as those of Shakwak Valley (Fig. 3.1, A18 - O4 & Fig. 3.2, H11 - O3), Donjek River (Fig. 3.1, A11 - J8), Duke River (Fig. 3.1, A14 - G12), Alsek River (Fig. 3.2, A4 - K4), Kaskawulsh River (Fig. 3.2, K4 - L1), and Duke Depression, where they are conspicuous by their relative absence. Severely weathered slope scars believed to be source zones for ancient landslides are not uncommon in the trunk valleys, but few are accompanied by identifiable debris accumulations, suggesting that the colluvium has since been eroded or reworked to the point of being unidentifiable. Rampton (1981) identified colluvium patterns at one site suggesting the landslide debris was dispersed by an active glacier.

Those landslides bordering trunk valleys that can be identified (*i.e.* Tepee Lake, Wolverine Plateau #2 & #3, Donjek River #1, Duke River) appear to be ancient. Tepee Lake Rock Slide (TLRS) is situated on the escarpment rim of a thick, plateau-like package of Neogene volcanic rocks (Wrangell Lava) overlooking Duke Depression to the north and Donjek River to the east. It is the largest and most clearly defined landslide of a number that have occurred along this declivity (see Wolverine Plateau #2 and #3, Appendix 1).

The source area of TLRS is a weathered, arcuate scar more than 1500 m in breadth, extending downward from the top of the escarpment. The exposed portion exceeds 175 m in height; landslide deposits and talus cover the lower portion. The headwall dips approximately 40 degrees to the north, truncating southwest dipping beds exposed in the slope. On the eastern flank of the slide, step-like scarps beneath a thin mantle of colluvium appear to reflect underlying bedrock topography (Plate 3.4). Relief between the crown and the toe varies from 425 to 575 m (Fig. 3.14). Colluvium from TLRS covers the valley floor beneath the escarpment to considerable thickness, and extends at least two km from the headwall, and perhaps as far as Tepee Lake. Its surface is subdued and uneven, and has been extensively modified.

Landslide colluvium at Wolverine Plateau #3 appears to abut glacial trim lines above Wolverine Creek, inferring that landsliding along the escarpment rim occurred before or during deglaciation (approximately 12,000-14,000 b.p.), and may be related to slope debuttressing. More recent slope failures along the escarpment are comparatively minor rockfalls and slumps. Rampton (1981) suggests landslide activity in this region was at a maximum during and immediately after deglaciation. Increased exposure of over-steepened slopes, changes in slope hydrologic and stress regime, and the removal of physical slope support are cited as contributing factors. Observations by Gardner (1980) in the southwest Canadian Rockies corroborate this view. A modern example of this phenomenon appears to be occurring at the terminus of Lowell Glacier (Plate 3.5). These suggest that the frequency of landsliding on slopes bordering the trunk valleys was greater in the past, and that these slopes are currently depleted of large incipient failures. Hence, the distribution of landslides in the trunk valleys supports an exhaustion model (Sec. 3.7) (Cruden *et al.*, 1993).

3.6.5 Seismicity

Landslides have long been known to be secondary effects of earthquakes (Radbruch-Hall *et al.*, 1976). The association between landslides and earthquakes in the Canadian Cordillera is documented by Mathews *et al.* (1978), Mathews (1979), Evans *et al.* (1987) and Wetmiller *et al.* (1989). Other examples have been studied in Alaska (Miller, 1960; Plafker, 1968), Peru (Plafker *et al.*, 1978), and elsewhere.

The record of historical seismicity in the Kluane-St. Elias region is largely incomplete. Since 1899, nine earthquakes greater than magnitude seven have occurred in Fairweather-Yakutat Zone, including the 1979 M7.2 Mt. St. Elias earthquake (Horner, 1983). Known historic earthquakes in Denali-Shakwak Zone are all less than magnitude seven. These include a M6+ event west of Kluane Lake in 1920 (Horner, 1988), and a M6.5 event west of Dalton Fault near the B.C. border in 1944 (Wetmiller *et al.*, 1989).

A seismograph installed at Whitehorse, Yukon, in 1971 allowed accurate detection of magnitude four earthquakes, and after improvements in 1978, as small as magnitude three (Wetmiller *et al.*, 1989). A strong motion accelerograph at Haines Junction, Yukon, has not been triggered (Horner, 1991; *pers. comm.*).

Between September 1978, and August 1990, 345 earthquakes were recorded in Denali-Shakwak Zone in Yukon. Their epicentre locations, magnitudes, and times of occurrence are listed in Appendix 2. The majority are concentrated in two groups along major tectonic faults (Fig. 3.15). The first is a dense cluster of epicentres near Cement Creek Fault that extends northwest, with decreasing intensity, to the Yukon-Alaska border. It includes the largest recorded earthquake in the data period (M_B5.4 on March 3, 1983). The second is a diffuse, but more extensive group that follows Denali and Duke River Faults from Kluane Lake southeast into British Columbia. Local seismicity clusters occur south of Kluane Lake, and also to the south of Dezadeash Lake. A microearthquake survey in the area immediately south of Kluane Lake confirmed low-magnitude seismicity at hypocentral depths less than 15 km (Horner, 1983). Seismicity levels on Denali Fault north of Kluane Lake, and on Duke River Fault between Cement Creek Fault and Kluane Lake are comparatively low. Epicentres not proximal to major faults have no distinct spatial or temporal pattern.

In a correlative study of landslides and 40 historical earthquakes worldwide, Keefer (1984) proposed a minimum threshold magnitude between four and five for earthquake-induced landslides. Large historical earthquakes in the Yukon study area are all greater than magnitude six. Of the 345 earthquakes recorded between 1978 and 1990, the majority are less than magnitude four, but there are a sufficient number greater than the threshold magnitude that seismicity may be considered a potential triggering mechanism.

It is not known whether seismicity levels in the past are comparable with current levels. Holocene glacial features in adjacent areas of the eastern Alaska Ranges (Richter, 1971; Plafker, 1977) have been offset by faulting that must have been accompanied by seismicity. In Yukon,

Holocene lineations in Shakwak valley have been attributed to movement on Denali Fault (Clague, 1979). These are cited as indirect evidence of seismicity in this region for at least part of the Holocene.

3.7 Exhaustion and Steady-State Regional Landslide Models

The temporal distribution of rock slides in any region should adhere to either a steady-state or exhaustion model. For a defined temporal interval, the probability of rock sliding remains constant through time for the steady-state model whilst decreasing for the exhaustion model, provided that the fundamental causes of slope instability (Sec. 3.5.1) remain constant or static. Thus, assuming that the mechanisms triggering rock slides are not temporally or spatially constrained, the steady-state model is characterized by a uniform temporal distribution, while the distribution for the exhaustion model is biased toward older movements.

Cruden et al. (1993) examined an area of the southeastern Canadian Cordillera where structurally controlled rock slides on over dip slopes predominate, concluding that the exhaustion model is more representative in that terrain.

Periglacial processes (French, 1985) are very active in the Yukon study area. Many landslides were difficult to distinguish because of this rapid cryogenic modification. As a corollary, the extent of modification was used to establish relative age and a qualitative temporal distribution. On this basis, the landslide population shows evidence of an exhaustion-type range of ages. However, notable exceptions to a regional exhaustion model coincide with zones of high seismicity, particularly in the Cement Creek area, where the apparent landslide ages depart from the exhaustion model, and are more in keeping with an active steady state model.

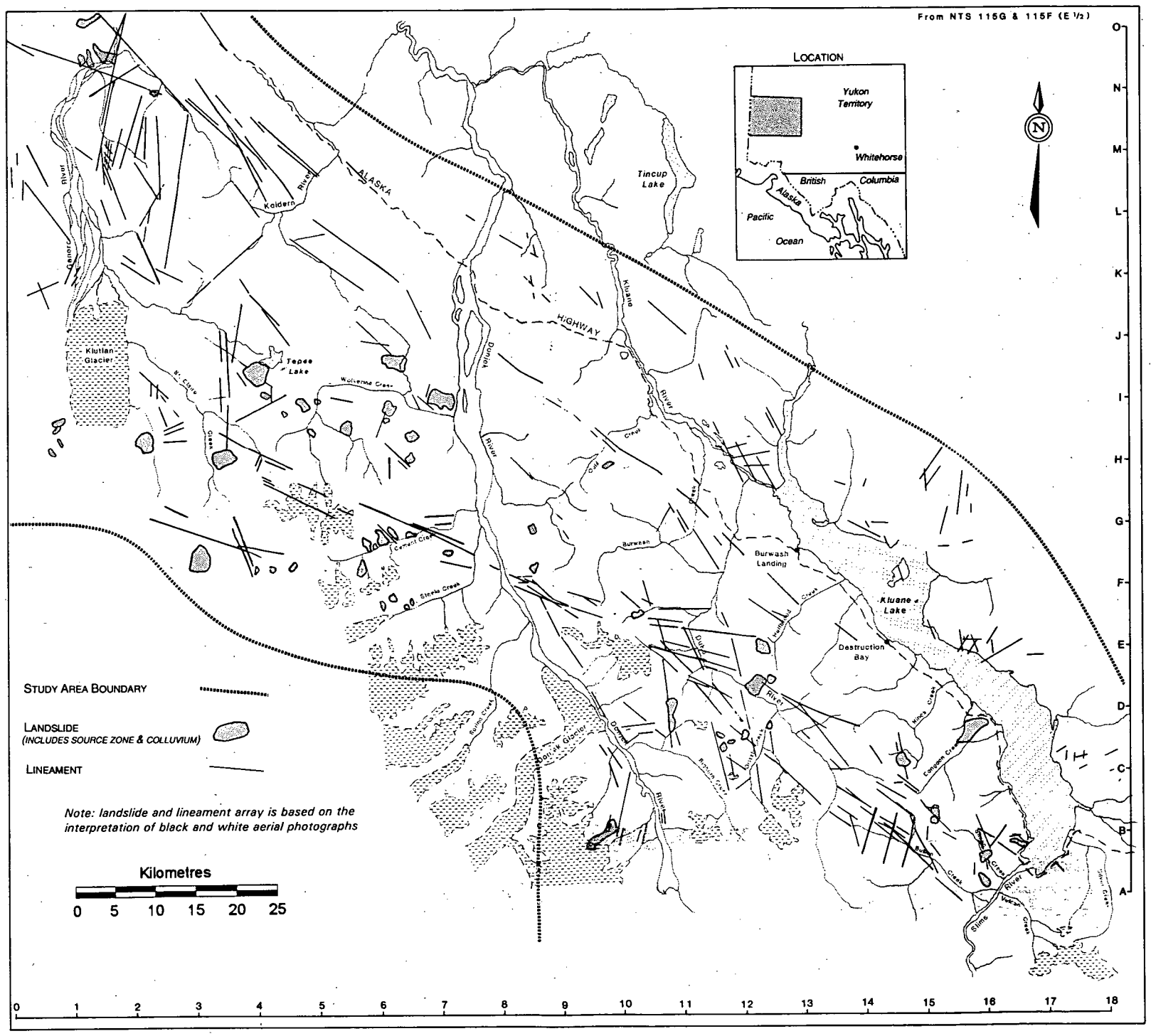

Figure 3.1. *Landslides and lineaments of the Kluane Lake map area. Landslides and lineaments (bold) are shown with local geographic features (light). The alpha-numeric grid on the border corresponds to locations and data in Appendix 1.*

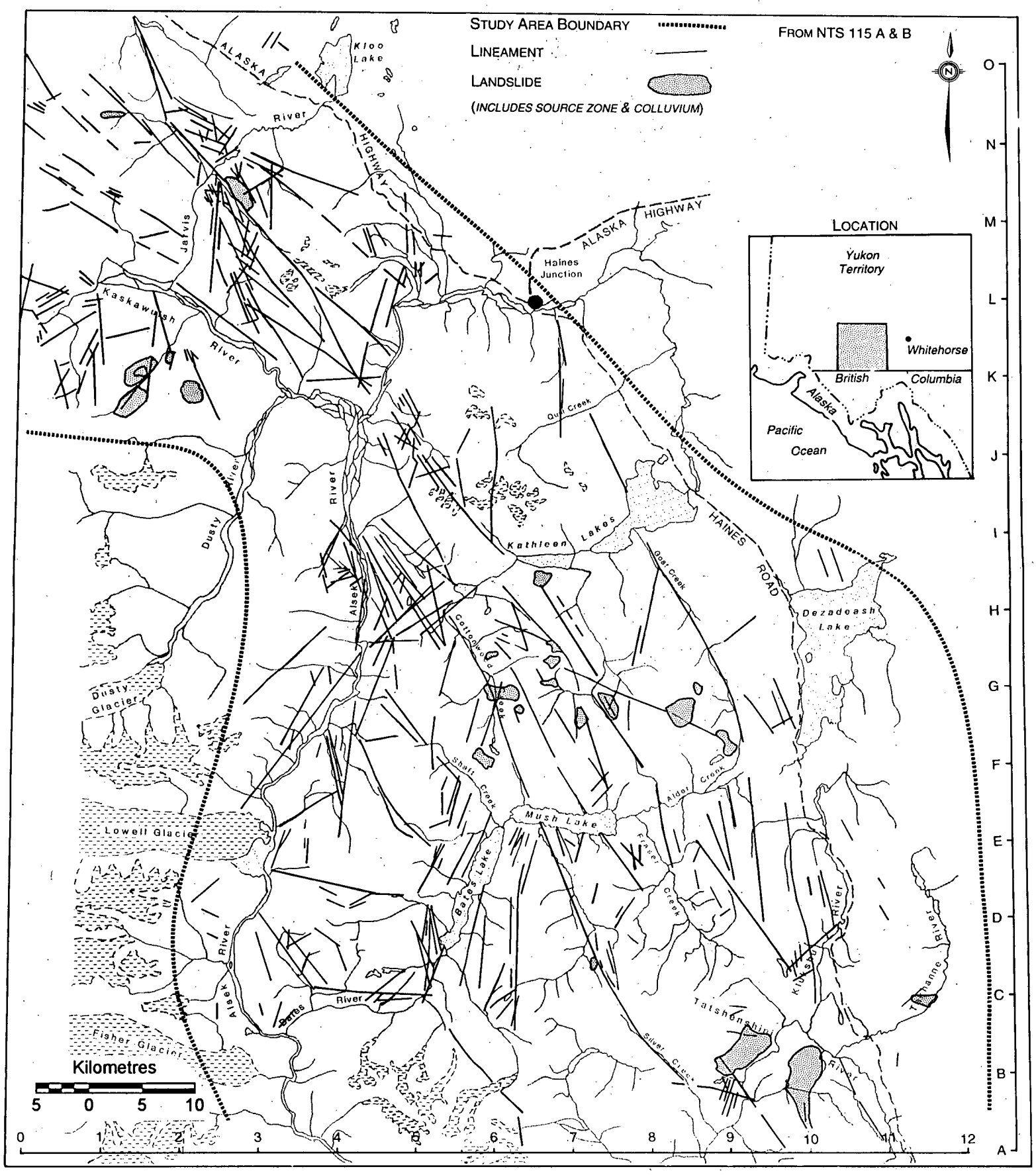

Figure 3.2. *Landslides and lineaments of the Mt. St. Elias and Dezadeash map areas. Landslides and lineaments (bold) are shown with local geographic features (light). The alpha-numeric grid on the border corresponds to locations and data in Appendix 1.*

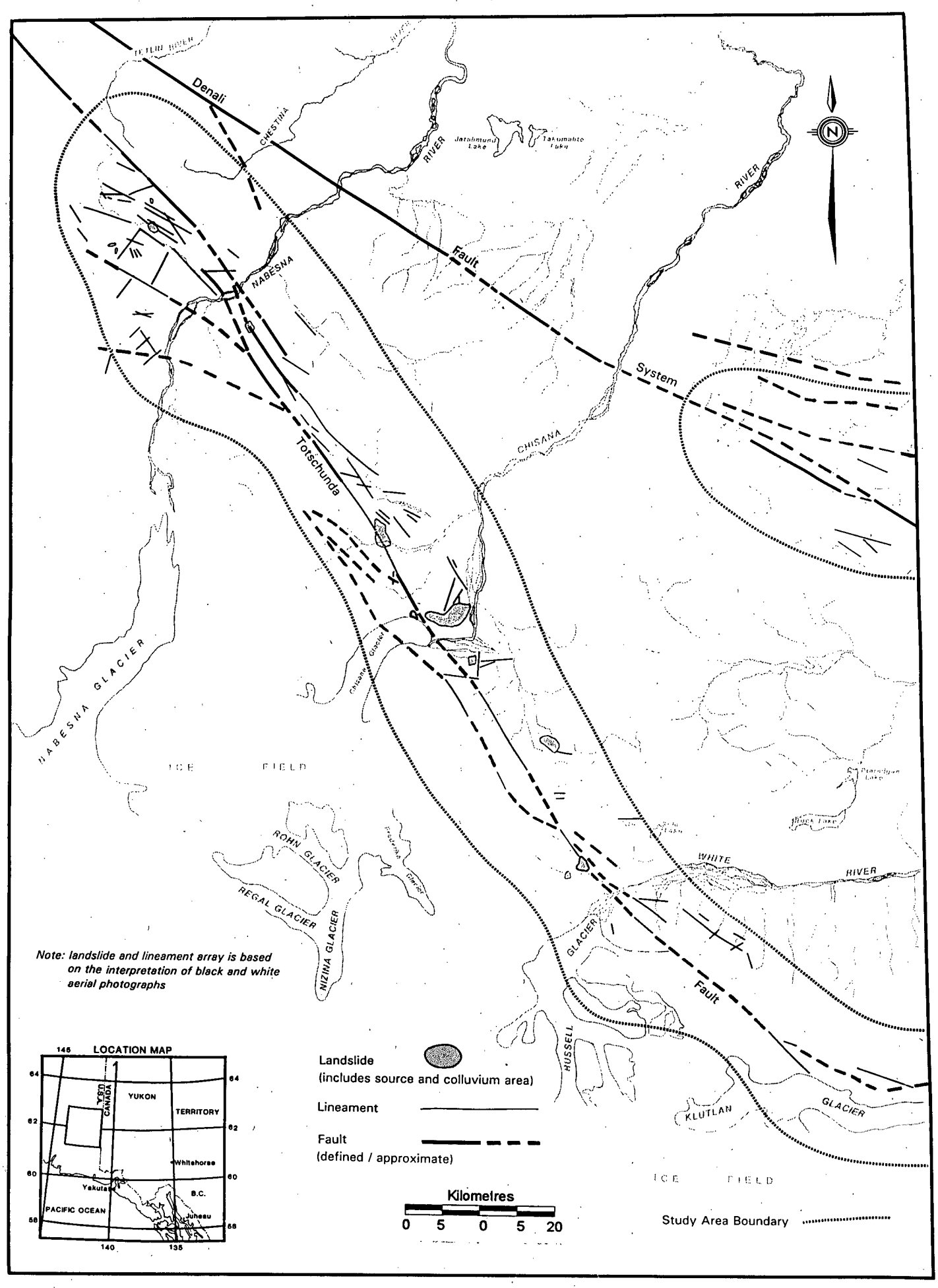

Figure 3.3. *Landslides, lineaments, and regional faults of McCarthy and Nabesna quadrangles, Alaska. Landslides, lineaments, and regional faults (bold) are shown with local geographic features (light).*

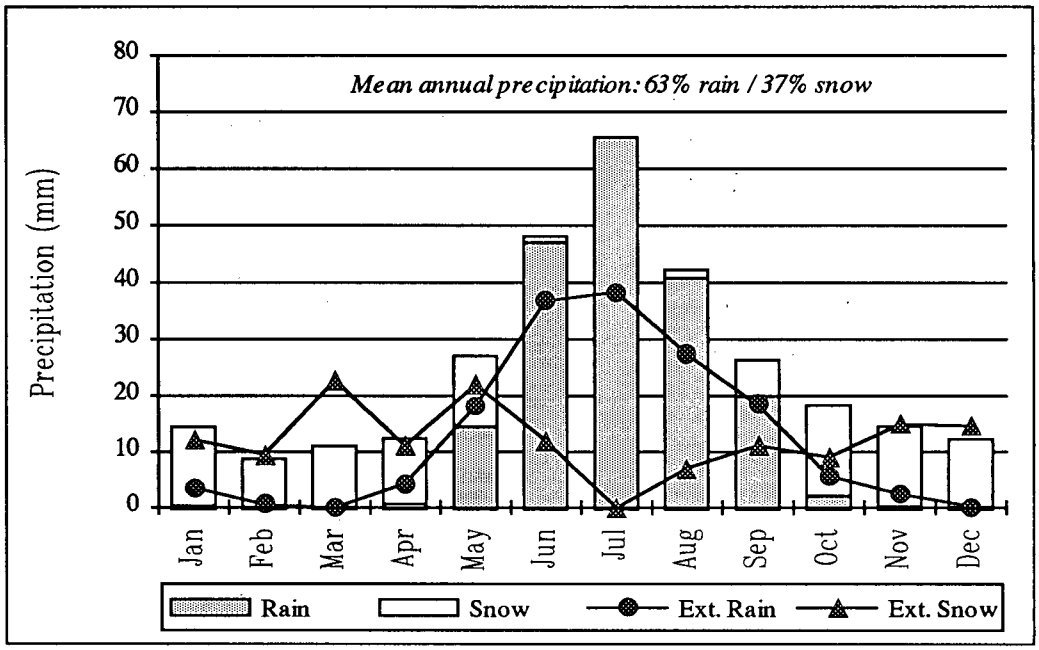

Figure 3.4. *Monthly mean precipitation and 24-hour precipitation extremes at Burwash Landing, Yukon (1966-1990). Snow is shown as its calculated water equivalent (Environment Canada, 1993).*

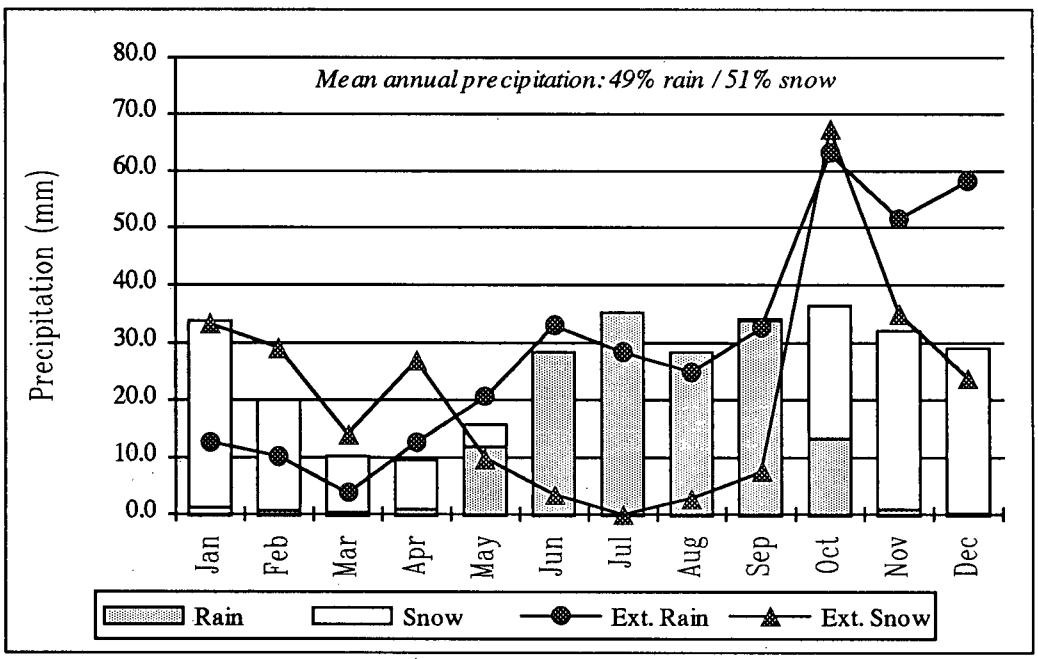

Figure 3.5. *Monthly mean precipitation and 24-hour precipitation extremes at Haines Junction, Yukon (1944-1985). Snow is shown as its calculated water equivalent (Environment Canada, 1993).*

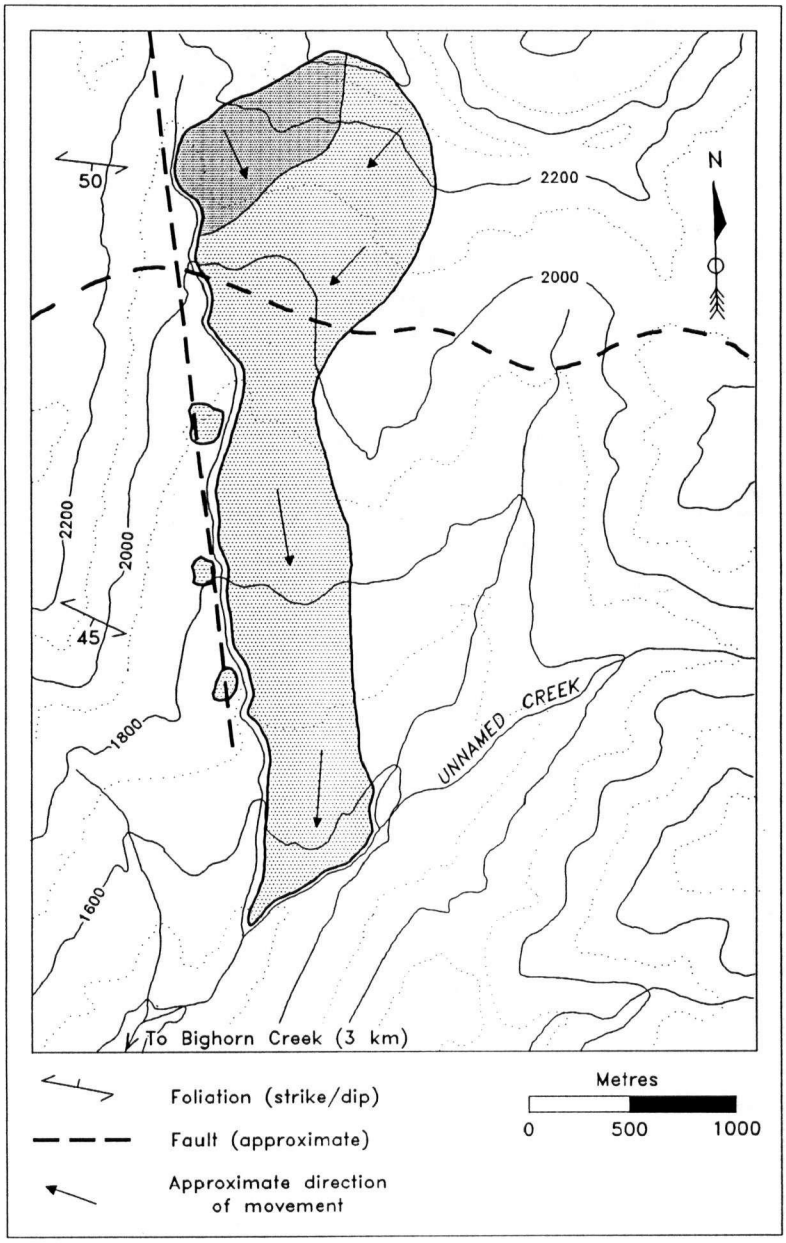

Figure 3.6. *Bighorn Creek Rock Avalanche. The slide area is lightly shaded; darker shading corresponds to intact rock blocks beneath the head scarp. Contour interval is 100 m.*

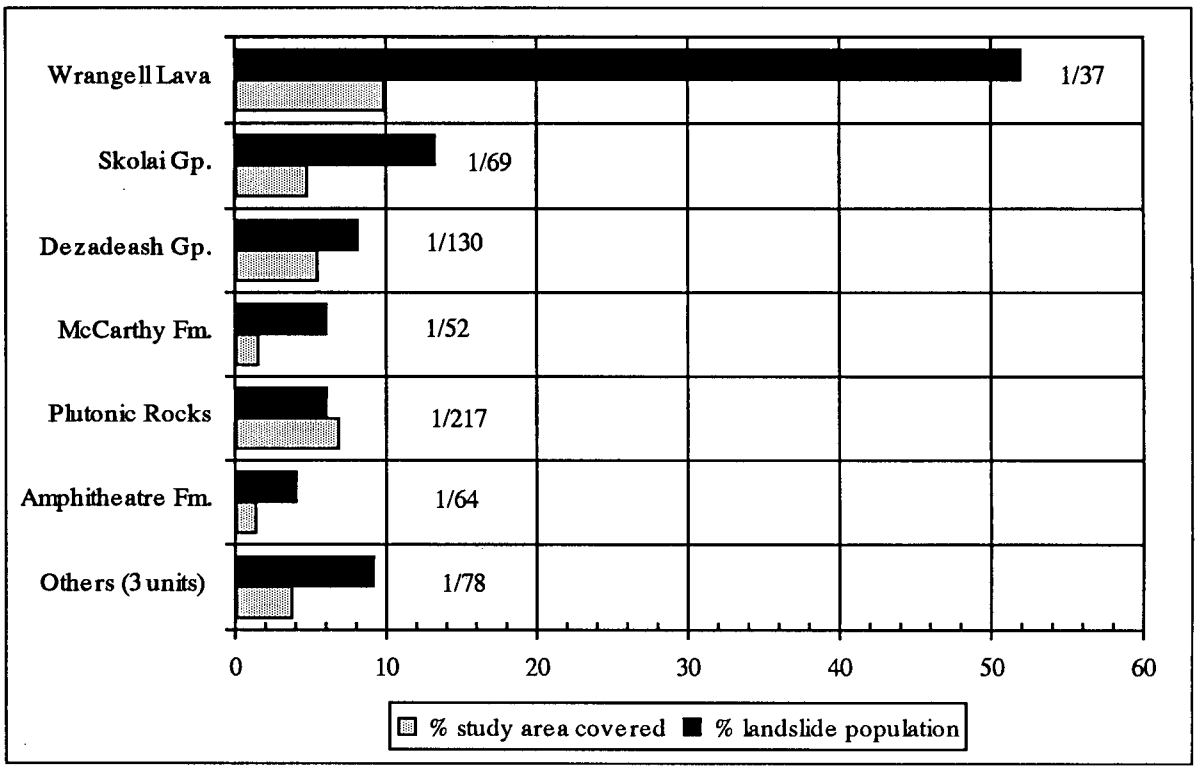

Figure 3.7. *Percent portions of the landslide population in each of the lithological divisions landslides occur in, together with the percent portion of the study area these divisions cover. The average population density in* km^{-2} *(landslide population in each bedrock division divided by the areal coverage of that division) is shown next to the corresponding bars.*

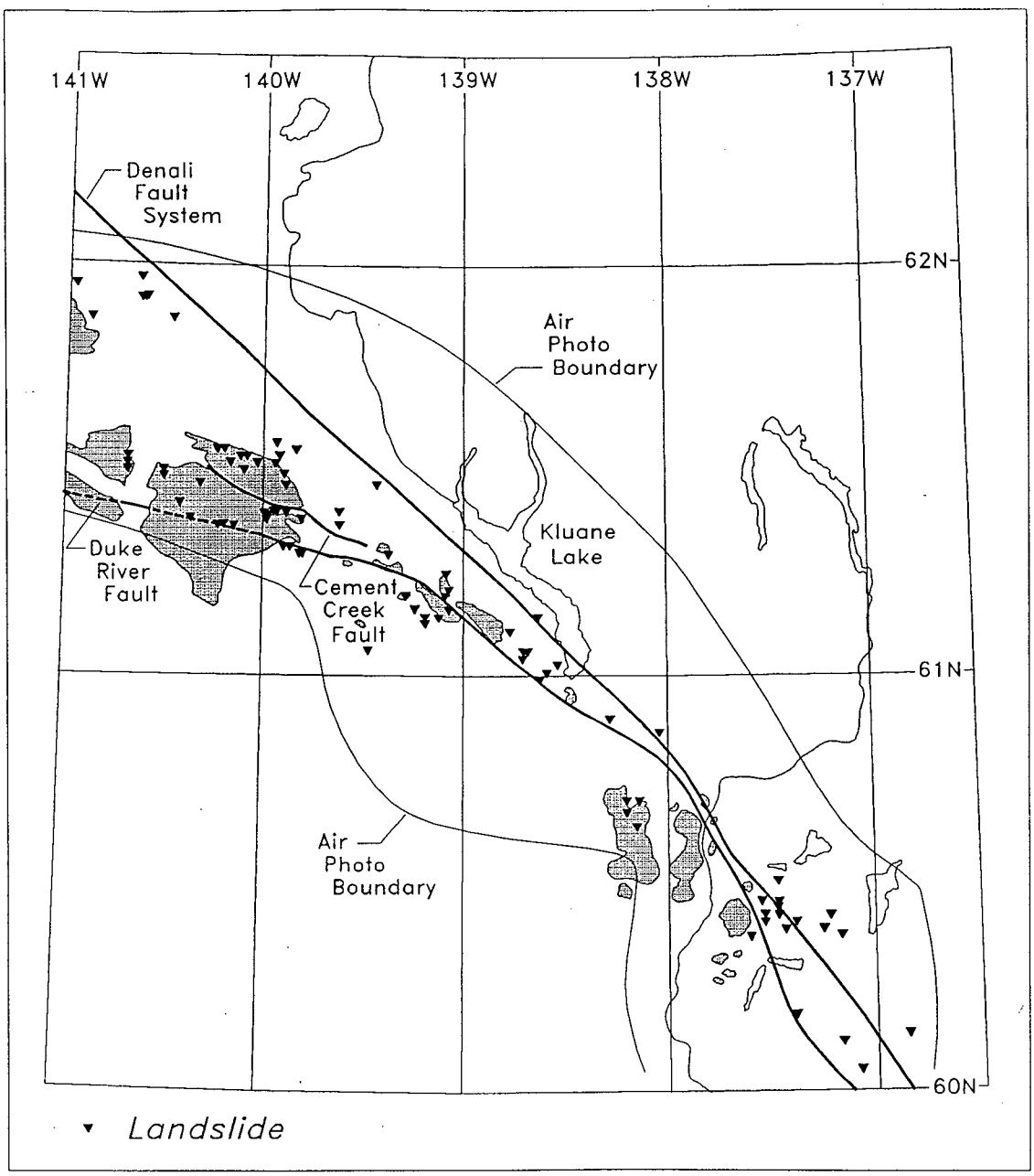

Figure 3.8. *Landslide locations (solid inverted triangles) are shown with the distribution of Neogene Wrangell Lava (shaded), and major faults.*

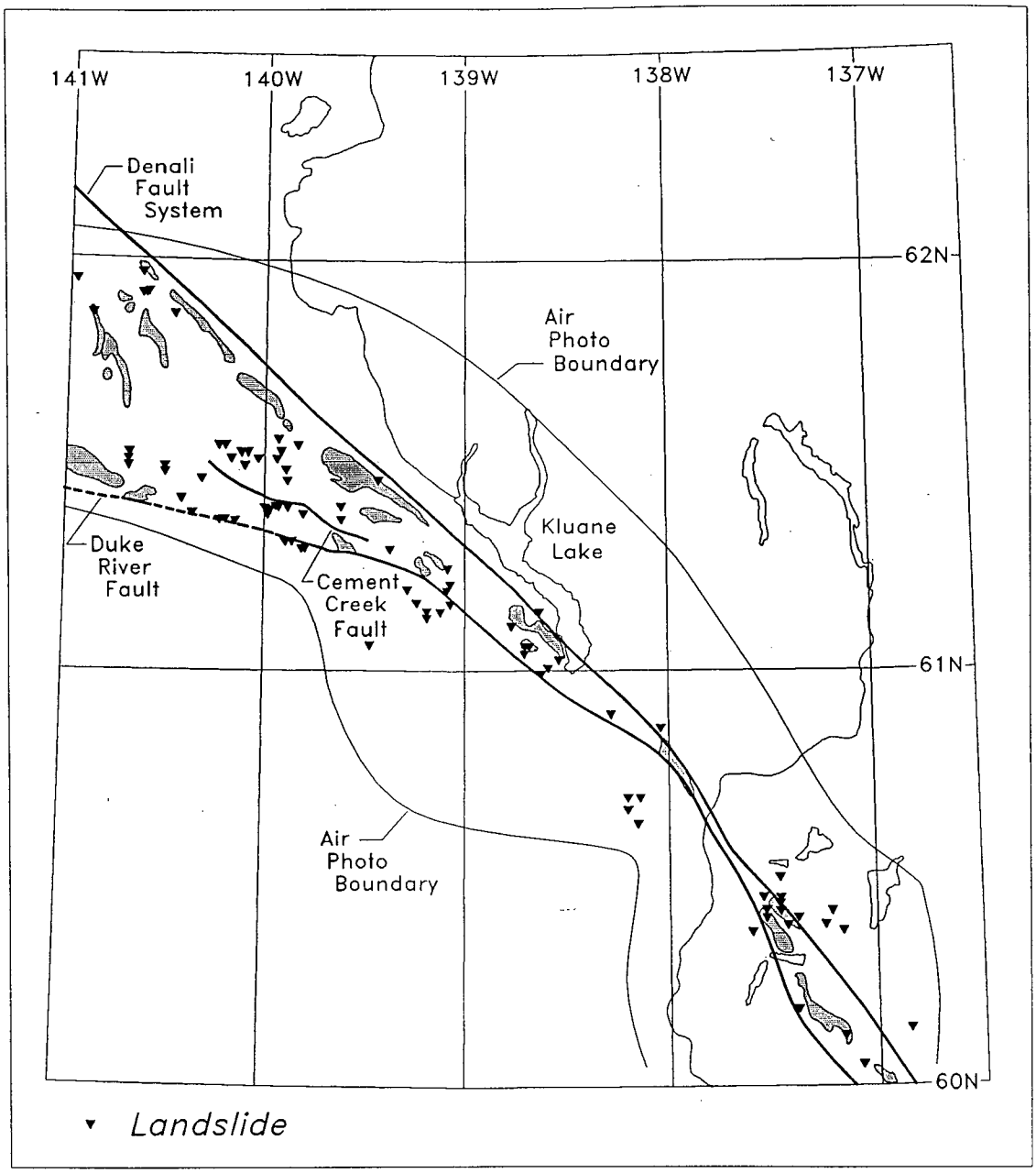

Figure 3.9. *Landslide locations (solid inverted triangles) are shown with the distribution of Permo-Triassic Skolai Group (shaded), and major faults.*

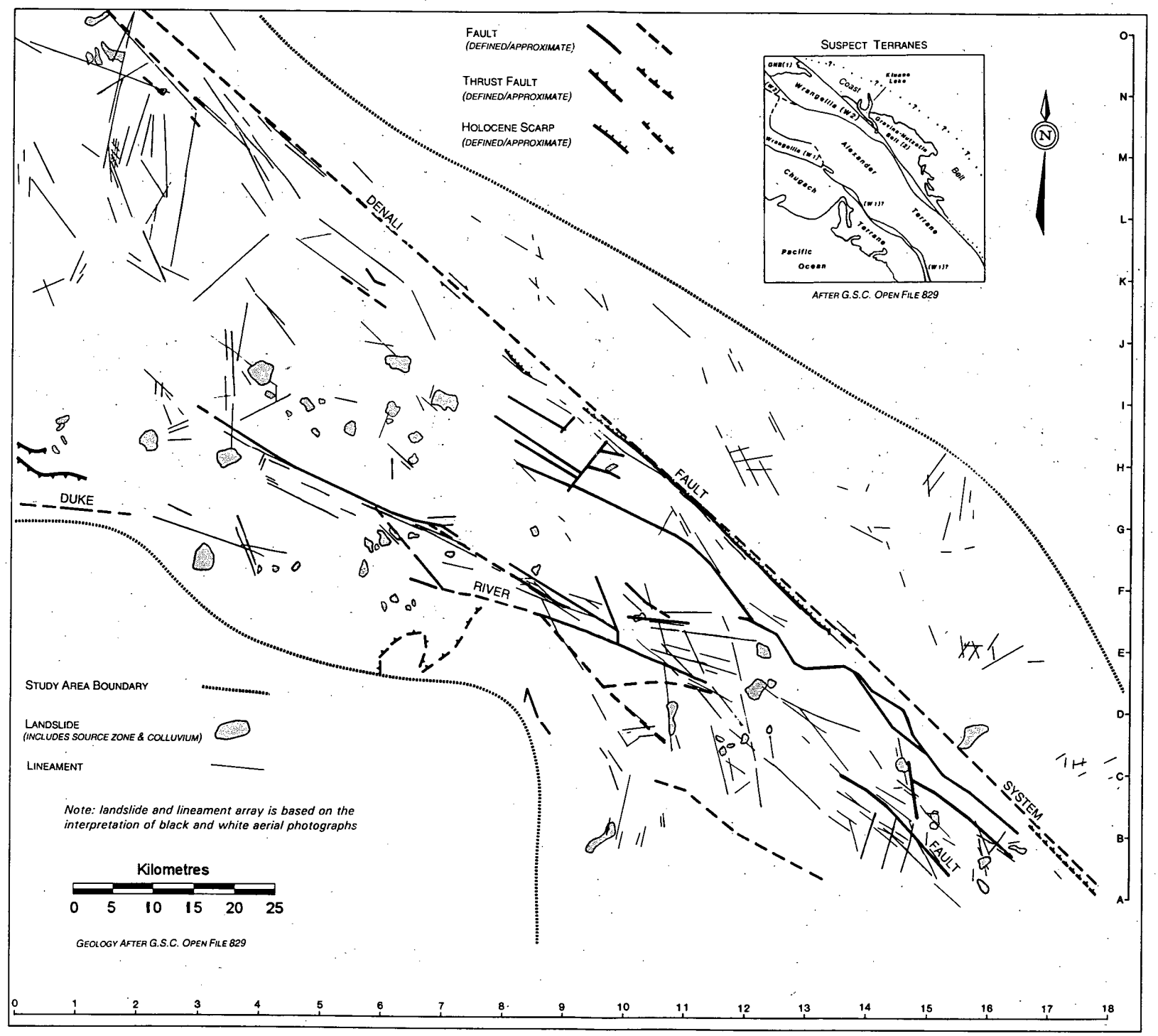

Figure 3.10. *Landslides, lineaments, and regional faults of the Kluane Lake map area. The alpha-numeric grid on the border corresponds to locations and data in Appendix 1.*

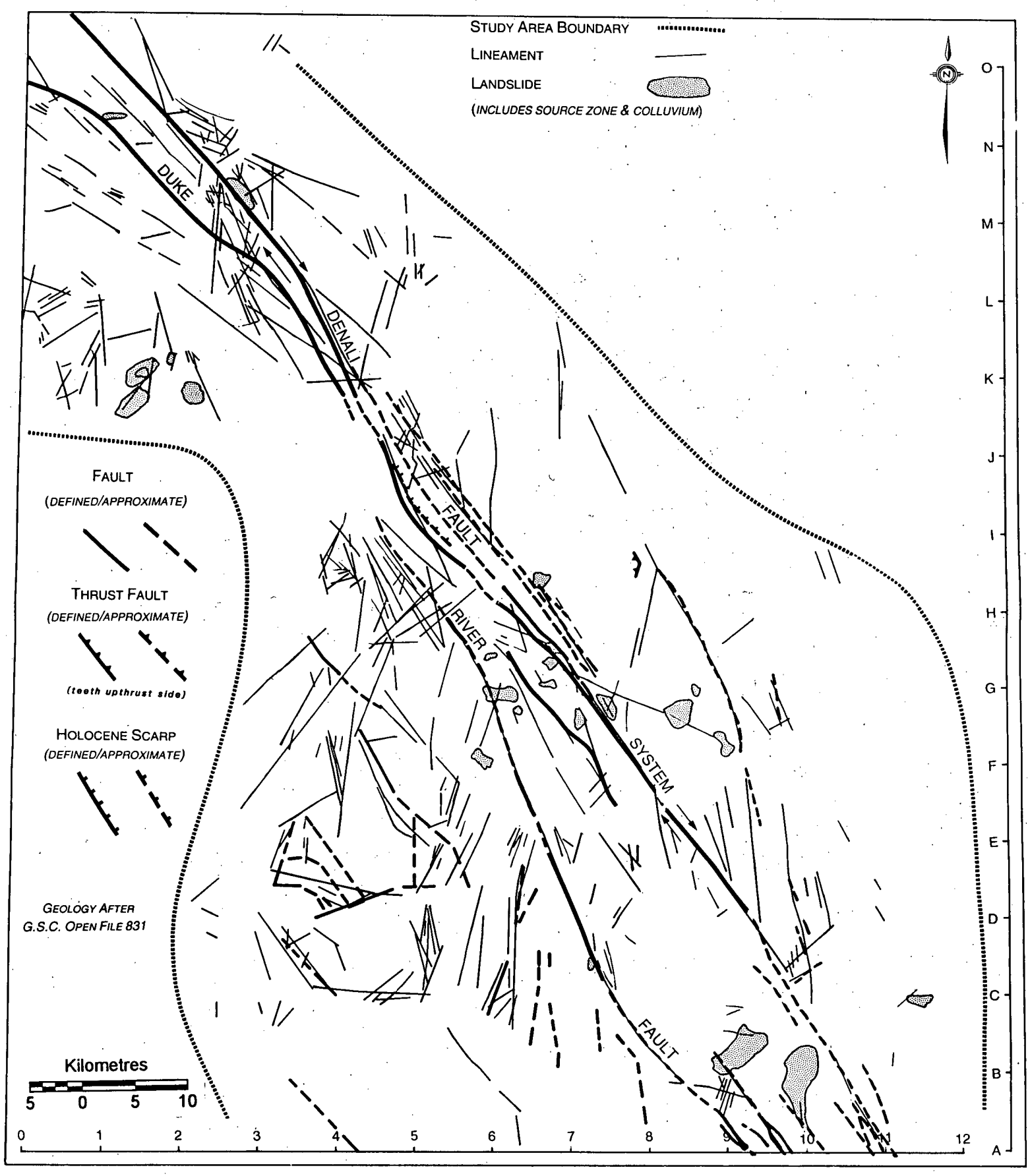

Figure 3.11. *Landslides, lineaments, and regional faults of the Mt. St. Elias and Dezadeash map areas. The alpha-numeric grid on the border corresponds to locations and data in Appendix 1.*

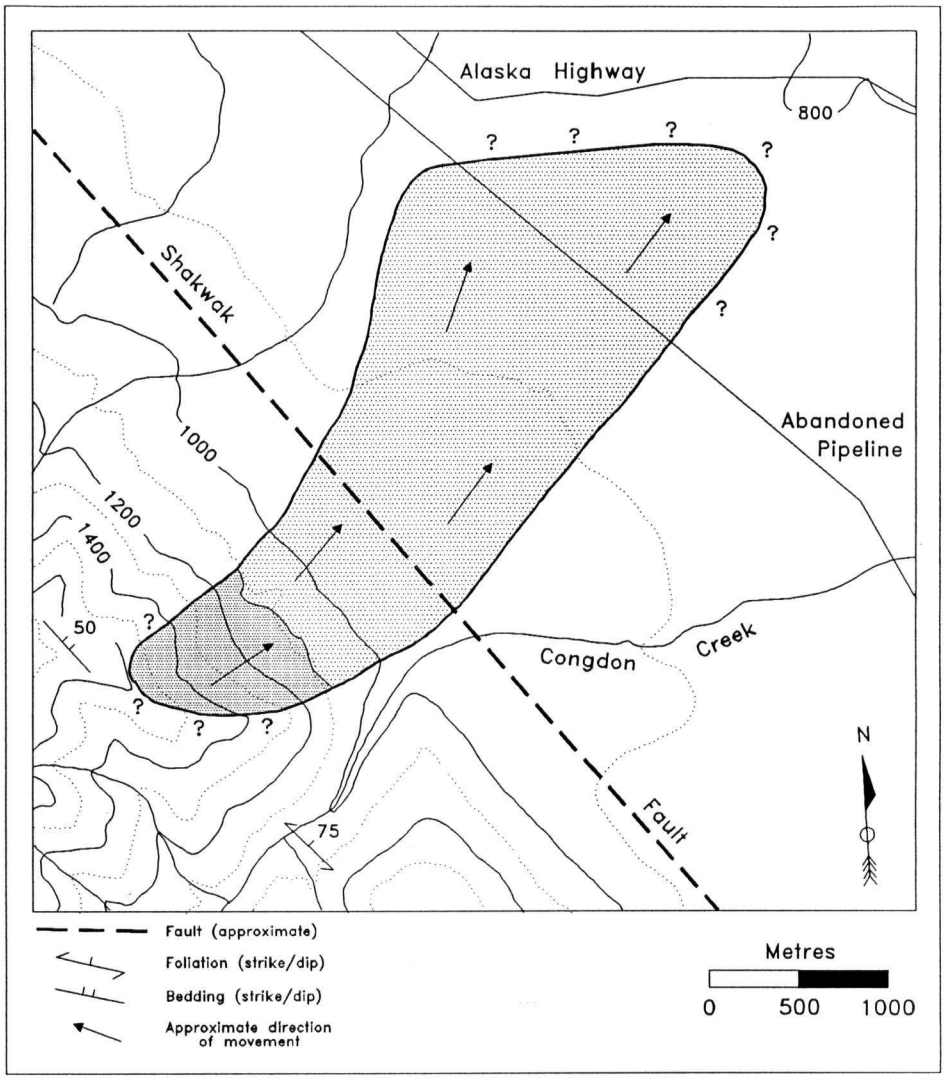

Figure 3.12. *Congdon Creek Rock Avalanche. The slide area is lightly shaded; darker shading corresponds to the interpreted source zone. Contour interval is 100 m.*

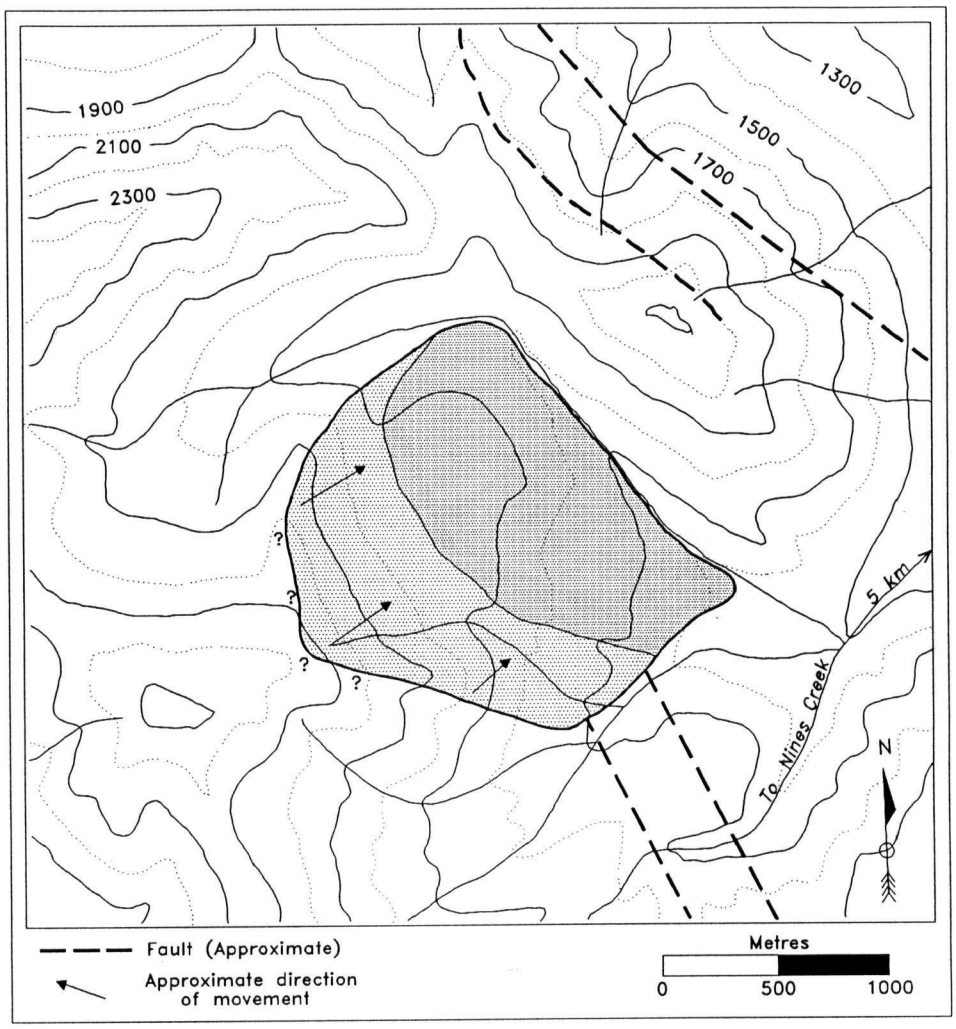

Figure 3.13. *Nines Creek Rock-Block Slide. The slide area is lightly shaded; darker shading corresponds approximately to the slide block. Contour interval is 100 m.*

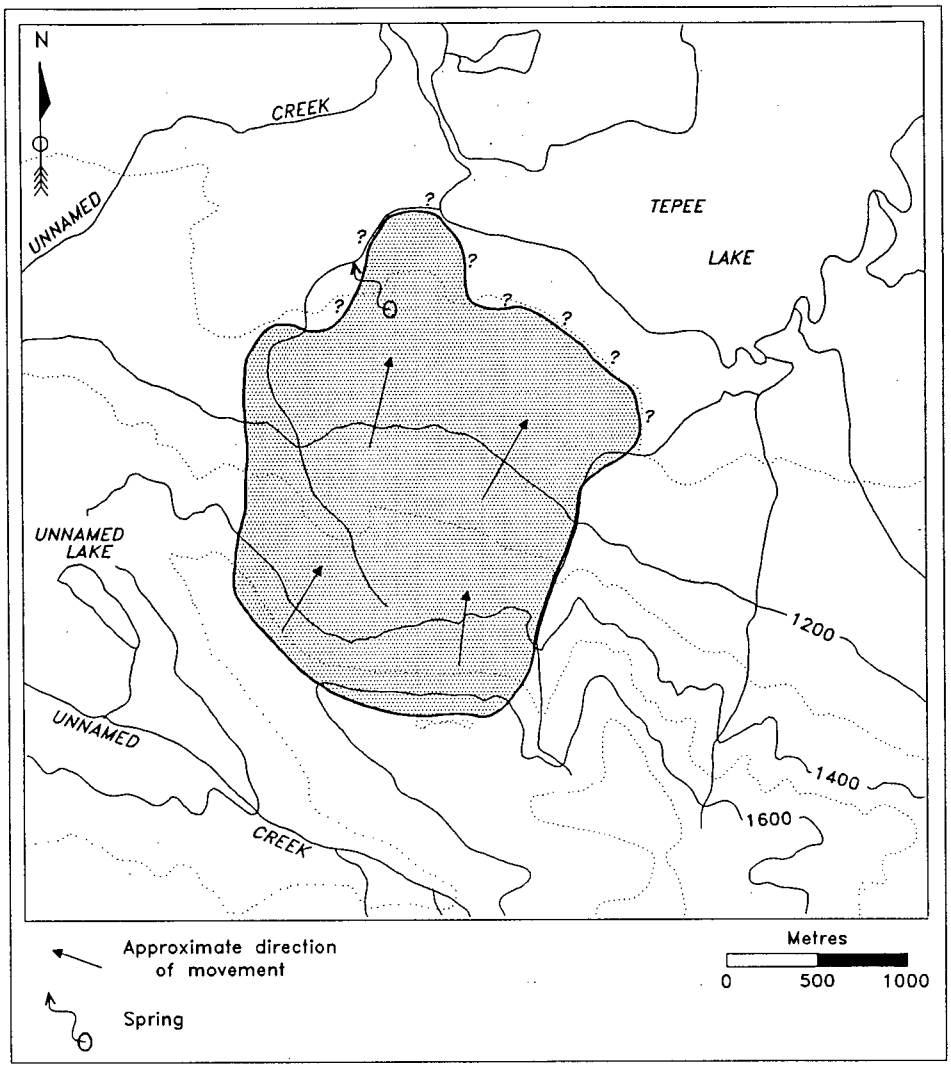

Figure 3.14. *Tepee Lake Rock Slide. The slide area is shown shaded. Contour interval is 100 m.*

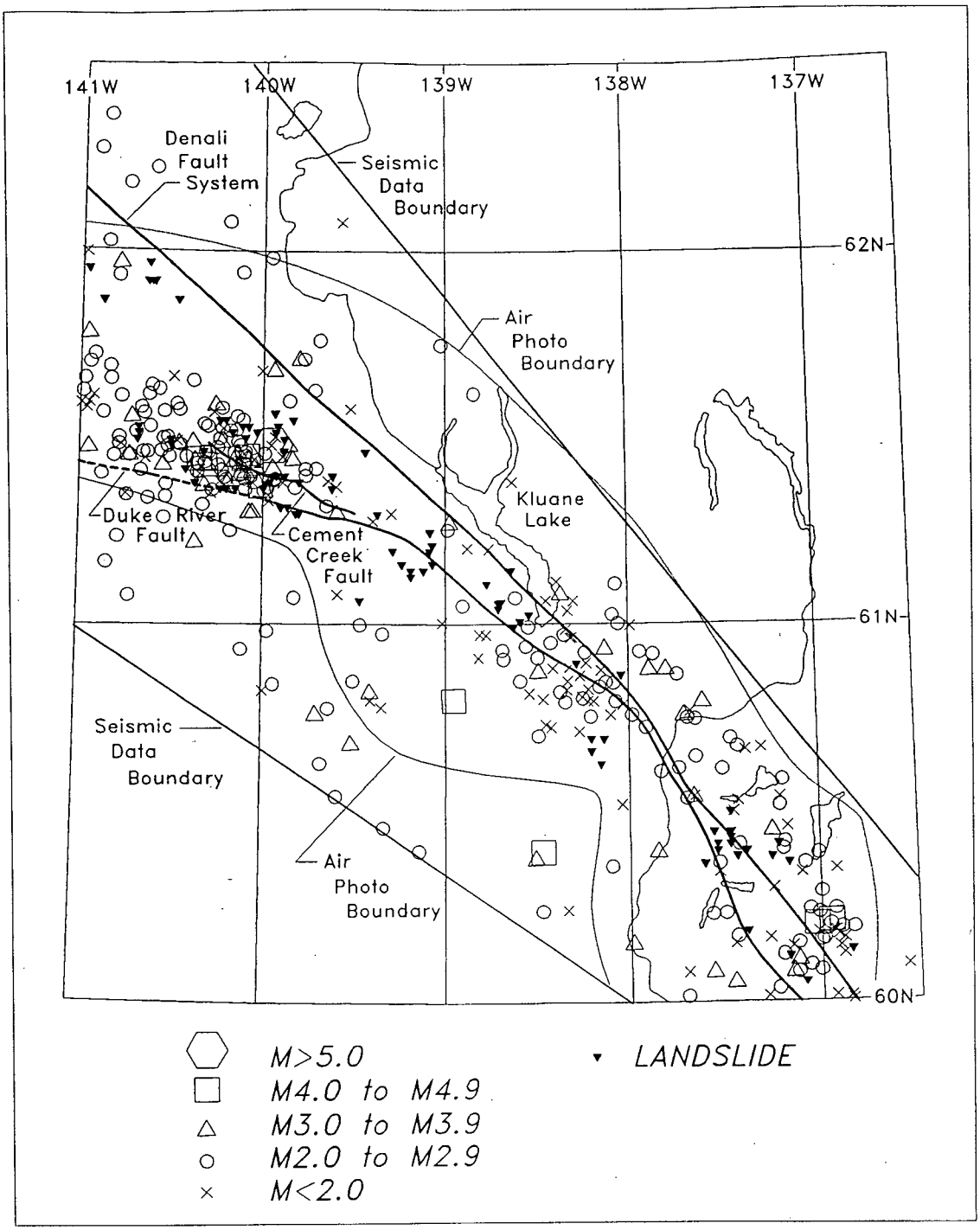

Figure 3.15. *Earthquake epicentre locations in Shakwak-Denali Zone (southwest Yukon) for the period September, 1978 to August, 1990. Epicentres are centred in each corresponding geometric symbol; location uncertainty is less than 10-15 km. Landslide locations are shown as solid inverted triangles. Major faults appear as heavy lines.*

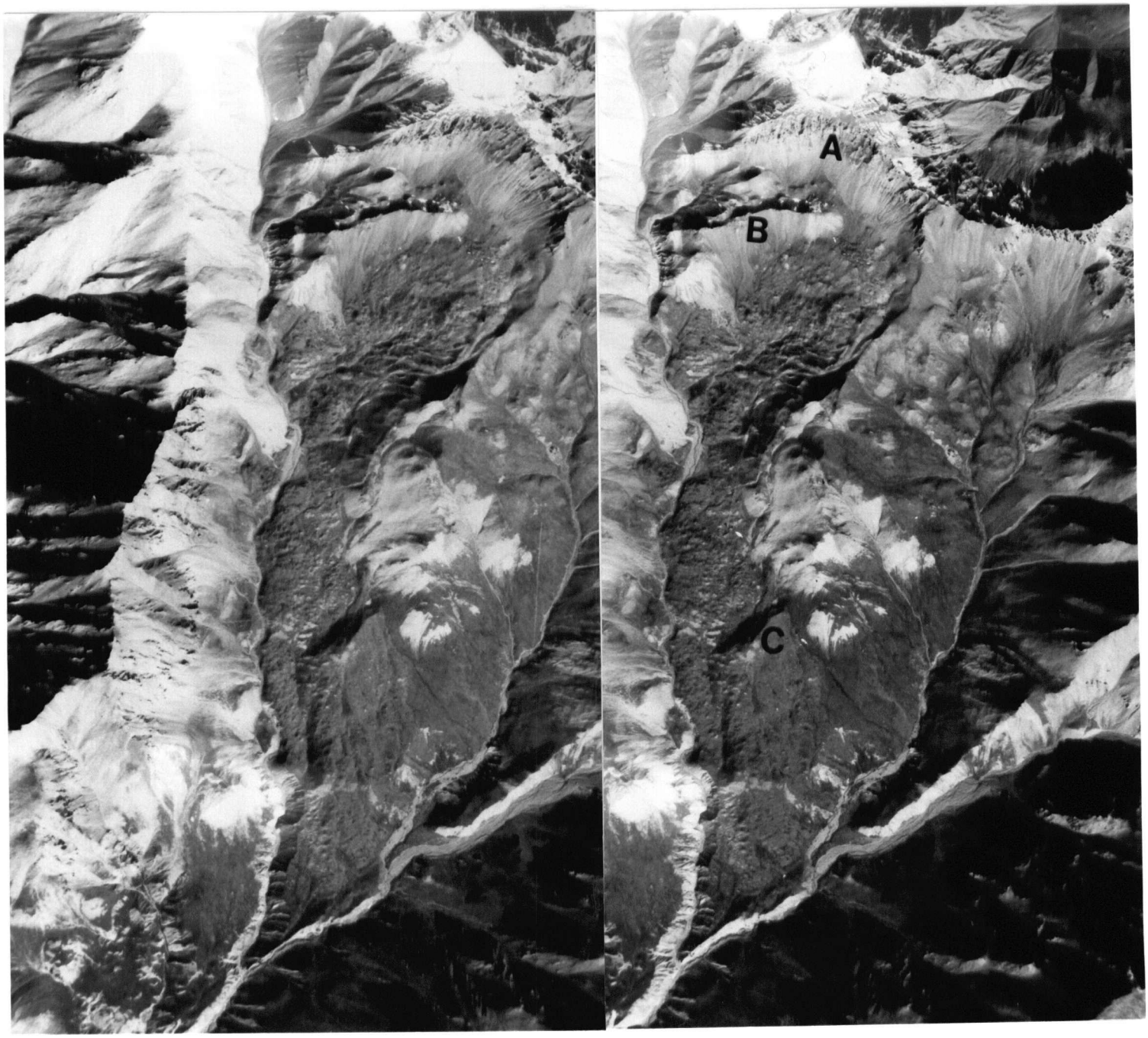

Plate 3.1. *Bighorn Creek Rock Avalanche. The debris train is clearly seen descending the narrow valley from the headscarp area (A). A large rock block has come to rest beneath the headscarp. Longitudinal debris ridges may be seen on the down slope side of the bedrock ridge at (C).*

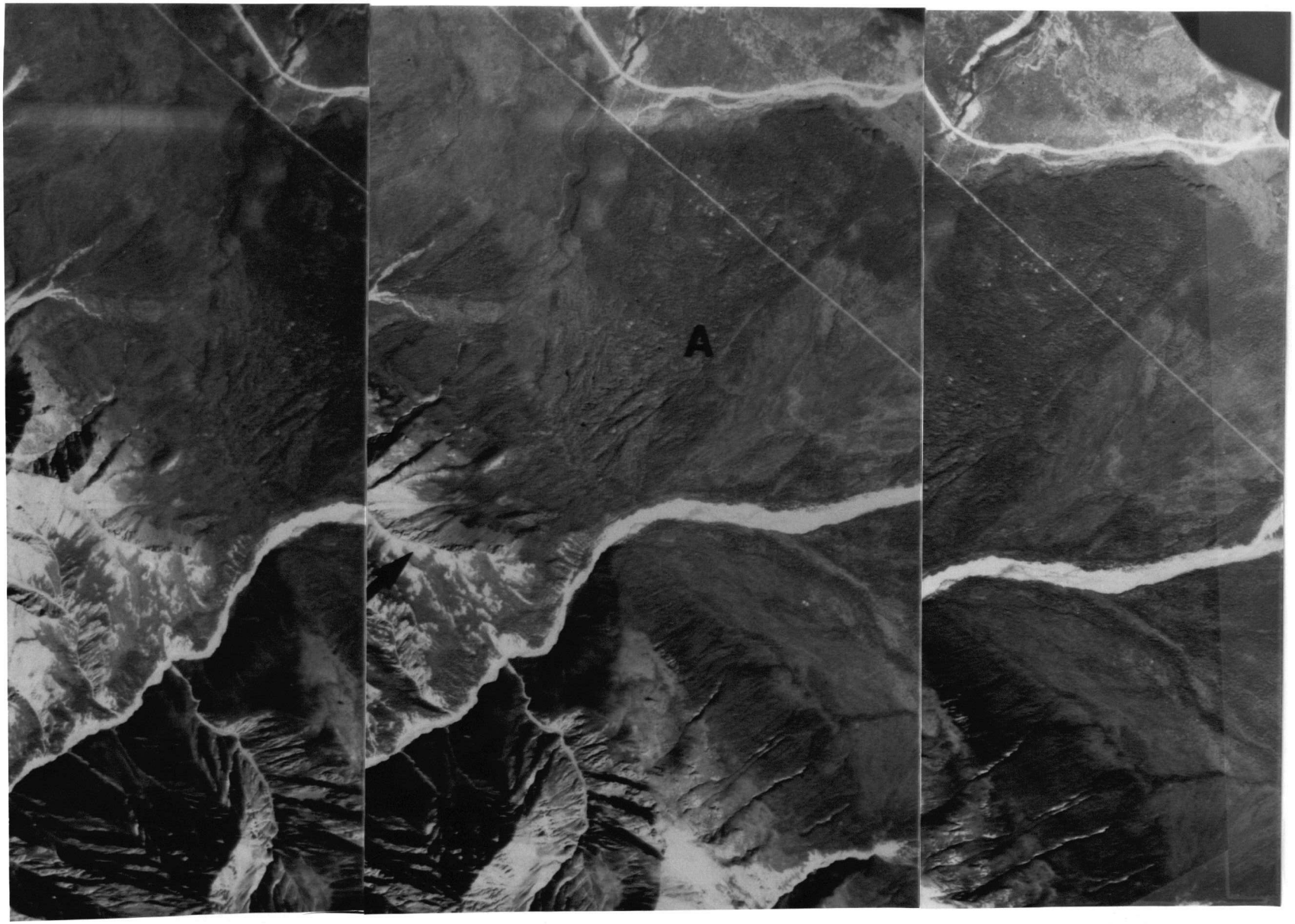

Plate 3.2. *Congdon Creek Rock Avalanche. Hummocky debris (A) is conspicuous on the surface of Congdon Creek alluvial fan; note the contorted ridges at the base of the slope. The suspected source area is indicated by the arrow.*

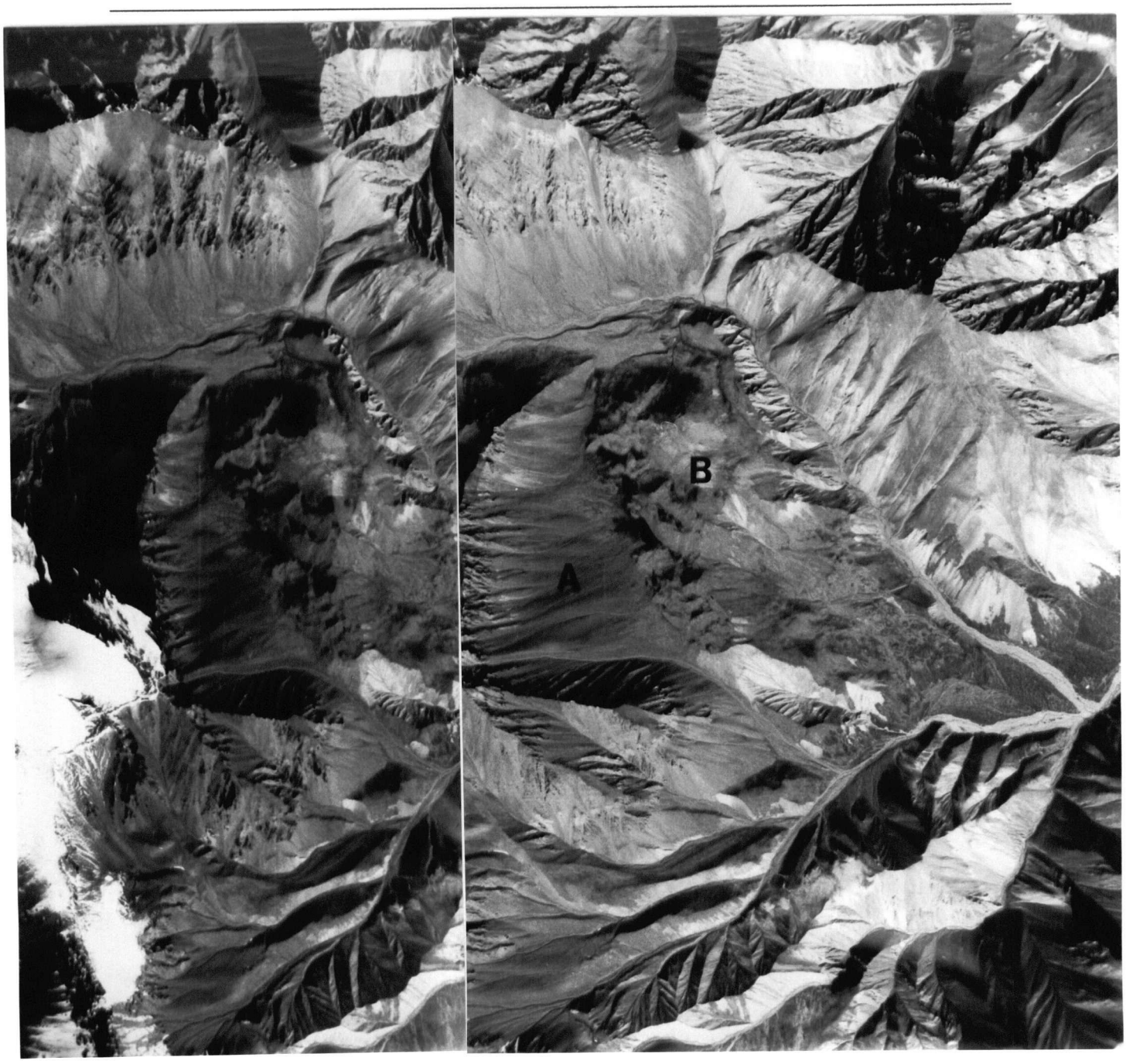

Plate 3.3. *Nines Creek Rock-Block Slide. The slide block (B) has translated as a coherent wedge. Debris avalanches off the flank of the block post-dating the original movement are seen below (B) and to the right. The rupture surface (A) is a remarkably planar feature.*

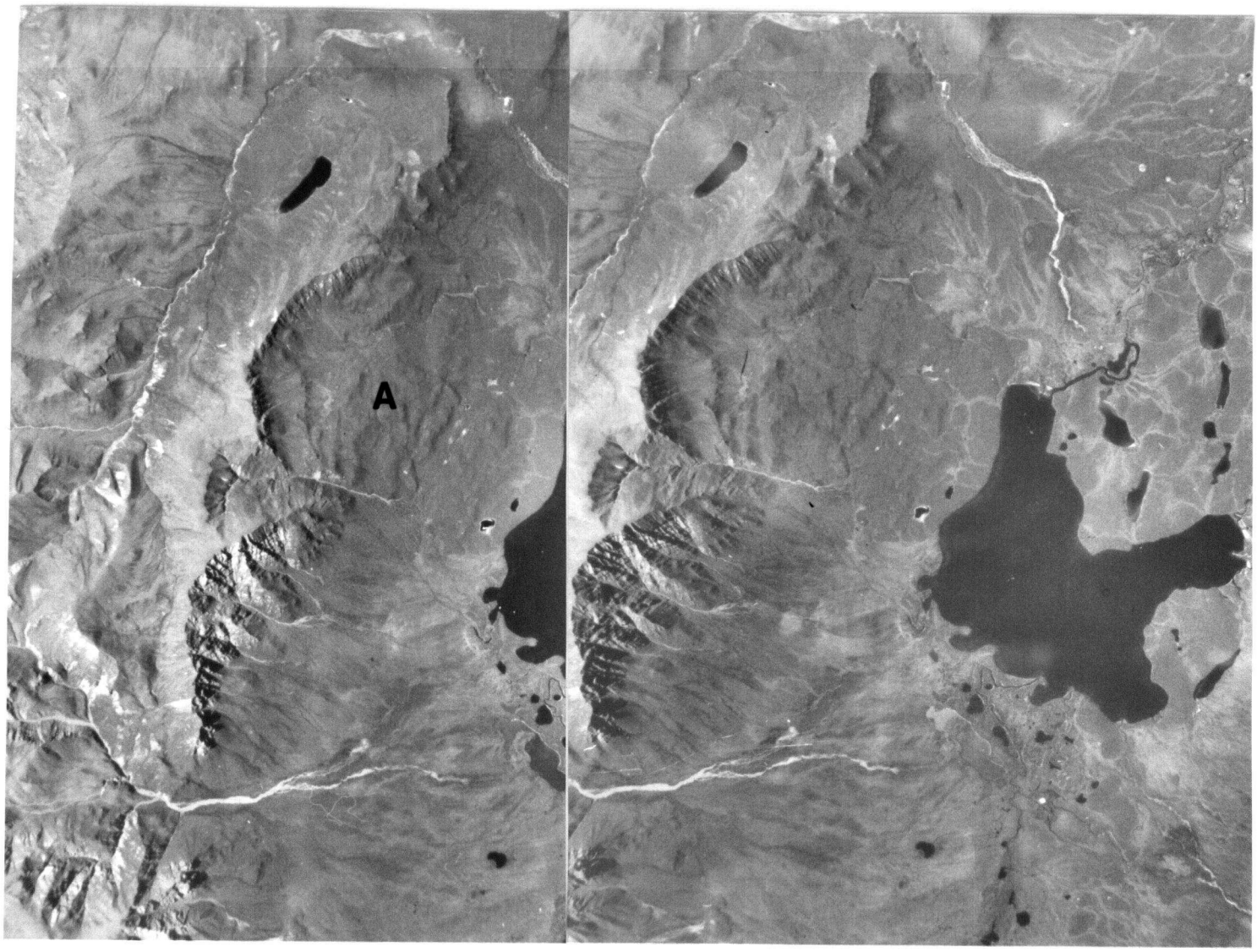

Plate 3.4. *Tepee Lake Rock Slide. This movement is characteristic of the several large, ancient landslides that occur along the rim of Wolverine Plateau. Hummocky, extensively modified colluvium is indicated (A). The position of the distal edge of the debris train is unknown.*

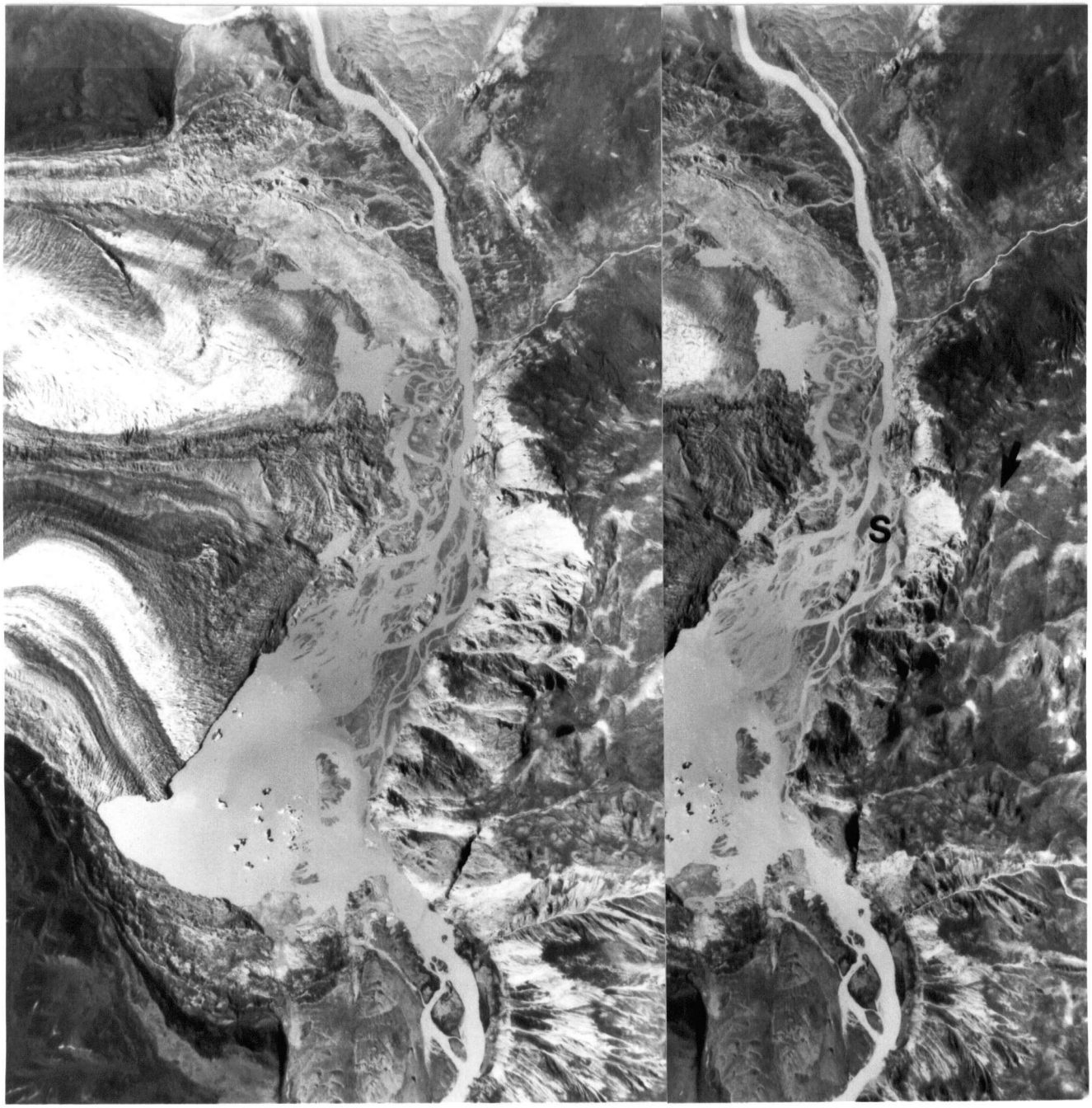

Plate 3.5. *Active slumping at the terminus of Lowell Glacier. Instability in the slope opposite the snout of the glacier (S) is probably exacerbated by repeated loading and unloading of the slope during glacial surges and recessions. Structures related to the fault (indicated by the arrow) are believed to significantly contribute to the relative stability of the slope.*

CHAPTER 4

Landsliding at Cement Creek

4.1 Introduction

The extent of penetrative discontinuity control in the landslide population, the spatial correlation between landslides and clusters of epicentres, and the anomalous departure of landslides in the epicentral cluster areas from the temporal exhaustion model discussed in the last chapter are cited as regional evidence of neotectonic effects. The Cement Creek area was studied in greater detail to confirm these effects and develop a framework for numerical simulations.

Field investigations undertaken in 1991 involved reconnaissance of the accessible landslides and local geology on the north slope of Cement Creek valley with the intent of determining the processes contributing to these movements.

4.2 Location

Cement Creek is located approximately 50 kilometres west of Kluane Lake in the eastern St. Elias Mountains. The location is in the Kluane Wildlife Sanctuary, just outside of Kluane National Park (Fig. 4.1). There is currently no human habitation or development in the region; roads constructed for mineral exploration extend into Burwash Uplands, 25 kilometres to the east.

4.3 Bedrock Geology of the Cement Creek Area

The bedrock geology of the Cement Creek study area is illustrated on Figure 4.2. Basement assemblages consisting of Pennsylvanian to Permian volcanics and volcanically derived sediments of Station Creek Formation (Skolai Group) are exposed north of Cement Creek Fault (Dodds, 1982a). Oligocene to Miocene continental clastic sediments of Amphitheatre Formation (Muller, 1967) are exposed locally in fault bounded panels and unconformably overlay Skolai Group rocks. Exposures near Cement Creek consist of well indurated, grey polymictic conglomerates, grey and buff sandstones, subordinate mudstones, and occasional interbedded coal seams. Local sectional thicknesses are on the order of 200 to 300 metres (Eisbacher *et al.*, 1977). Miocene or younger rhyolitic to dacitic sub-volcanic intrusions outcropping north of Cement Creek Fault may be associated with porphyritic felsic dykes intruding lower Wrangell Lava (Muller, 1967).

Stratigraphically uppermost and predominant in this area is Wrangell Lava (St. Clare Province; Muller, 1967; Souther *et al.*, 1975), a succession of Miocene to Pliocene andesitic and basaltic flows with minor interbedded sediment, tuff, and volcanic ash. Wrangell Lava overlies Amphitheatre Formation near Cement Creek but is locally absent north of Cement Creek Fault. Sections of the Wrangell pile locally exceed 700 metres in thickness (Skulski *et al.*, 1986), and are as thick as 1200 metres immediately south of the area on Figure 4.2 (Souther, 1974). The informal upper, middle, and lower lithostratigraphic divisions defined by Souther *et al.* (1975) are retained here. Lower and Middle Wrangell Lava near Cement Creek comprise rusty weathering, blocky flows up to ten metres in thickness. The flows are commonly separated by comparatively thin (typically less than 0.2 metres), densely compacted, ochre to mauve weathering, typically altered horizons comprised of angular intra-Wrangell and Wrangell derived clasts up to 20 cm in diameter, in a clay matrix. Wrangell Lava is dissected by several intersecting sets of joints in most exposures. Conspicuous sub-vertical joints are apparent

wherever there has been recent ground movement along Cement Creek. These joints are attributed to valley stress relief during deglaciation or stream incision.

Cement Creek Fault appears to be a westward extension of the Wade Mountain Fault Zone (Read *et al.*, 1975). Where exposed near Cement Creek, it is a sub-vertical zone of sheared and bleached rock approximately 20 metres wide (Power, 1988). An unnamed fault extends from Cement Creek Fault southeast toward Duke River Fault (Dodds, 1982a). Both faults dislocate Lower and Middle Wrangell Lava, but overlying surficial deposits are undisturbed. Minor sub-vertical faults cutting Lower Wrangell Lava have sub-horizontal slickensides and are believed to be splays from Cement Creek Fault. These observations imply that transcurrent movement on these faults persisted until at least Miocene or Pliocene time. However, Quaternary sediments near the extrapolated northwestern trace of Cement Creek Fault are tilted (Souther *et al.*, 1975), suggesting later displacement has occurred.

Tertiary rocks are folded about west-northwest trending axes, with the intensity of deformation greatest near Cement Creek Fault and to the west where folds become overturned (Dodds, 1982a).

4.4 Geomorphology of the Cement Creek Area

Terrain development in Cement Creek valley reflects intense Late Cenozoic regional deformation, and the effect of Quaternary glacial advances. Relief in this area is moderately high, the result of rapid regional uplift (Horner, 1988) and intense Holocene erosion.

Topographic expression is characterized by angular, glaciated mountain peaks exceeding 2500 metres with steep, glacially scoured bedrock slopes, and by steep sided, deeply incised stream valleys. Cement Creek valley has a broad, roughly v-shaped, but asymmetric profile, varying from less than one to several kilometres in width. Valley slope angles typically vary between 20 and 40 degrees, and on the north side of the valley, possess some degree of conformity with underlying bedding. In aerial photographs the upper elevation limit of

Pleistocene glacial scour in Cement Creek Valley appears to be approximately 1700 metres. Alpine glaciers locally persist to elevations as low as 2200 metres.

Glacially derived surficial deposits blanket bedrock on the lower valley slopes. A 1.25 m section exposed on the northern lip of Cement Creek canyon comprises, from top to bottom: (a) a thin organic mat (< 0.25 m, variable); (b) a uniform clean sand (≈ 0.4 m), and; (c) a gritty, predominantly silt layer with sub-angular volcanic clasts to 10 cm in diameter (≈ 0.6 m). The lower horizon may be a partially reworked ice contact deposit. The surficial deposits do not appear to be draped over the lip of the canyon currently occupied by Cement Creek, suggesting that it has incised on the order of 100 m since deglaciation.

Coarse diamicton from debris torrent deposits are not uncommon in many of the tributary streams to Cement Creek. Active slope processes include deep-seated bedrock movement, comparatively small scale slumping of unconsolidated surficial deposits where there is active stream erosion, and solifluction in some of the Quaternary deposits mantling upper valley slopes.

4.5 Landslide Distribution at Cement Creek

Landslides in Cement Creek valley predominate on the northern valley wall above Cement Creek (Plate 4.1; Fig. 4.3). Field work undertaken in 1991 involved reconnaissance of sites one through four; sites five and six were not visited. Landslides are numbered as they appear in Appendix 1.

No datable materials were recovered in the field. However, based upon the degree of physical surficial modification their ages range from recent (site 1) to ancient (site 3).

All of the landslides are seated in Lower and Middle Wrangell Lava (Fig. 4.2). For landslides on the northern wall of Cement Creek valley, slip is facilitated where generally south-dipping, fold tilted beds are exposed. An investigation of the landslide at site one by Power (1988) concluded that rupture had mainly occurred along discrete, comparatively low-strength horizons that separate the volcanic flows (Section 4.3). This landslide is described in Section

4.6. This is the general mode of failure at site four (described below), and probably at site three as well, but the advanced age of the latter prevented reliable verification.

The landslide at site four appears to have occurred in at least two temporally separate events. The temporal distinction is made on the basis of the relative degree of weathering of the rupture surface(s). The rupture surface corresponding to the presumed earlier movement is a weathered, well-exposed, slightly undulating plane in the eastern portion of the slide area. The western portion, which corresponds to the later movement, is a smooth, comparatively unweathered surface that is overlain by colluvium except near the crown of the slope (Plate 4.2). Both rupture surfaces are locally parallel to bedding orientations measured near the crown of the slide, although the more recent landslide appears to have failed on a deeper structural plane. A small downhill-facing scarp in the western portion of the crown area orthogonally truncates bedding and trends approximately parallel to the bedding strike. The origin of this scarp is unclear, but it is believed related to shear displacement along ubiquitous sub-vertical joints observed in the volcanic rocks, and may be related to coseismic or gravitational deformation.

Slope movement(s) at site two are seated in a zone of extremely sheared and altered rock coinciding with the position of the unnamed fault (Fig. 4.2). Moderately northeast dipping beds exposed in the headscarp are crosscut by smooth, somewhat weathered, high-angle planes parallel to the fault. Retrogressive slope movements post-dating the initial failure appear to be seated on these planes.

4.6 Recent Landsliding at Cement Creek

In the spring of 1983, a local pilot reported the occurrence of a large landslide in the Cement Creek area. A detailed investigation in 1986 included geological and geophysical measurements, as well as a microgeodetic survey (Power, 1988).

The landslide is situated on the southern margin of a small plateau north of Cement Creek (Site 1, Fig. 4.3). A 90 metre deep Holocene canyon incised by Cement Creek forms the

southern edge of the plateau. It is seated in tightly folded Lower Wrangell Lava approximately 300 metres south of Cement Creek Fault (Fig. 4.2).

Ground cracks circumscribing a low hill, which now comprise the headscarp, are clearly visible in pre-1983 aerial photographs (Plates 4.3, 4.4). These are evidence of incremental slope movements prior to the 1983 landslide. The landslide has developed as a rock block slide affecting an estimated area of 0.6 km^2 and with an approximate volume at $10\text{-}12 \times 10^6$ m^3. It is encompassed by a roughly circular headscarp five to eight metres high, and, although it is dissected by several deep medial cracks, the displaced mass is largely coherent.

Groundwater discharge at the toe occurs only where surface water has infiltrated dilated sub-vertical faults and tension cracks at the toe of the slide; no seepage was observed in adjacent undisturbed bedrock. These observations do not preclude the presence of groundwater and associated pore-pressure gradients in the slope.

The landslide has undergone finite displacement estimated at 30-40 metres and currently appears to be metastable. Kinematic analysis by Power (1988) suggests the landslide's left flank has undergone oblique slip along bedding on the northern limb of an asymmetric, southeast plunging syncline intersecting its southwest corner (Fig. 4.2).

On the basis of investigations completed as part of this study, most of the rupture surface is believed to coincide with low-strength intraflow horizons (Sec. 4.3), except near the headscarp where bedding is truncated. Slip has occurred where south-dipping beds daylight in the canyon wall several tens of metres above Cement Creek. Massive lava columns up to 60 metres high have separated from the toe along sub-vertical joints. Below the toe, a thick blanket of rubbly debris extends downward into Cement Creek.

If it is assumed that this slope was at or near a state of limiting equilibrium prior to 1983, it may also be assumed that one or more temporally spaced trigger mechanisms disturbed equilibrium and initiated the 1983 movement. Surface water infiltration through pre-existing joints, which appear to go to considerable depth, is unlikely because the landslide was observed

in the late winter, long before seasonal snow melt began. Moreover the presence of continuous permafrost (Heginbottom *et al.*, 1987) all but precludes infiltration. Toe erosion is clearly not a factor because Cement Creek was already incised well below the toe elevation of the incipient failure. The most likely trigger mechanism is ground shaking attributed to strong motion during a burst of seismicity in the Cement Creek area coinciding with the time of the 1983 movement. Two moderate earthquakes on March 30, 1983, one a M5.4 event with the epicentre 13 km from this landslide, the other a M4.8 event with the epicentre less than 5 km away. These were followed by a series of lower magnitude after shocks during April, 1983, and generally elevated levels of low-magnitude seismicity for several months afterward (Fig. 4.4).

4.7 Summary

Landslides in the Cement Creek area are seated in the Lower and Middle stratigraphic divisions of Wrangell Lava. The predominant mode of slope failure was observed to be basal slip along tilted intraflow surfaces that are exposed in steep valley slopes. Evidence collected in the field and from aerial photographs shows that finite, incremental slope deformation may precede large magnitude movement. Landslides are observed to move as coherent, block-like bodies at less than critical displacements.

Landslide processes have been particularly active in the Cement Creek area during the Holocene. The spatial and relative temporal landslide distribution departs from the regional slope exhaustion model. Neotectonic effects, especially earthquake strong motion, are believed to be important mechanisms triggering slope movement. Numerical analysis of slope deformation induced by earthquake loading was undertaken to test this hypothesis. An overview of the most commonly used numerical dynamic analysis methods are presented in Chapter Five, as well as discussion and verification of the selected method.

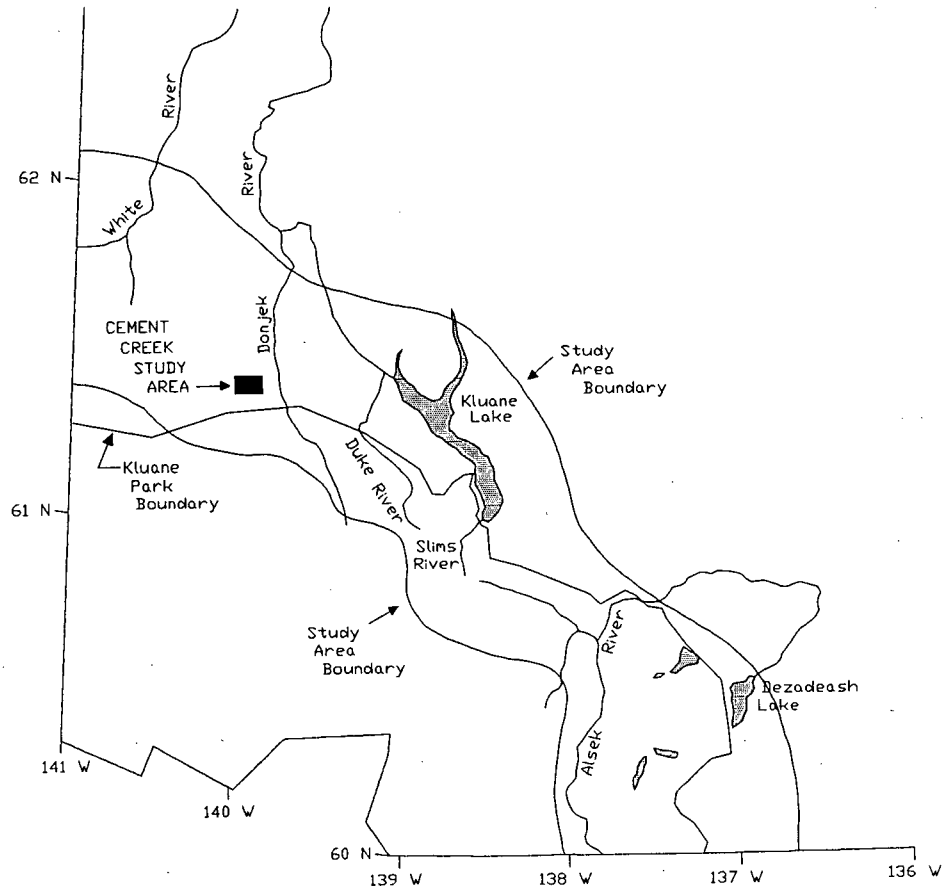

Figure 4.1. *Location of the Cement Creek study area in southwest Yukon.*

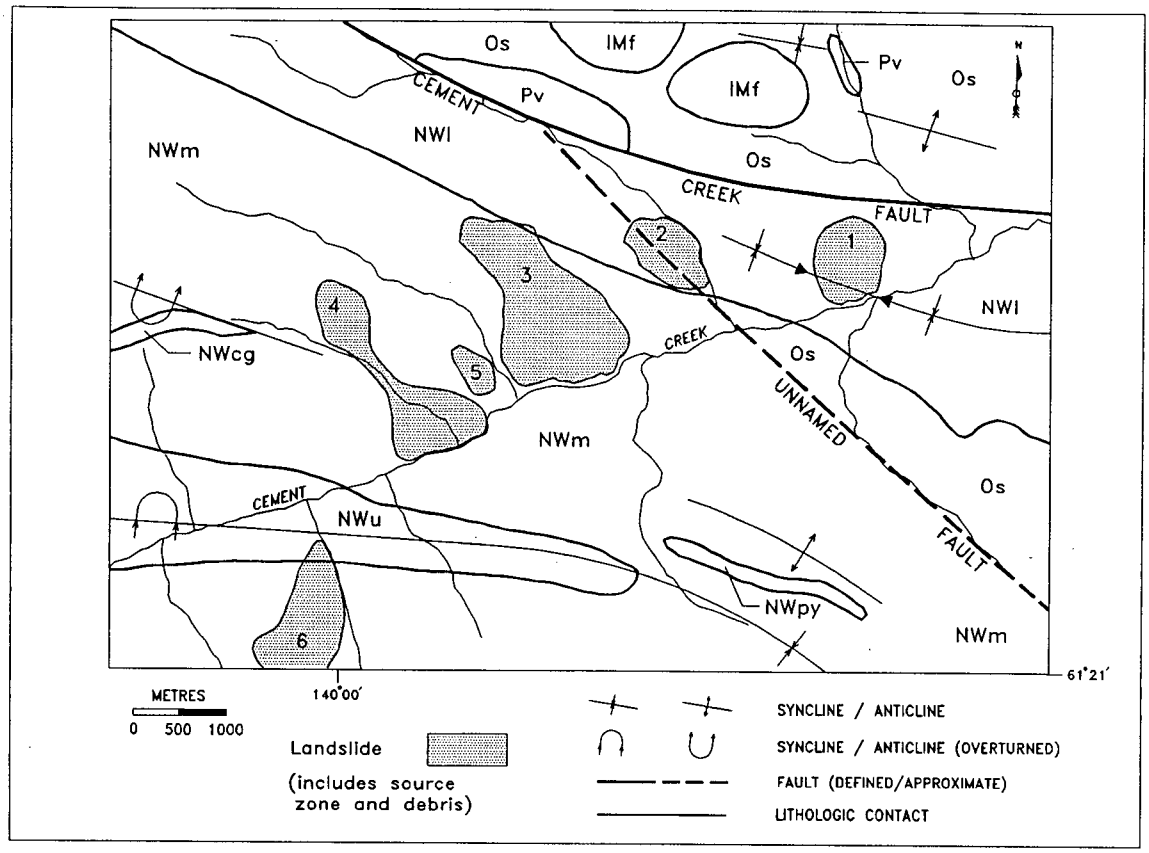

Wrangell Lava - St. Clare Province (Miocene and Pliocene)

NWu: basalt, trachybasalt, andesite flows and pyroclastic rocks; minor volcanic conglomerate.

NWm: porphyritic and non-porphyritic basaltic andesite flows, interbedded with felsic ash flows, tuff, and volcanically derived sediments.

NWl: thick, blocky, mainly non-porphyritic basaltic andesite flows with locally interbedded siltstone; overlain by thin closely stacked basaltic flows.

NWcg: intra-Wrangell volcanic conglomerate; clasts all Wrangell derived.

NWpy: intra-Wrangell acid tuff or ash flows.

Wrangell Intrusions (Miocene)

IMf: subvolcanic intrusive bodies of latite, trachyte, or rhyo-dacite; in part or all intra-Wrangell.

Amphitheatre Formation (Paleogene)

Os: well indurated grey polymictic conglomerates, grey and buff sandstones, subordinate mudstone and shale, and occasional interbedded coal seams.

Station Creek Formation (Skolai Group) (Pennsylvanian and Lower Permian)

Pv: predominantly pyroclastic rocks; including volcanic breccia and agglomerate, grading up into tuff; rare argillite and basic flows.

Figure 4.2. *Bedrock geology of the Cement Creek area showing folds and major faults (after Dodds, 1982a). Lithological descriptions are after Dodds (1982a). Landslide locations are shown shaded.*

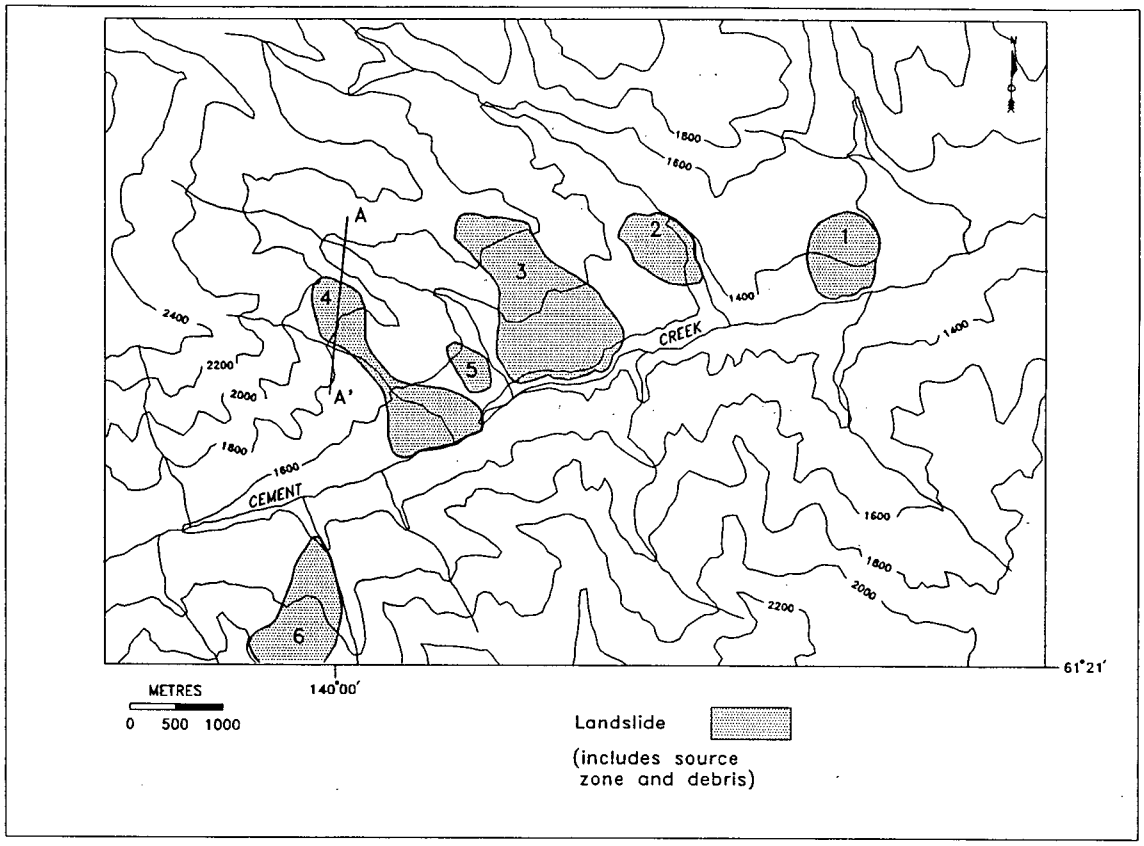

Figure 4.3. *Topography of the Cement Creek area (200 m contour interval). Landslides locations are shown shaded. Cross section A-A' corresponds to the profile on Figure 6.1.*

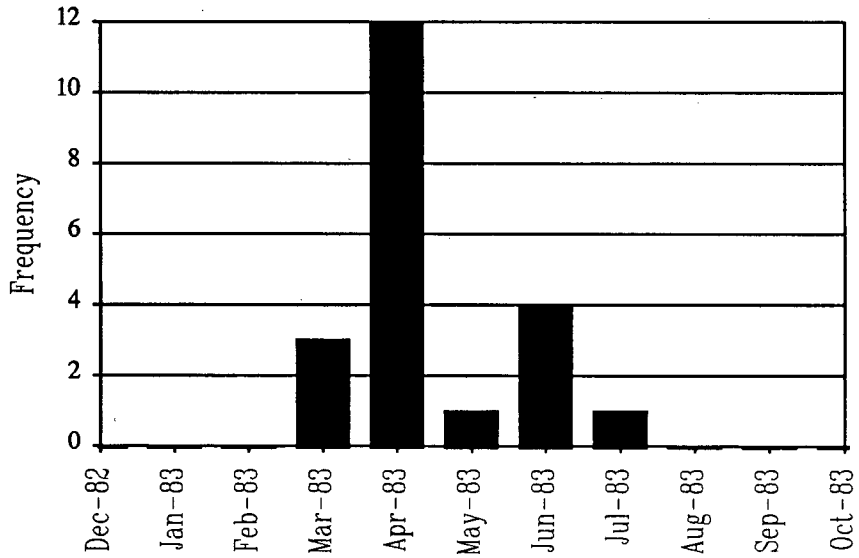

Figure 4.4. *Frequency (number) of earthquakes occurring in a 15 km radius of Cement Creek between December, 1982, and October, 1983. Data courtesy of D.H. Weichert, Pacific Geoscience Centre.*

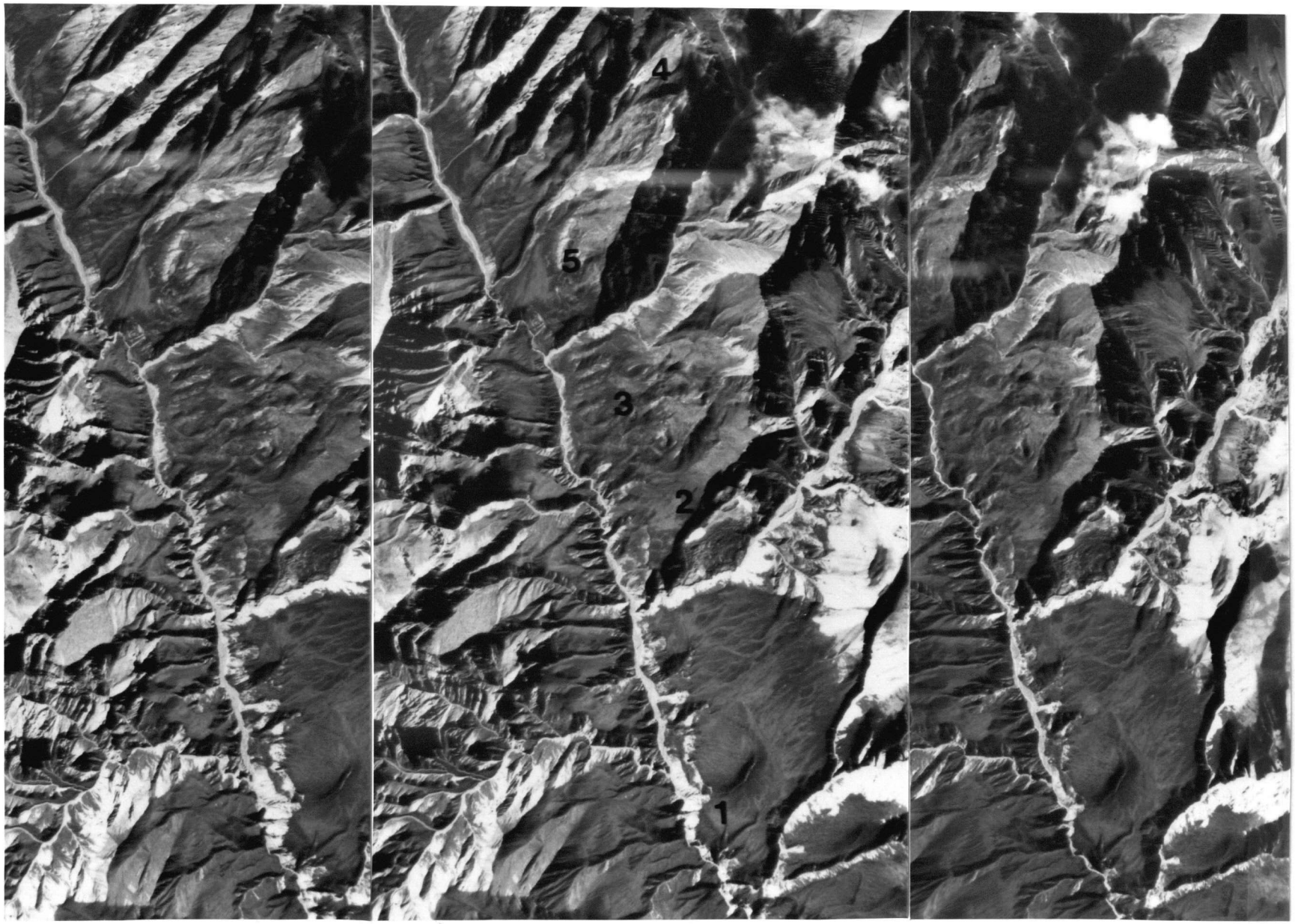

Plate 4.1. *Large landslides on the north wall of Cement Creek Valley. The landslides are numbered as they appear on Figures 4.2 and 4.3, and also as they appear in Appendix 1.*

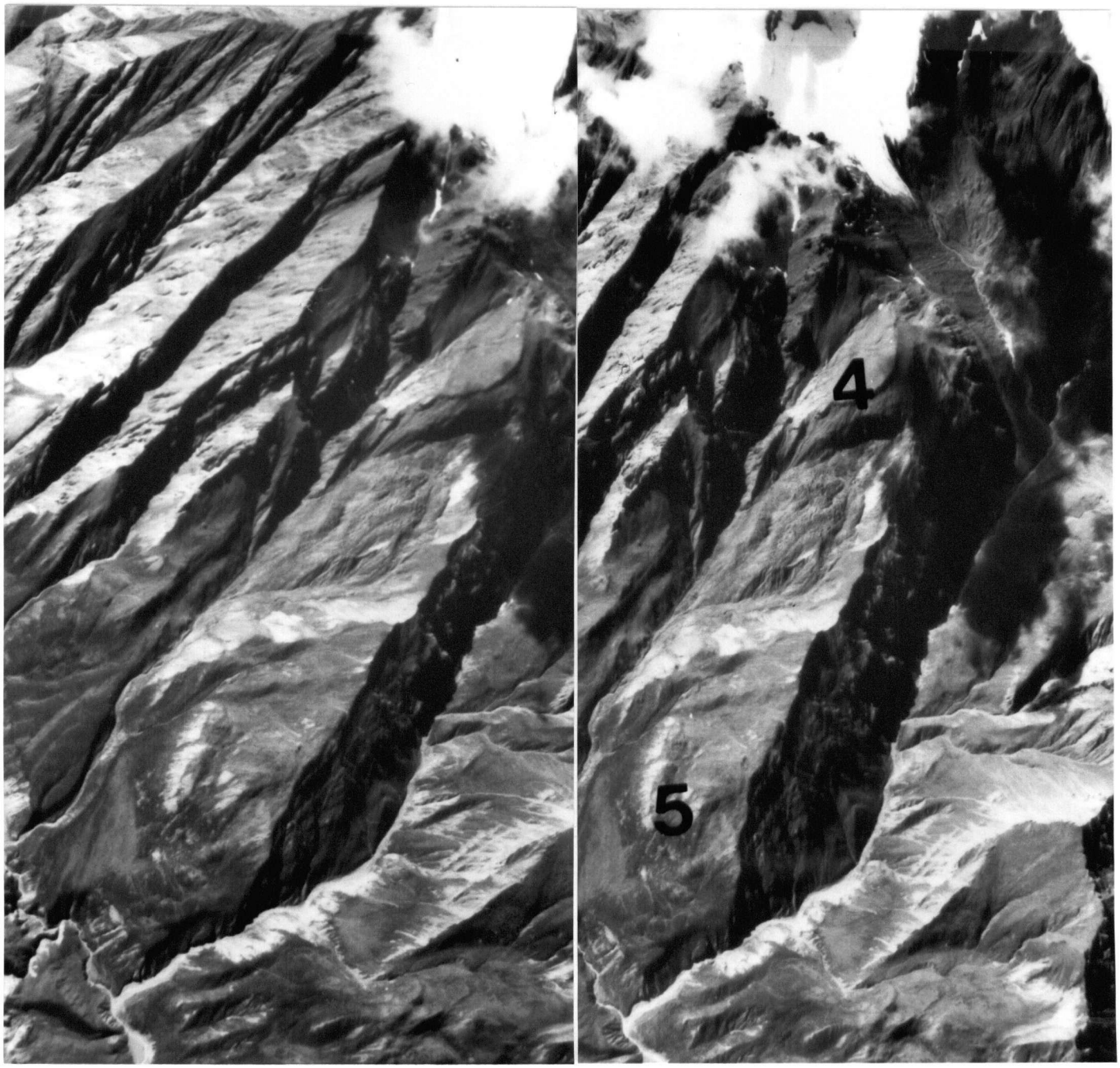

Plate 4.2. *Cement Creek #4 Rock Slide. The landslide area is contained in the slope indentation below numeral (4). The photographs are oriented with west toward the top of the frames.*

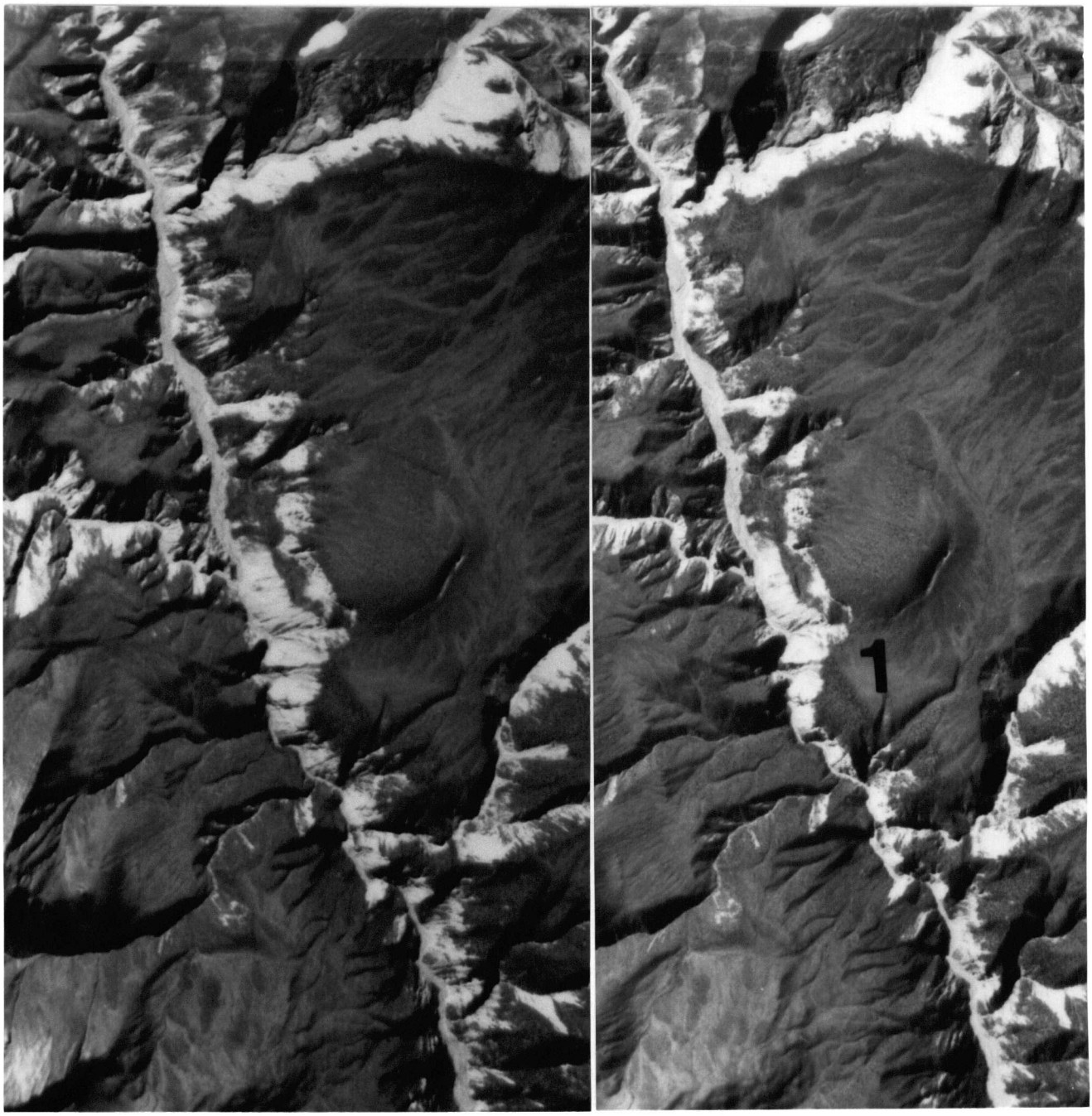

Plate 4.3. *Cement Creek #1 Rock Slide. The landslide is roughly centred on the domal hill in the middle of this pre-1983 photograph. The photographs are oriented with west toward the top of the frames. Ground cracks circumscribing the hill are clearly seen on its northern perimeter. A bench on the wall of Cement Creek Canyon at the toe of the slide is believed to be locally co-planar with the rupture surface.*

Plate 4.4. *Post failure oblique view of Cement Creek #1 Rock Slide. The photograph was taken looking east down Cement Creek Valley. Incremental displacement along the pre-1983 circumferential ground cracks is clear. A debris stream originating from the western portion of the toe overlies the canyon slope.*

CHAPTER 5

Overview of Dynamic Analysis Methods and Verification of UDEC

5.1 Introduction

This chapter focuses on two distinct but related topics. The first is a broad overview of the numerical methods available for seismic response analysis of rock slopes. The second is an introduction to the distinct element method (program UDEC), the method selected for the analyses in Chapter 6. Limited verification of shear wave-propagation and elasto-plastic shear displacement modelled by UDEC are compared with closed-form solutions.

5.2 Methods of Dynamic Numerical Analysis

Among the numerical methods available for the dynamic response analysis of slopes are limit-equilibrium, continuum and discontinuum formulations. Each of these methods is discussed as a class of analytical technique, including the addition of Newmark analysis (Sec. 5.2.2) which is considered a corollary of limit-equilibrium analysis. This overview is not intended to be rigorous, and may not necessarily include state-of-the-art developments in all aspects of this field, but rather is included to familiarize the reader with the most widely known numerical methods, as well as their comparative strengths and weaknesses.

5.2.1 Limit-Equilibrium Methods

Limit-equilibrium (pseudo-dynamic) analytical methods are well established in both soil and rock mechanics. In principle, these methods consider the force equilibrium of a rigid-elastic

body sliding on a defined rupture surface, and typically utilize a factor of safety criterion to evaluate the stability of the system. The factor of safety is defined as the sum of the forces resisting movement divided by the sum of the driving forces. Dynamic loading is accounted for by including an inertial body force in the static stability calculation [5-1a], that corresponds to an arbitrarily oriented ground acceleration. Slope failure is assumed to occur if the dynamic factor of safety (F_{dy}) becomes less than unity along the potential rupture plane. An expression for F_{dy} of the simple block system on Figure 5.1 is given below [5-1b] (adapted, after Crawford *et al.*, 1982):

$$F_{dy} = \frac{\sum(\text{static resisting forces})}{\sum(\text{static driving forces})} + \sum(\text{dynamic forces}) \qquad [5\text{-}1a]$$

$$= \frac{\left[{}^{cl}/_{W}\right] + \left[\cos\beta - K\sin\left(\beta - \theta\right)\right]\tan\phi}{\left[\sin\beta + K\cos\left(\beta - \theta\right)\right]} \qquad [5\text{-}1b]$$

where c denotes cohesion and W is the weight of the block. Similar expressions can be derived to accommodate different geometries (Naumann, 1990), and more complex failure criteria (Sarma, 1975).

The limit-equilibrium method is attractive because of its simplicity, but is limited by several assumptions implicit in its formulation: 1) sliding occurs on a continuous surface with known orientation, and with uniform strength properties that obey a perfectly plastic Mohr-Coulomb criterion; 2) the sliding body is rigid, and the body forces acting upon it are resolved through its centre of mass; 3) the ground accelerations are considered continuous, and therefore; 4) any induced displacement along the slip surface results in total slope failure. Assumptions (1) and (2) generally preclude adequate representation of most rock slopes, which are comprised of jointed, discontinuous rock with non-linear elasto-plastic deformation behaviour. Assumption (3) is unrealistic because ground accelerations during earthquake loading are transient.

5.2.2 Newmark Analysis

Newmark (1965) recognized that for a given slope or structure, the critical accelerations during a seismic event are transient. Under such loading, the factor of safety may be less than unity for discrete intervals, and hence a slope may undergo permanent, finite displacement without complete failure. The formulations presented by Newmark (1965) incorporate the preceding ideas into a limit-equilibrium type of analysis, and embody a number of different failure geometries. Slopes are represented as rigid, elastic bodies sliding on continuous surfaces of known orientation. A variety of force-displacement relationships may be assigned to the slip plane. The basic methodology of Newmark has been extended and modified a number of times since its introduction (*i.e.* Sarma, 1975; Crawford *et al.*, 1982; Ghosh *et al.*, 1989).

Consider the example of a block sliding on a cohesionless horizontal plane (Fig. 5.2a) (Newmark, 1965). The base has time varying motion, $y(t)$, and the sliding block has motion $x=y+u$, where x is the net motion and u is its motion relative to the base. The resistance to sliding, Ng, where N is a coefficient and g is the acceleration due to gravity (assumed constant), is equal in magnitude and oppositely directed to the minimum acceleration required to just set the block in motion. In this case the value of N is equal to $\tan(\phi)$, where ϕ is the intrinsic (Coulomb) friction angle of the plane.

For simplicity, the acceleration of the base is given as a rectangular pulse (Fig. 5.2b) of magnitude Ag and duration t_0; the resistance Ng is shown as a dashed line. In Figure 5.2c the velocities of the base and the sliding block are shown. The base has velocity V at time t_0 which remains constant. At time t_m the sliding block also attains velocity V, and relative motion between the base and the block ceases because their velocities are equal. The shaded area on Figure 5.2c represents the relative displacement, u_m, between the sliding body and the base for a single acceleration pulse, and may be calculated from the expression:

$$u_m = \frac{V^2}{2gN}\left(1 - \frac{N}{A}\right) \qquad [5\text{-}2]$$

Equation [5-2] (Newmark, 1965) assumes equal resistance to motion for accelerations of both positive and negative magnitude. For the case of an unsymmetrical sliding resistance, such as a block sliding on an inclined plane, [5-2] does not account for greater sliding resistance in the "uphill" direction, nor does it account for cumulative displacement in the direction of the lowest sliding resistance that would occur after multiple acceleration pulses. Such cases are routinely handled using available computer algorithms, or by using empirical displacement relationships such as those derived by Newmark (1965).

5.2.3 Continuum Methods

The finite element method is by far the most extensively used continuum formulation for the evaluation of the seismic response of slopes and structures in soil and rock (Clough *et al.*, 1966; Dezfulian *et al.*, 1970; Valliappan *et al.*, 1985; Alheid *et al.*, 1988). Other continuum formulations such as FLAC (Cundall *et al.*, 1988) offer an alternative, but have not enjoyed the popularity of the finite element method.

Continuum methods represent the model domain as a continuous medium. The domain is normally discretized into a number of deformable elements that may be virtually any size or shape. The individual elements are connected at their boundaries by a finite number of nodal points. Approximate solutions for the system are obtained at the nodes. Finite element formulations readily incorporate pore pressures, non-homogeneous and transient stress regimes, as well as the anisotropy, heterogeneity, and nonlinear behaviour that is associated with geological materials (*i.e.* Goodman *et al.*, 1968; Idriss *et al.*, 1974; Finn *et al.*, 1988). These features allow more realistic behaviour in geomechanical models and offer the user far greater flexibility with problem geometry than the methods described in Sections 5.2.1 and 5.2.2.

The evaluation of earthquake response with the finite element method requires solution of the following system of differential equations:

$$[M](\ddot{u}) + [C](\dot{u}) + [K](u) = \{R(t)\} \qquad [5\text{-}3]$$

where $[M]$, $[C]$, and $[K]$ respectively are matrices of terms for the mass, damping, and stiffness of the assembled elements; (u) are nodal displacement vectors, with single and double dots denoting the first and second derivatives with respect to time; and $\{R(t)\}$ is the earthquake load vector. Equation [5-3] may be solved by a number of methods, including mode superposition (Clough *et al.*, 1966) and step-by-step integration (Wilson *et al.*, 1962). A more comprehensive description of the theory and applications of dynamic analysis with the finite element method is provided by Desai *et al.* (1972).

The continuum approach to the dynamic analysis of geological media has several limitations. Representation of the inherent heterogeneity and discontinuity in most rock masses often requires the formation and solution of large matrices [5-3]. In practical terms these may be unsolvable in a medium possessing either complex heterogeneity or a high density of discontinuities. In practice these problems may be somewhat alleviated by assuming some degree of homogeneity, by employing an equivalent continuum model (Goodman *et al.*, 1968), or by assuming that displacements will occur along a few "key" discontinuities in the problem domain. However, these assumptions may fail to adequately characterize the behaviour of a heterogeneous, discontinuous medium, and can artificially constrain the number of degrees of freedom of the system. Further, in general terms, the elements normally used to model discontinuities do not readily accommodate large displacements (Wang *et al.*, 1993), and stiffness matrices must be reformed whenever there are significant displacements between nodes. For these reasons, problems involving large displacements, such as those that may occur in a slope undergoing critical earthquake loading, may be time-consuming and potentially difficult to solve.

5.2.4 Discontinuum Methods

Discontinuum techniques are formulated specifically to analyze the behaviour of particulate or discontinuous systems. The majority fall within a general class of methods known as discrete element methods. Itasca (1992) reviews the four sub-classes of discrete element analyses. They are the: 1) distinct element method; 2) modal methods; 3) discontinuous deformation analysis, and; 4) momentum-exchange methods. A hybrid rigid-block model is proposed by Wang *et al.* (1993). Of these four methods, only the distinct element and modal methods have been developed to the point where they may be used for dynamic analysis of general systems. The focus of the following discussions will be oriented toward the distinct element method. Applications of the distinct element method to dynamic analysis of surface structures have been demonstrated (Bardet *et al.*, 1985; Brady *et al.*, 1988; Lorig *et al.*, 1991).

In discrete element methods, the model domain is divided into an assemblage of elements or blocks that are separated by discontinuities (joints). The blocks may be rigid or deformable, depending upon the formulation that is used. Block to block interactions occur along the joints, which have prescribed constitutive laws that define the behaviour of the interactions. The distinct element method retains all the flexibility of the finite element method with regard to input (*i.e.* heterogeneity, non-linear behaviour) and problem geometry. The solution procedures used in discrete element methods vary somewhat, particularly in the case of deformable blocks. The procedure specific to the distinct element method is discussed in Section 5.3.

In general terms, rock masses may be characterized as blocky, discontinuous systems. This is particularly true of near-surface rock where confining stresses are usually small when compared with intact rock strength, and the predominant mode of deformation is by slippage or separation along discontinuity planes. This type of deformation is accentuated by dynamic loading. The distinct element method is well suited for the analysis of such systems. An important feature of the distinct element formulation is that the block elements may undergo

finite displacement and rotation (including complete detachment), and can form new contacts that result from relative motions of the blocks (Itasca, 1992). Contact and motion logic for the elements are not affected by large displacements.

A disadvantage of the distinct element method is that the critical time step used in the calculation cycle must sometimes be made very small to ensure numerical stability. The time step is related to material stiffness and element or zone size. Because of this, some simulations can take considerable time.

5.3 Description and Formulation of UDEC

Since it was first introduced in 1971 (Cundall, 1971), the distinct element method has undergone nearly continuous development that is reviewed by Pritchard (1989). The generalized two-dimensional formulation of the distinct element method is a computer program marketed by Itasca Consulting Group known as UDEC (Universal Distinct Element Code) (Itasca, 1992). The following discussions deal specifically with UDEC Version 1.83.

5.3.1 General Formulation

UDEC utilizes a time domain algorithm that solves the equations of motion for a block system with an explicit finite difference method. The solution procedure is known as dynamic relaxation (Otter *et al.*, 1966), wherein the nodal points (or elements) in the system are displaced according to Newton's Second Law, a process that is justified on physical grounds (Cundall, 1987). Element displacements are adjusted so that unbalanced forces within the system are minimized, and the equilibrium or steady-state solution is approached incrementally. The physical principles and solution procedure are discussed by Cundall (1980) and Lemos *et al.*, (1985). A brief description of the basic principles and the calculation cycle implemented in UDEC follow, including adaptations of the code that are specific to dynamic analysis.

5.3.2 Element Representation

UDEC allows the use of either fully-deformable or rigid elements. Fully deformable elements are normally used in wave propagation problems such as earthquake response analysis, or when a high degree of accuracy is desired in the solution of quasi-static problems. The use of rigid elements is permissible if less accuracy is desired, or when element deformation is not considered important to the solution of the problem. The majority of analyses performed in this study use fully-deformable elements, and they will form the basis of the following discussion.

There are seven different constitutive relationships available for fully-deformable elements in UDEC. A homogeneous, isotropic, elastic constitutive relationship with a linear stress-strain law is normally used for dynamic analysis of discontinuous rock under low confining stress, where strain is anticipated to occur predominantly along discontinuities. Although high transient stresses may occur in a rock mass during dynamic loading, the load interval usually lasts only a few tens of seconds or less. Because of this, plastic deformation of the model elements may be ignored without significant error.

5.3.3 Interface Constitutive Relationships

Force and displacement behaviour at the element interfaces (contacts) may be assigned bi-linear or non-linear elasto-plastic constitutive relationships. In the bi-linear model, the response to normal and shear loading at edge-to-edge interfaces (joints) between elements are governed by incremental linear stress-displacement relations:

$$\begin{aligned} \Delta\sigma_n &= k_n \Delta u_n \\ \Delta\sigma_s &= k_s \Delta u_s \end{aligned} \qquad [5\text{-}4]$$

where k_n and k_s are the joint normal and shear stiffnesses, and Δu_n and Δu_s are the incremental normal and shear displacements. Corner-to-edge and corner-to-corner contacts utilize a force-displacement law formulated identically to [5-4], except that the shear and normal stiffness are in units of force/length rather than stress/length. The maximum shear stress (or force) is limited according to the Mohr-Coulomb friction criterion:

$$|\sigma_s| \leq c + \sigma_n \tan\phi = \sigma_{s(\max)} \qquad [5\text{-}5]$$

where c denotes cohesion, and ϕ is the basic joint friction angle. Tensile strength can also be included in the calculation.

The non-linear, or Continuously-Yielding (C-Y) joint model is intended to simulate post-peak strain softening that occurs in rock joints due to cumulative shearing damage on the joint surface. The implementation utilizes a bounding surface concept (Dafalias *et al.*, 1982, *in* Itasca, 1992) and is described in detail by Cundall *et al.* (1988) and Itasca (1992). The stress responses to normal and shear loading are expressed incrementally as:

$$\begin{aligned} \Delta\sigma_n &= k_n \Delta u_n \\ \Delta\sigma_s &= F k_s \Delta u_s \end{aligned} \qquad [5\text{-}6]$$

and the joint normal and shear stiffnesses k_n and k_s are given by:

$$\begin{aligned} k_n &= a_n \sigma_n^{e_n} \\ k_s &= a_s \sigma_n^{e_s} \end{aligned} \qquad [5\text{-}7]$$

where a_n, e_n, a_s, e_s are model parameters The exponential form of [5-7] simulates the increases in shear and normal stiffness observed in rock joints[1] with increasing normal stress (Bandis *et al.*, 1983). A generalized shear stress-displacement curve for monotonic loading under constant normal stress is shown on Figure 5.3. The factor F in [5-6] is an internal factor governing the instantaneous shear modulus, and is formulated:

$$F = \frac{(1-\sigma_s / \tau_m)}{1-r} \qquad [5\text{-}8]$$

where τ_m is the bounding strength, and r is an internal factor for restoring elastic stiffness immediately after load reversal. It is seen in [5-8] that the value of F depends upon the ratio between the actual and the bounding stress. The value of the bounding strength curve is calculated from the expression (Itasca, 1992):

$$\tau_m = \sigma_n \tan \phi_m \mathrm{sgn}(\Delta u_s) \qquad [5\text{-}9]$$

where ϕ_m can be considered the friction angle that would apply to the joint if it was to dilate to its maximum dilation angle, and is continually reduced by a semi-empirical method as joint damage accumulates.

A potential error[2] was found in the algorithm for the C-Y joint model. During simulations of monotonic shear tests, the shear stress-displacement curves were found to be insensitive to joint cohesion. The reasons for this behaviour may be related to the lack of a cohesion term in [5-9], or an algebraic flaw in the algorithm.

---

1 The normal stiffness in filled discontinuities, depending upon the filling thickness, may be considered normal stress independent, or nearly so (Barton *et al.* 1987, pp. 88-89).

2 Currently being discussed with the manufacturer.

5.3.4 Gridpoint Calculation Cycle

A deformable element representation is obtained by internally discretizing each block with a triangular finite difference mesh. Each triangle is assumed to obey a constant strain law. Gridpoints are assigned at the triangle vertices, and a lumped mass based upon the average shared mass of the adjacent triangular zones is assigned to the central gridpoints.

The gridpoint calculation cycle begins with summation of the forces, F_i, acting upon a given gridpoint i:

$$F_i = F_i^x + F_i^c + F_i^l \qquad [5\text{-}10]$$

where the superscripts x, c, and l denote force contributions from external, contact, and internal sources respectively. Contact forces apply only to those gridpoints laying on the boundary of the element. The equation of motion for the gridpoint is based upon Newton's Second Law (Brady *et al.*, 1988):

$$\frac{\partial \dot{u}_i}{\partial t} + \alpha \dot{u}_i = \frac{F_i}{m} + g_i \qquad [5\text{-}11]$$

where u_i is a vector of the gridpoint displacement components with the single dot denoting the first derivative with respect to time, α is the viscous damping term, m is the gridpoint lumped mass, F_i is the sum of the forces from [5-8], and g_i is the component of gravitational acceleration. Integration of [5-11} using a central finite difference approximation yields the expression:

$$\dot{u}_i^{(t+\Delta t/2)} = \left[\frac{\dot{u}_i^{(t-\Delta t/2)} \left(1 - \alpha\Delta t/2\right) + \left(\left(F_i^{(t)}/m\right) + g_i\right)\Delta t}{1 + \alpha\Delta t/2} \right] \qquad [5\text{-}12]$$

where the superscripts in parentheses denote the time that the corresponding term is evaluated. Inspection of [5-12] (Lorig *et al.*, 1991) reveals that if velocity $\dot{u}_i^{(t-\Delta t/2)}$ is known, then the velocity $\dot{u}_i^{(t+\Delta t/2)}$ may be calculated directly from the force components acting at the gridpoint.

The dynamic algorithm used in UDEC is limited by the assumption that velocities and accelerations remain constant during the calculation time step, Δt. The method relies on the physical concept that a finite time interval is required for a disturbance to pass through a block system. If the time step size is chosen so that a displacement cannot propagate from one element to the next in one time step, the equations of motion for all the elements become uncoupled and the numerical procedure is stable (Pritchard, 1989). With deformable elements, the size of the time step must obey constraints related the size of the triangular finite difference zones and the stiffness of the system (Itasca, 1992).

The increment of gridpoint displacement may be calculated from the new velocity:

$$\Delta u_i = \dot{u}_i \Delta t \qquad [5\text{-}13]$$

With the displacement of each gridpoint known, the position of the element boundary may be updated and new contact stresses and displacements for the next time step may be calculated from the interface constitutive relations. Incremental strains, ε, and rotations, θ, in each zone are evaluated at each time step, and are related to gridpoint node displacements according to the definitions of two-dimensional strain:

$$\begin{aligned} \dot{\varepsilon}_{ij} &= \frac{1}{2}\left(\dot{u}_{i,j} + \dot{u}_{j,i}\right) \\ \dot{\theta}_{ij} &= \frac{1}{2}\left(\dot{u}_{i,j} + \dot{u}_{j,i}\right) \end{aligned} \qquad [5\text{-}14]$$

where the single dot denotes the first derivative with respect to time; the subscripts i and j on the left hand side of [5-14] are directional indices; and the subscripts i, j on the right hand side of

[5-14] denote partial derivatives with respect to the i and j directions. New stresses in each zone are calculated from the expression:

$$\Delta\sigma_{ij} = \lambda\Delta\varepsilon_v\delta_{ij} + 2\mu\Delta\varepsilon_{ij} \qquad [5\text{-}15]$$

where λ and μ are the Lamé constants; $\Delta\sigma_{ij}$ are the elastic increments of the stress tensor; $\Delta\varepsilon_{ij}$ are the incremental strains; $\Delta\varepsilon_v$ is the increment of volumetric strain, and; δ_{ij} is the Kronecker delta function (Itasca, 1992). The explicit incremental calculation approach is a valuable feature because it is comparatively easy to incorporate non-linear or post-peak constitutive behaviour into the algorithm.

The calculation cycle described in Equations [5-10] to [5-15] provides new gridpoint velocities and displacements, contact forces, and zone stresses that are applied as initial conditions for calculations in the next time step.

5.3.5 Damping

In most numerical analyses, some form of damping must usually be applied to account for energy losses that occur in physical systems. In soil and rock these losses are frequency independent and predominantly hysteretic. They can be attributed to internal deformation of intact geological materials, displacement along planes of discontinuity, frictional heating, or the movement of fluids within the system.

Both mass- and stiffness-proportional damping are available in UDEC. They may be used individually, or both types may be applied in combination in what is termed Rayleigh damping. Rayleigh damping is defined in the following manner. For any mode i of a multiple degree of freedom system, the fraction of critical damping, λ_i, with corresponding frequency, ω_i, may in principle be determined from:

$$\lambda_i = \frac{1}{2}\left(\frac{\alpha}{\omega_i} + \beta\omega_i\right) \qquad [5\text{-}16]$$

where α is the mass-proportional constant, and β is the stiffness-proportional constant (Idriss *et al.*, 1974). From inspection of [5-16] it is seen that Rayleigh damping is clearly not frequency independent. The mass-proportional component is dominant at lower frequencies, while the stiffness-proportional component is dominant at higher frequencies. However, for most systems, there exists a band of frequencies wherein Rayleigh damping remains roughly constant, and frequency independent damping may be simulated (Itasca, 1992). These frequencies are related to the natural modes of the system and to the input excitation signal.

The damping forces in UDEC are applied at the gridpoints of the system. With mass-proportional damping the forces are proportional to the absolute velocity and mass of the node, but are applied in a direction opposite to the velocity (Itasca, 1992). For stiffness-proportional damping, either contact forces or zone stresses are applied that are proportional to stiffness and the relative velocity or strain rate (Itasca, 1992). The limitations of velocity proportional damping are summarized by Cundall (1987).

In static and quasi-static problems, either mass-proportional or an adaptive viscous damping scheme is used. The adaptive scheme adjusts the viscous damping term in [5-11] in proportion to the change in kinetic energy of the system at each time step, in a manner that simulates critical damping (Itasca, 1992). However, Pritchard (1989) notes that in quasi-static problems with certain geometries, erroneous body forces may be created.

In dynamic problems either mass- or stiffness-proportional or Rayleigh damping may be used. For problems that involve large element displacements, it is generally inappropriate to use mass-proportional damping because motion may be artificially inhibited. In such systems stiffness-proportional or a modest amount of Rayleigh damping may be the preferred choice (Itasca, 1992).

5.3.6 Adaptations to Dynamic Analysis

Geomechanical models at the scale of surface and underground engineered structures are usually best represented by an unbounded medium. Numerical representations that discretize a finite region of space in the vicinity of the structure require that the artificial numerical boundary enforce conditions analogous to an infinite space or half-space. Fixed or elastic boundaries are usually sufficient for static or quasi-static analyses. However, difficulties can arise in dynamic analyses because; 1) outward propagating waves can be reflected back into the system, and; 2) the boundaries may fail to adequately represent the motion of the half-space or infinite-space adjacent to the discretized domain. Non-reflective boundaries and a dynamic free-field have been implemented in UDEC to deal with these problems respectively.

5.3.6.1 Non-Reflective Boundaries

In principle, the problem of outward propagating waves may be remedied by extending the model boundaries a sufficient distance from the region of interest that allows material damping to dissipate the energy. In materials with a high level of natural damping this solution may be viable. However, in materials such as rock that have a small amount of natural damping this can be impractical, in terms of both computer storage requirements and run time. An alternative method proposed by Kuhlmeyer *et al.* (1969) is to incorporate energy absorptive boundaries. Such a scheme was adopted in UDEC. Non-reflecting boundaries providing viscous normal and shear tractions are implemented as independent dashpots attached to the model boundaries (Fig. 5.4). The tractive forces are formulated as:

$$\tau_n = -\rho C_p v_n$$
$$\tau_s = -\rho C_s v_s \qquad [5\text{-}17]$$

where v_n and v_s are the components of velocity normal and parallel to the boundary, ρ is the mass density of the material at the boundary, and, C_p and C_s are the p- and s-wave velocities respectively (Kuhlmeyer *et al.*, 1969). The tractions are calculated at every time step and applied as boundary loads. Numerical instability may arise because the tractive forces are calculated with velocities lagging by half a time step (Itasca, 1992).

5.3.6.2 Dynamic Free-Field

The reasoning that necessitates non-reflective boundaries applies equally to the rationale for the implementation of the dynamic free-field. The purpose of the free-field is to simulate the motion of an infinite space or half-space that is assumed to exist at the model boundary The free-field is a one-dimensional explicit finite difference calculation performed in parallel to the model system, and is coupled to gridpoints along the lateral boundaries of the model by viscous dashpots (Fig. 5.4). The free-field consists of a column of unit width that is discretized into n elements of equal length Δy, with $n+1$ lumped mass gridpoints. The elastic properties of the free-field are representative of the model system, including contributions from discontinuities.

The free-field calculation is independent of the horizontal coordinate, x, and therefore element deformations are expressed as:

$$\varepsilon_{xx} = 0, \quad \varepsilon_{yy} = \frac{\partial u_y}{\partial y}, \quad \gamma_{xy} = \frac{\partial u_x}{\partial y} \qquad [5\text{-}18]$$

where ε_{yy} and γ_{xy} are the elastic normal and shear deformations in the y direction, and; u_x and u_y are relative displacements of the free-field (Itasca, 1992). The free-field calculation provides element stresses σ_{xx}^f and σ_{xy}^f, and gridpoint velocities v_x^f and v_y^f. The coupling of the free-field to the model elements is shown on Figure 5.5. Free-field stress contributions to the model are

provided at discrete points along the block edge at the same y-coordinates as the free-field gridpoints. At an arbitrary gridpoint *i* the applied forces are:

$$P^{i}_{x,y} = \frac{1}{2}\left[\left(\sigma^{f}_{xx,xy}\right)^{j-1} + \left(\sigma^{f}_{xx,xy}\right)^{j}\right]\Delta y \qquad [5\text{-}19]$$

where the subscripts *x* and *y* denote directions, and the subscripts *xx* and *xy* denote normal and shear stresses corresponding to the directional subscripts of the free-field elements *j* and *j-1*. The applied forces at the corner gridpoints of the model element (for example corner A, Fig. 5.5) are:

$$R_{x,y} = -\rho C_{p,s}\left(v^{A}_{x,y} - v^{fA}_{x,y}\right)l \qquad [5\text{-}20]$$

where l is one-half the block edge length. The free-field velocity at point A is obtained by linear interpolation between its adjacent gridpoints *i* and *i-1*.

5.4 Verification of UDEC

The formulation and constitutive relationships of UDEC have been validated with analytical solutions in a number of static and dynamic simulations (Cundall, 1971; Cundall *et al.*, 1988; Itasca, 1992). However, no verification data are available for: 1) the accumulation of permanent strain on discontinuities in response to dynamic loading, and; 2) the response of a geological medium to upward propagating seismic waves. These are key considerations with regard to the incremental deformation behaviour of rock slopes.

Closed-form solutions to these problems have been formulated, and are available in widely available software. Comparative analyses were performed between the encoded closed-form solutions and UDEC to verify its performance.

5.4.1 Comparison of Newmark's Method and UDEC

Newmark (1965) offers the first rigorous treatment of earthquake induced ground displacement. It is in essence a closed-form solution for the shear displacement of a geometrically and mechanically simple slope system. The methodology described in Section 5.2.2 is readily adaptable to digital analysis of arbitrary ground accelerations. The program selected for Newmark analysis is TNMN (Taga Inc., 1989).

Comparative analyses between TNMN and UDEC were performed using a single rigid block sliding on an inclined plane, similar to the system depicted on Figure 5.1. The input acceleration signal is assumed oriented parallel to the slip plane. To attain this condition in UDEC the block system is rotated until the slip plane is horizontal, and the input signal is applied to the bottom boundary of the model. The resolved vertical and horizontal components of gravity are applied to the system as shown in Figure 5.6. Although the appearance of the UDEC model is different, the physical system represented in each of the models is identical. Material properties used in each of the analyses are listed in Table 5.1 following page).

Yield accelerations in the down-slope and up-slope directions for the block system are 0.185g and 0.532g respectively. Gravity is assumed vertical and constant at -9.81 m/s^2 in all analyses. A sinusoidal acceleration signal with peak amplitude 0.200g (1.96 m/s^2), frequency 0.5 Hz, and duration 12 seconds was input to the TNMN model. The peak amplitude was selected to ensure down-slope displacement, without the possibility of up-slope displacement for oppositely directed acceleration pulses. Because UDEC utilizes velocity rather than acceleration input, a sinusoidal velocity signal of amplitude 0.624 m/s, frequency 0.5 Hz and duration 12 seconds was applied to produce the desired peak acceleration of 1.96 m/s^2 (0.200g). The velocity signal produces accelerations with a cosine wave form, but this presents no ambiguity when compared with the sinusoid wave in TNMN, because the number of critical acceleration peaks in each case is the same.

Table 5.1. *Material Properties Used in Comparative Analyses*

Program	TNMN	UDEC
Mass Density (kg/m^3)	2500	2500
Friction Angle of Slope Material (Degrees)*	20	20
Elastic Modulus (GPa)	N/A**	40.0
Poisson's Ratio	N/A**	0.25
Joint Normal Stiffness (GPa)	N/A**	4.0
Joint Shear Stiffness (GPa)	N/A**	4.0

* no cohesion was used in these analyses
** not applicable

The results of the TNMN (Newmark) analysis shown on Figure 5.7 indicate an accumulated relative block displacement of 3.14 cm. This result compares with the accumulated relative displacement of 3.12 cm obtained with UDEC (Fig. 5.8). Accelerations of the base and sliding block in the UDEC model are shown on Figure 5.9. The base block has a uniform amplitude of ± 1.96 m/s^2. The base block has a yield acceleration of 1.82 m/s^2, a difference of 1.6% from the theoretical value of 1.85 m/s^2. Initially high accelerations (2.66 m/s^2) occurring in the first few cycles of the simulation result from abrupt velocity gradients in the static system at the beginning of the dynamic run. Figure 5.9 show that these "spikes" produce a nominal up-slope displacement of 4.7×10^{-5}m that can be ignored without incurring significant error in the calculation.

In summary, these data show that UDEC obtains results comparable to the closed form solution encoded in TNMN for the accumulation of permanent deformation along discontinuities due to dynamic loading. The comparison is valid only for the bi-linear elasto-plastic joint model available in UDEC and the perfectly plastic strain law assumed in TNMN. TNMN has no equivalent to the continuously-yielding (non-linear) joint deformation model in UDEC.

5.4.2 Comparison of Shake4 and UDEC

Program Shake (Schnabel *et al.*, 1972) is a numerical implementation of the closed-form solution for horizontal displacements occurring due to one-dimensional shear wave propagation in horizontally layered media. The conceptual representation of the Shake model domain consists of a linearly viscoelastic one-dimensional "column" of rock with horizontal, infinitely extending layers, that is bounded at its base by an elastic half-space. The input disturbance (an acceleration) may be applied at any vertical coordinate in the column, but is assumed to propagate vertically upward from the half-space. Only horizontal motion of the medium is permitted. The program calculates (in the frequency domain) the response of the system in terms of either, or all of, acceleration, velocity, displacement, or shear stress history in the time domain, or in the frequency domain Fourier or power spectra. The program assumes that each layer of material comprising the system is completely defined by its thickness, mass density, shear stiffness, and critical damping ratio (Schnabel *et al.*, 1972). A modified version of the program called Shake4 (version 6) was used for these analyses.

The comparison model is a homogeneous column 30 m high comprised of material with mass-density and shear stiffness equivalent to moderately jointed volcanic rock (Lama *et al.*, 1978c). Because UDEC utilizes a two-dimensional model domain, the column was assigned a 15 m width in the UDEC analyses. To attain boundary conditions analogous to Shake4, the dynamic free-field calculation (Sec. 5.3.5.2) was used to simulate the motion of a horizontally infinite medium surrounding the column, and a non-reflective boundary (Sec. 5.3.5.1) was used at its base to simulate wave energy dispersion in the elastic half-space. The material properties for each model are listed in Table 5.2. The constitutive properties of the non-reflective boundary are calculated from the criteria proposed by Goodman *et al.* (1968).

Table 5.2: *Material Properties Used in Comparative Analyses*

Program	Shake4	UDEC
Mass-Density of Material (kg/m3)	2600	2600
Elastic Modulus (GPa)	21.0	21.0 (11.4)*
Poisson's Ratio	0.25	0.25 (0.18)*
Joint Normal Stiffness (GPa)	N/A	2.0
Joint Shear Stiffness (GPa)	N/A	2.0

* parentheses correspond to equivalent elastic properties of the viscous boundaries

The implementation of damping in Shake4 is frequency independent (Schnabel *et al.*, 1972), while in UDEC damping must be applied at a central frequency such that frequency independent damping is emulated (Sec. 5.3.4). Viscous damping was applied to the UDEC model at the frequency of the first natural mode of the column (15.0 Hz). Stiffness proportional damping is ineffective in this model because it has no contacts. However, viscous damping opposes block motion (Sec. 5.3.4) and may interfere with the model response. For this reason the critical damping ratio was kept to a modest level of 2.0% in both the Shake4 and UDEC analyses.

A series of sinusoid acceleration signals between 1.0 and 13.0 Hz at discrete intervals of 2.0 Hz were applied to each model. The maximum acceleration at the base of the model was limited to 0.10g. Peak acceleration response was evaluated at nine vertical intervals in each model (including the base) and response spectra were compiled. Forcing frequencies at or past the first natural mode of the column were not tested. The reasons for this are that; 1) the theoretical dynamic amplification at resonance is 25 times the base acceleration ($\approx$ 2.5g) and represents an acceleration observed only under special conditions in natural systems (Wetmiller *et al.*, 1988), and; 2) for the purposes of earthquake response analysis, only those frequencies under

10 Hz are usually of interest. Acceleration response spectra at four uniformly spaced depth intervals are shown on Figures 5.10a through 5.10d. The acceleration data corresponding to these spectra are listed in Table 5.3.

Table 5.3: *Peak Acceleration Values of Response Spectra**

Frequency (Hz)	surface	-7.5m	-15m	-22.5m
1.0	0.987, 0.987	0.986, 0.986	0.985,0.985	0.983,0.983
3.0	1.032, 1.031	1.029, 1.028	1.019, 1.018	1.004, 1.003
5.0	1.132, 1.134	1.123, 1.124	1.094, 1.095	1.048, 1.047
7.0	1.318, 1.318	1.296, 1.296	1.233, 1.231	1.129, 1.123
9,0	1.659, 1.660	1.615, 1.621	1.484, 1.486	1.274, 1.268
11.0	2.373, 2.391	2.279, 2.289	2.003, 2.007	1.568, 1.558
13.0	4.503, 4.451	4.253, 4.199	3.532, 3.476	2.424, 2.362

* Paired acceleration values in m/s^2 correspond to [UDEC, Shake4] respectively.

The response spectra for each model exhibit excellent agreement. The mean difference between the calculated peak acceleration values is less than 0.2% at frequencies of 11.0 Hz or less. The mean differences at 13.0 Hz are less than 1.8%, with a maximum difference of 2.6% recorded at a depth of 22.5 m. This result is probably due to the increasingly sensitivity of the dynamic amplification factor to small changes in the effective forcing frequency as the natural (resonance) modes of the system are approached. Also implied in these results is the effectiveness of the dynamic free-field boundary for simulation of elastic far field motion during dynamic analysis.

5.5 Summary

An overview of the numerical methods available for dynamic analysis was presented in Section 5.2. The distinct element method possesses many features that make it the appropriate choice for modelling of discontinuous rock masses. The generalized two-dimensional formulation of the distinct element method known as UDEC is described in Section 5.3. UDEC simulations of dynamically induced linear-plastic joint displacement and one-dimensional shear wave propagation were verified by comparison with closed-form solutions. The results agree well, and demonstrate that UDEC is capable of simulating physically correct behaviour in simple systems.

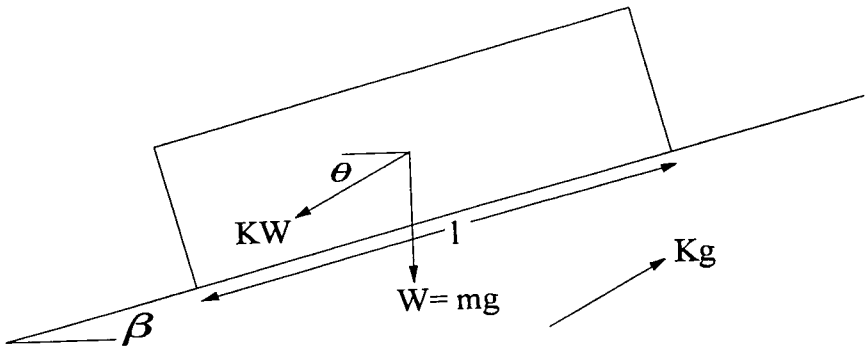

Figure 5.1. *Physical framework for limit-equilibrium analysis. The slope is β degrees from horizontal. An arbitrary acceleration pulse Kg at angle θ from horizontal produces a body reaction force KW in the block.*

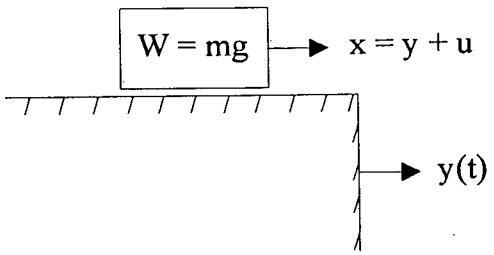

Figure 5.2a. *Block sliding on a horizontal plane (after Newmark, 1965).*

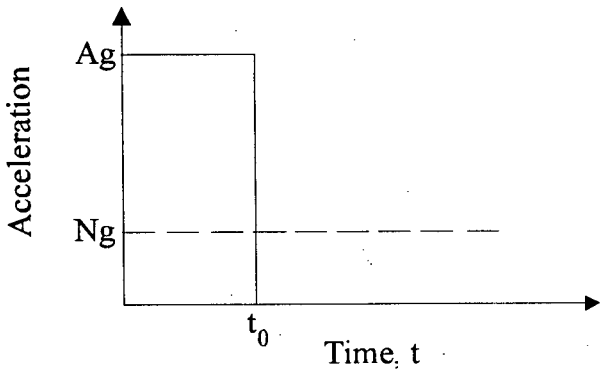

Figure 5.2b. *Rectangular acceleration pulse of magnitude Ag (solid line) is shown with the block critical acceleration Ng (dashed line) (after Newmark, 1965).*

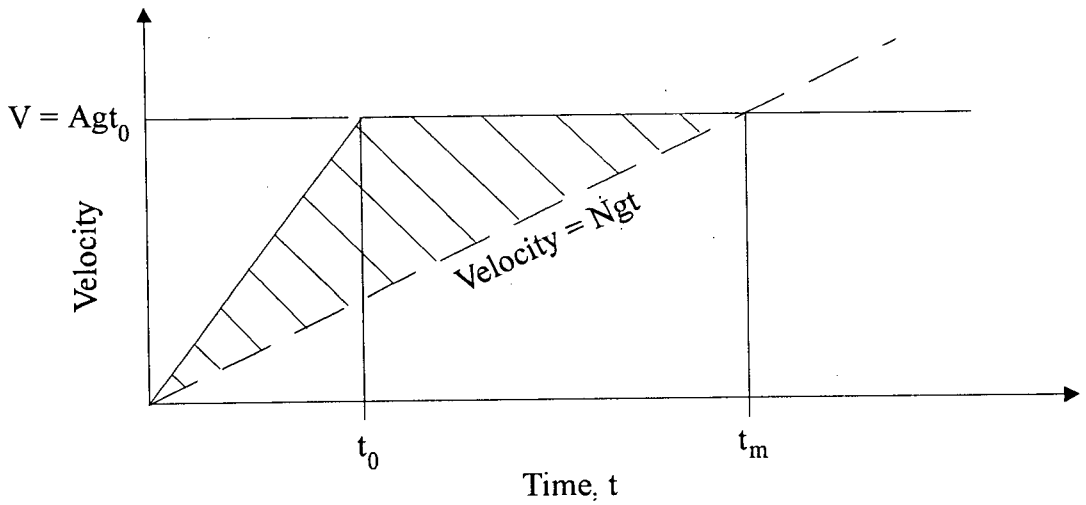

Figure 5.2c. *Schematic plot of base and sliding block velocities with time. The area of the hatched region is equal to the relative displacement of the sliding block (after Newmark, 1965).*

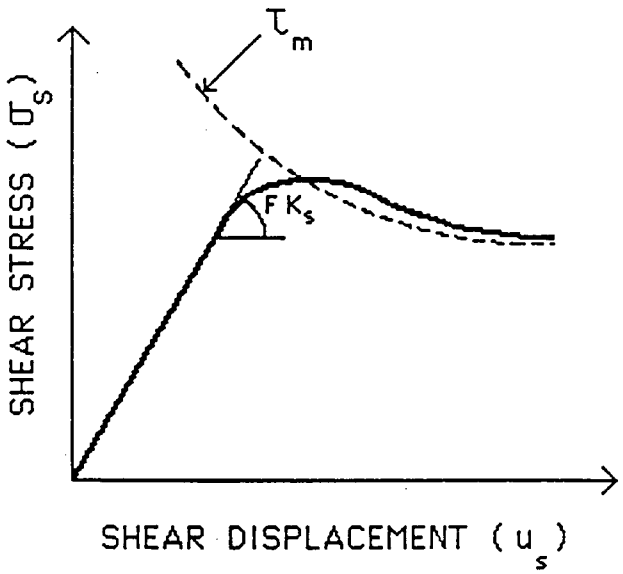

Figure 5.3. *Shear stress-displacement curve under monotonic loading and constant normal stress for the C-Y joint model (after Itasca 1992). The instantaneous tangent modulus Fk_s is shown, as well as the bounding strength curve τ_m.*

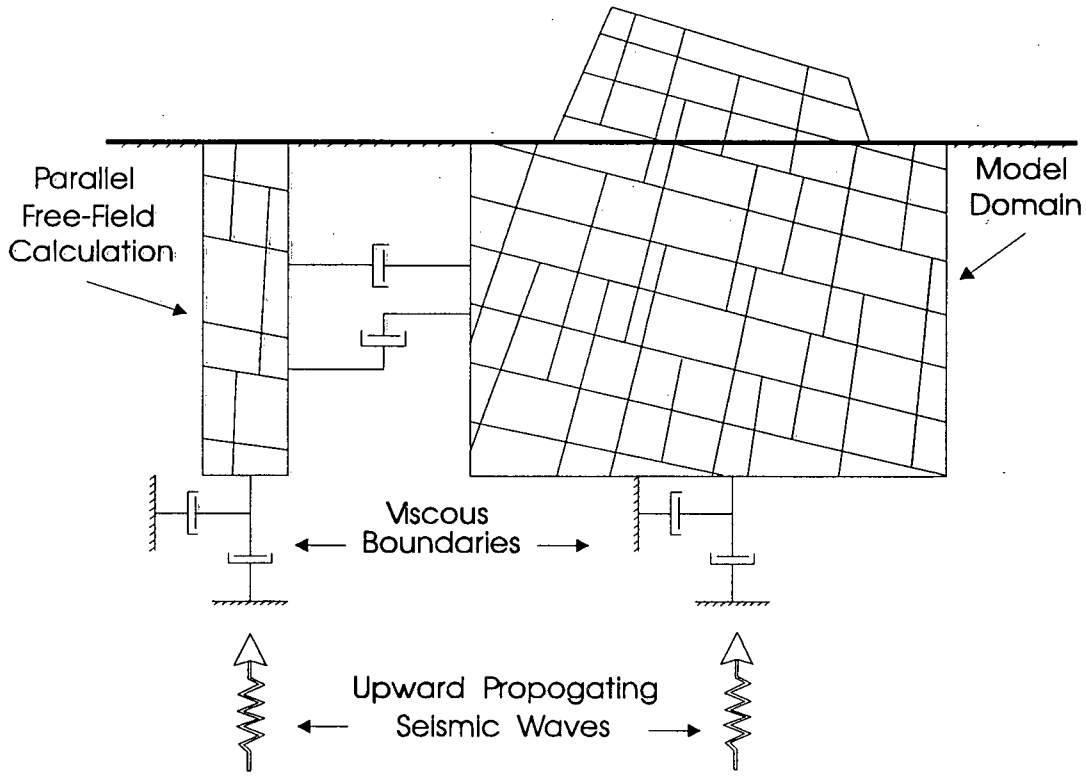

Figure 5.4. *Schematic representation of the dynamic free-field and non-reflective boundary implementations in UDEC (after Itasca, 1992).*

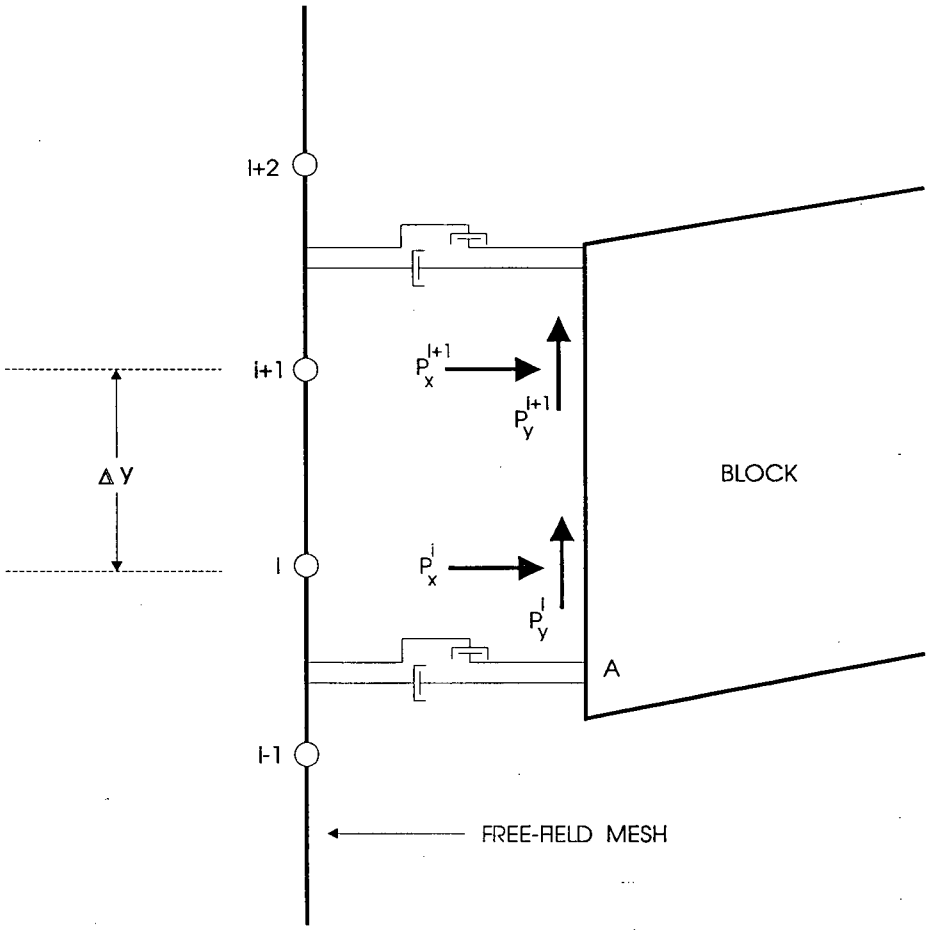

Figure 5.5. *Schematic representation of the linkage between the dynamic free-field calculation and the model domain in UDEC (after Itasca, 1992).*

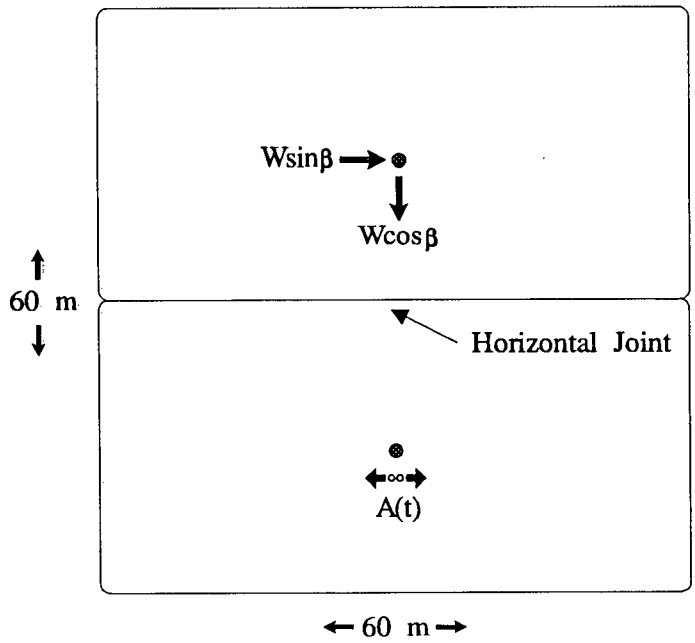

Figure 5.6. *The UDEC model used for comparative analysis of Newmark's method. The force components acting upon the top block are equivalent to those that would be present if the model was rotated β degrees clockwise.*

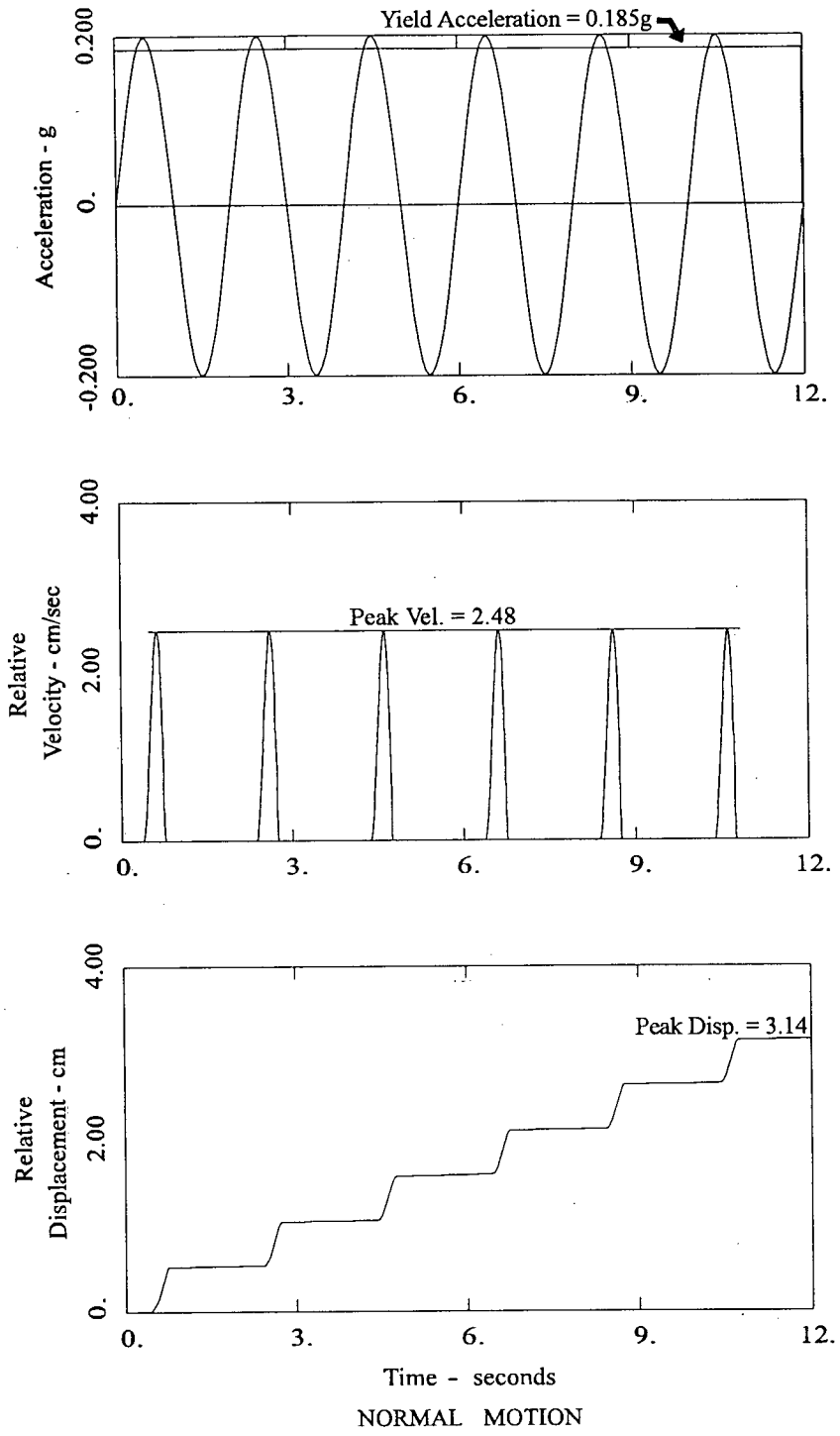

Figure 5.7. *Results of TNMN (Newmark) analysis. The input acceleration signal is shown in the top frame. Peak relative velocity and accumulated relative displacement between the block and the base are shown in the middle and bottom frames respectively.*

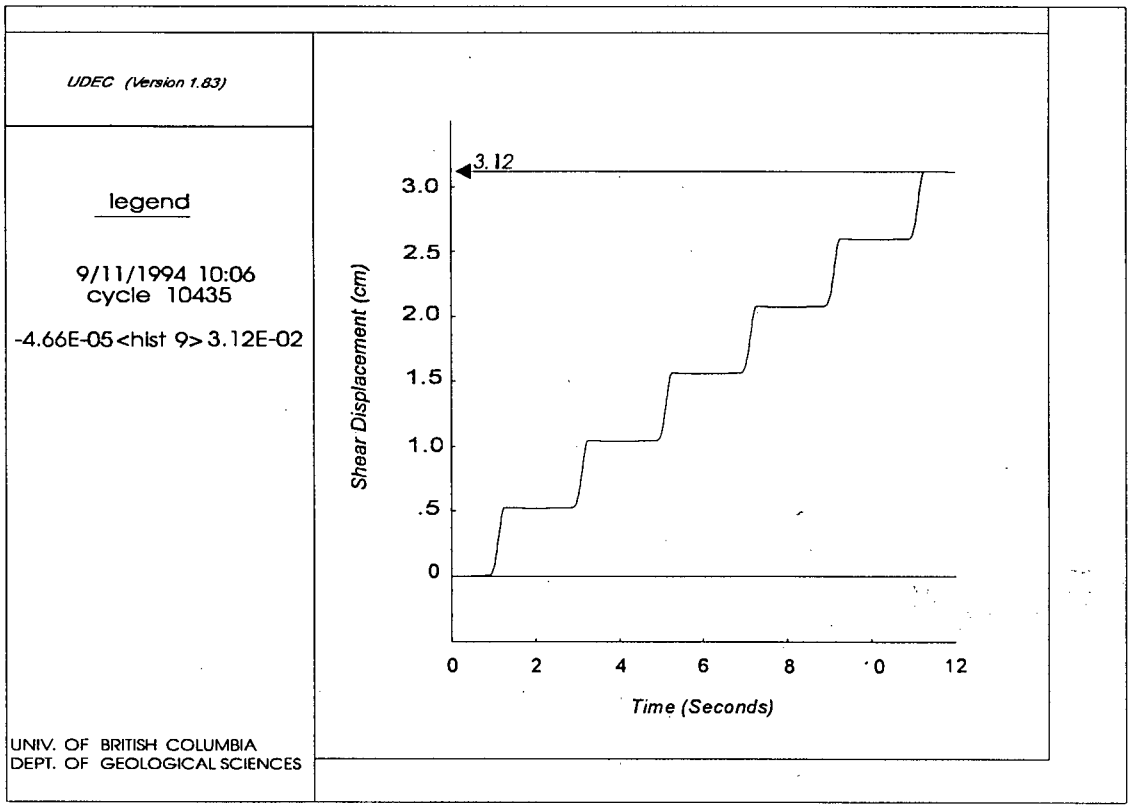

Figure 5.8. *Results of UDEC shear deformation analysis. Accumulated relative displacement between the bottom (non-sliding) and top (sliding) block is shown plotted against model simulation time.*

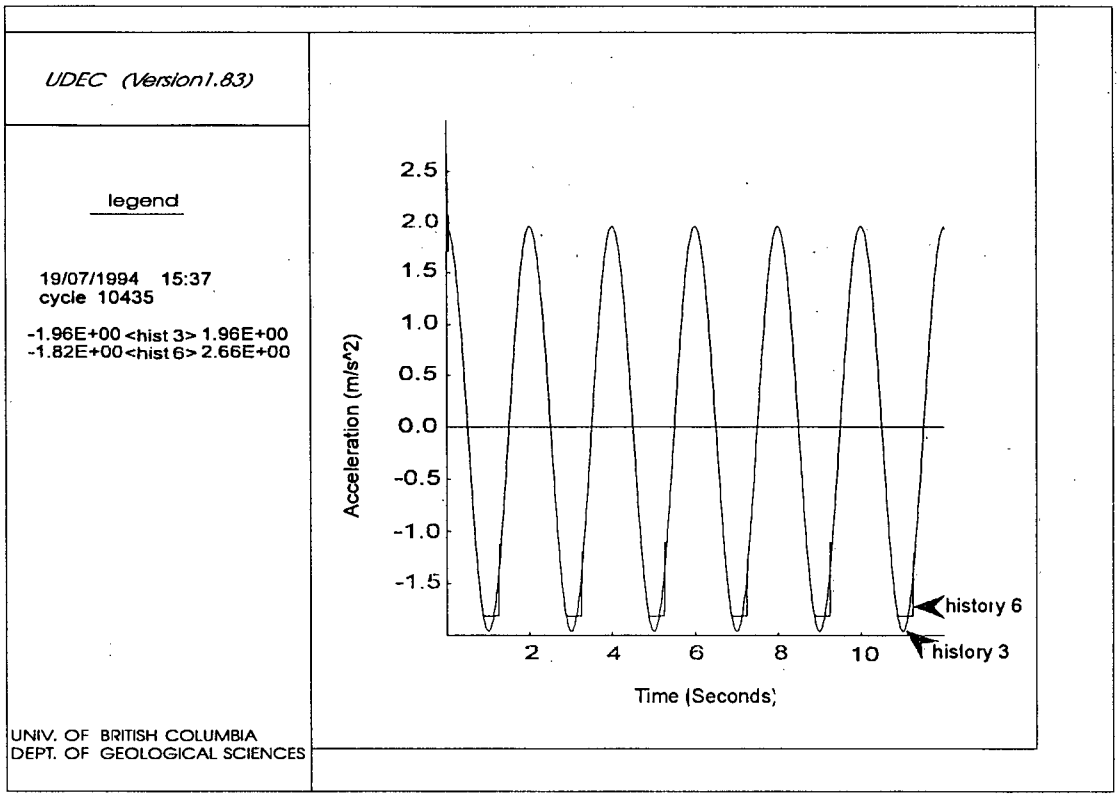

Figure 5.9. *UDEC shear deformation analysis block accelerations. The bottom block representing the base acceleration is history 3. The sliding block is represented by history 6.*

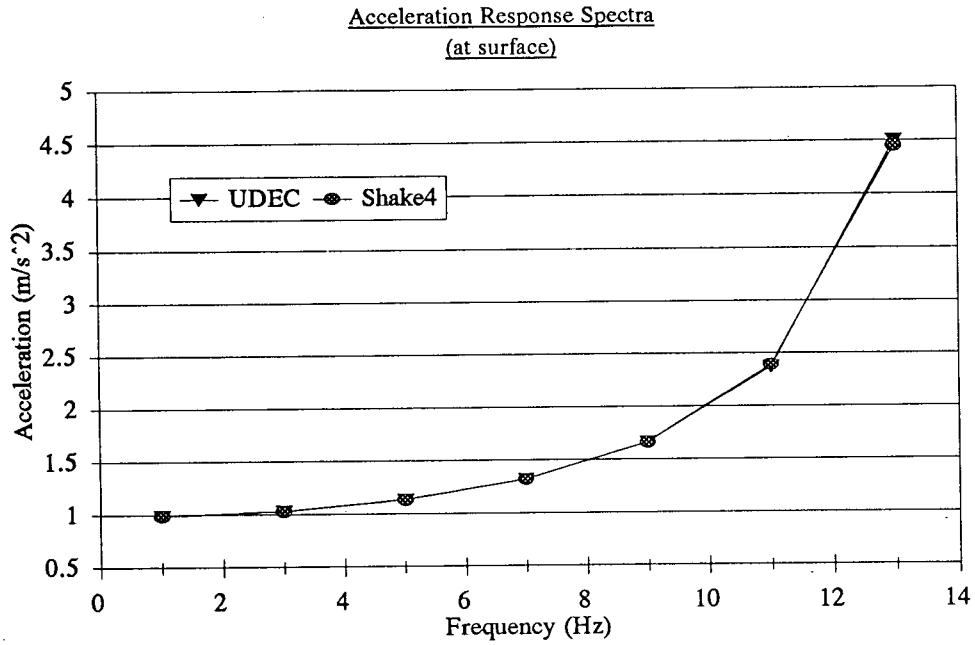

Figure 5.10a. *Peak acceleration response spectra for UDEC and Shake4 (at surface).*

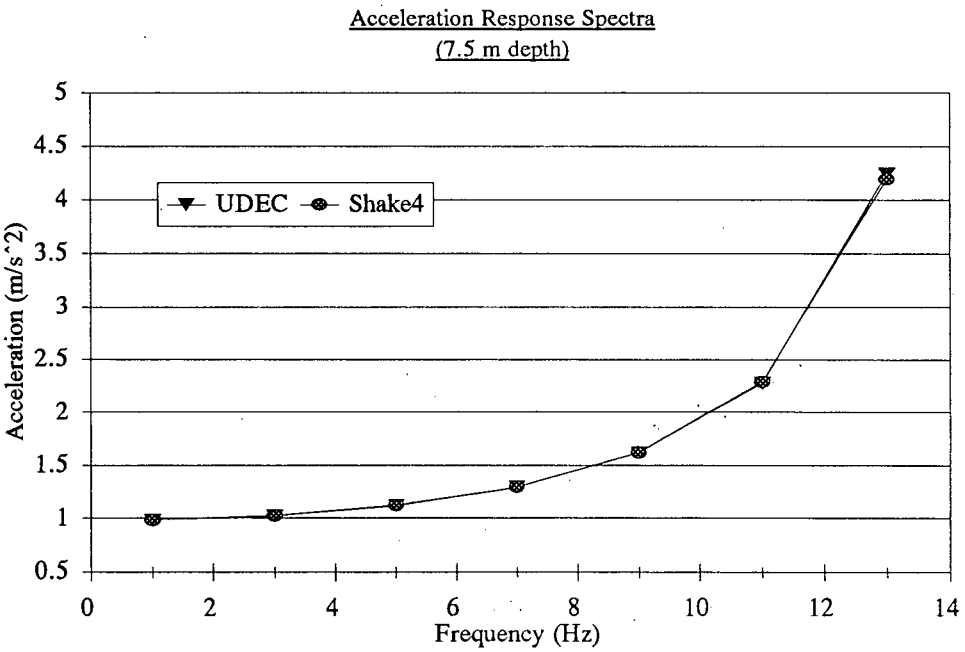

Figure 5.10b. *Peak acceleration response spectra for UDEC and Shake4 (at 7.5 m depth).*

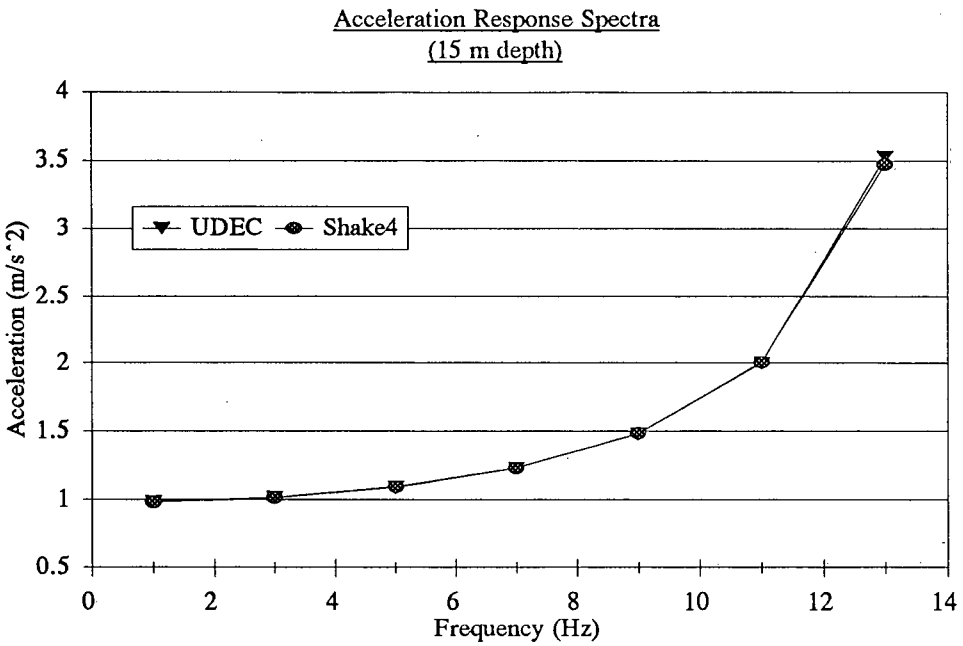

Figure 5.10c. *Peak acceleration response spectra for UDEC and Shake4 (at 15 m depth).*

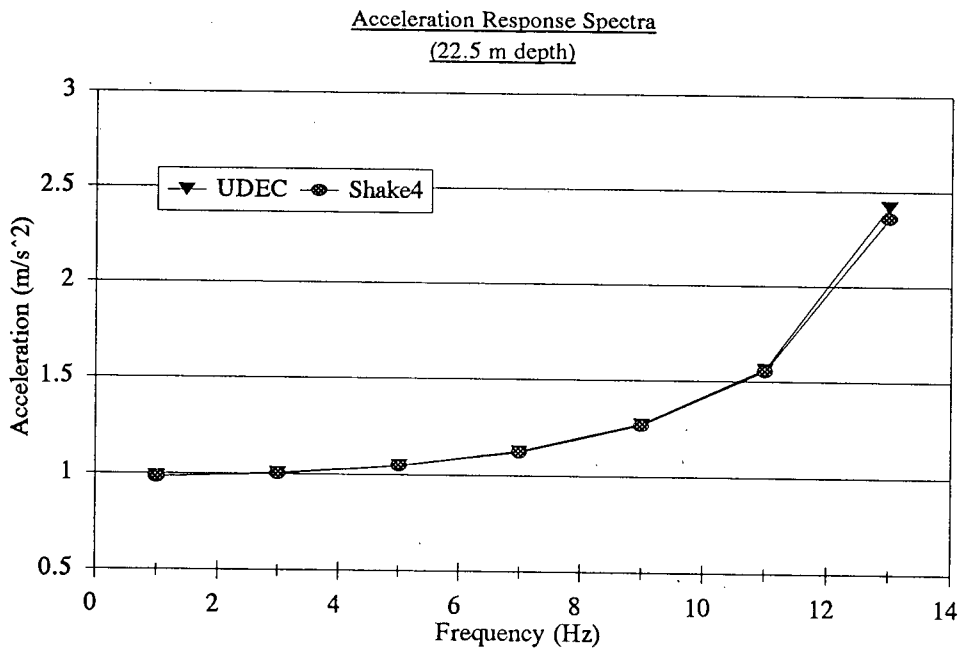

Figure 5.10d. *Peak acceleration response spectra for UDEC and Shake4 (at 22.5 m depth).*

CHAPTER 6

Dynamic Analysis Of Slope Deformation At Cement Creek

6.1 Introduction

The generalized deformation behaviour of rock slopes at Cement Creek in response to earthquake loading is analyzed with UDEC in this chapter. The aim is to determine whether seismicity may be considered a viable landslide triggering mechanism, and to gain insight into seismogenic deformations of rock slopes. No analyses of this type have been undertaken in the Yukon study area until now.

6.2 Modelling Approach

The UDEC model described here is based upon geomorphic observations and geological measurements obtained during field reconnaissance of the Cement Creek area. Detailed structural, lithological, and geomechanical data pertinent to this area are not available. The approach to numerical modelling of data-limited systems in rock mechanics is discussed by Starfield *et al.* (1988). The principal tenets of their methodology are:

1) the model should be a simplification of reality. Its design should be motivated primarily by the questions necessitating the model, rather than the details of the system being modeled.

2) the intent of the analyses is qualitative rather than quantitative. Modelling is performed to gain an understanding of the behaviour of the system, rather than to make absolute predictions about it.

With these principles in mind, it is seen that the investigation procedure is heuristic, rather than a deterministic process.

6.3 UDEC Model Geometry and Characteristics

The predominant mode of failure observed at landslide sites on the north wall of Cement Creek valley is by shearing along penetrative surfaces in the rock mass. Structural deformation in the bedrock underlying these slopes is intense, and precludes the design of a model that is representative of all of the landslides. One landslide for which there is limited reliable data and excellent exposure of the failure surface is Cement Creek #4. In view of this, generalized structural and slope geometries based upon Cement Creek #4 landslide were adopted for the analyses.

Cross section A-A' (Fig. 4.3) passes through Cement Creek #4 landslide in the approximated direction of slippage on the basal plane. Topographic profile A-A' corresponding to the section line is shown on Figure 6.1. Elevations for the profile were taken from NTS topographic map sheets 115 F/8 (Tempest Mountain) and 115 G/5 (Steele Creek). The pre-landslide topography indicated on Figure 6.1 was reconstructed from slope profiles adjacent to the slide area, and reflects the measured orientation of the underlying structural planes.

The UDEC model is illustrated on Figure 6.2. The geometry is simplified from that shown in the profile on Figure 6.1. To increase numerical efficiency, the size of the model was scaled downward. The base of the model is fixed in the vertical direction, and assigned a viscous-boundary condition to simulate energy dissipation in the half-space beneath the model (Sec. 5.3.6.1). The left and right lateral boundaries were similarly assigned viscous-boundary conditions, and were coupled to a parallel free-field calculation (Sec. 5.3.6.2).

Discretization of the model domain represents a balance between numerical efficiency and the importance of providing enough detail to characterize the behaviour of the system. Achieving this balance is a trial-and-error process. Because it is impractical to discretize the

model at the frequency of field measurements, discontinuities are included explicitly at a coarse scale, and constitutive properties equivalent to the intervening jointed rock mass are assigned to the model elements.

Two discontinuity sets are incorporated in the model. The principal set divides the model domain into 20 degree dipping blocks with thicknesses varying between 23 and 24 metres (Fig. 6.2). These coarsely emulate the bedding surfaces separating the individual flows in the volcanic rocks. The topmost block is further split into two 12 metre thick layers, a spacing that approximates the upper limit of the measured bedding thickness in the field (Sec. 4.2). Their inclination conservatively corresponds to measured dips that vary between 18 and 27 degrees in the crown area of Cement Creek #4 landslide. With the exception of Cement Creek #2, all of the landslides investigated at Cement Creek have failed along these planes (Sec. 4.4).

The second discontinuity set subdivides the two topmost blocks into an array of quadrilateral prisms at a 12.5 metre spacing. These prisms are the only elements in the model that may translate freely. They correspond to the sub-vertical joints that were observed at the toe of Cement Creek #1, where rock columns have detached from the main body of the landslide. They roughly parallel the free-face of the landslide mass, and persist for considerable distance up slope from the toe (Power, 1988). These structures are probably present at Bighorn Creek Rock Avalanche as well, where massive, coherent rock blocks have detached from the head scarp (Sec. 3.6.2).

6.4 Slope Pore Pressure

No hydrogeolgical data are available for slopes in the Cement Creek area. It is widely acknowledged that the pore pressure regime in a slope can have a significant effect on stability (*i.e.* Hodge *et al.*, 1977). However, as noted in Section 4.6, the presence of continuous permafrost generally prohibits infiltration of surface water, except where pre-existing discontinuities have been dilated by slope movement. Because of this, as a simplifying

assumption, all analyses are performed with the slope in an unsaturated (zero pore pressure) state. The potential destabilizing effect of surface water infiltration into dilated discontinuities is recognized, but is not analyzed in this study.

6.5 UDEC Model Parameter Selection

UDEC allows the use of a variety of constitutive laws for the model elements and discontinuities. Strength and deformation constants for the rock mass and joints are required input parameters for UDEC. No specific data for these parameters are available for rocks in the Cement Creek area. Representative values were selected from published sources, except where noted below. The general references used are Lama *et al.* (1978*a, b, c*), Pasamehmetoglu *et al.* (1981), Bandis *et al.* (1983), Barton *et al.* (1987), and Lu (1993).

6.5.1 Rock Mass Characterization

The model elements in all of the analyses utilize an elastic, isotropic constitutive model with linear stress and strain laws and a Mohr-Coulomb failure criterion. The elements are internally discretized with a deformable finite-difference mesh that complies with the wave transmission restrictions of Kuhlmeyer *et al.* (1973). Confining stresses throughout the model are low when compared to the intact rock strength. Because of the confining stress state, plastic deformation of the elements is not considered significant, and model deformation is expected to occur predominantly along discontinuity planes.

The rock mass model parameters are summarized in Table 6.1.

Table 6.1: *Rock Mass Parameters Used in the UDEC Analyses*

Parameter	Rock Mass	Viscous Boundary
Density (kg/m^3)	2,600	2,600
Elastic Modulus (MPa)	16,000	9,600
Poisson's Ratio	0.25	0.16
Bulk Modulus (MPa)	9,000	4,690
Shear Modulus (MPa)	6,000	3,810
Friction Angle (deg)	45*	N/A*
Cohesion (MPa)	2.0*	N/A*
Tensile Strength (MPa)	0.2*	N/A*

* the parameter is not strictly required for problem calculation.

The elastic modulus of the rock mass was back-calculated from seismic refraction data obtained at Cement Creek #1 landslide by Power (1988). Beneath a comparatively thin low-velocity layer, his data indicate a single refractor with an average p-wave velocity of 2725 m/s. The p-wave velocity, C_p, is related to the deformation constants of an elastic, isotropic media by the relation:

$$C_p = \left(\frac{\left(K + 4/3\, G\right)}{\rho} \right)^{1/2} \qquad [6\text{-}1]$$

where ρ is the mass density of the media, and K and G are the bulk and shear moduli respectively. Assuming Poisson's Ratio of 0.25, [6-1] yields a dynamic elastic modulus of 16.1 GPa.

The calculated dynamic modulus is between 30 and 65 percent less than elastic moduli in andesites measured in small-scale tests, but is well in accordance with increased deformability and decreased rock strength for in-situ conditions noted by Heuze (1980). Similar behaviour in a number of independent tests are compiled by Lama *et al.* (1978b). The differences between small-scale and in-situ elastic constants is attributed to the increasing influence of flaws and discontinuities within the rock mass at larger scales (da Cunha, 1990).

Cohesion and tensile strength data are available for small-scale tests (Pasamehmetoglu *et al.* 1981, Lama *et al.* 1978*a*), but representative in-situ values are not. No guidelines for an appropriate scale reduction could be found, and hence small-scale test values were arbitrarily reduced by an amount proportional to the modulus reduction, although there is no physical justification for this assumption.

Parameters of the viscous boundary are based upon those of the rock mass adjusted to account for the presence of discontinuities. The equivalent elastic modulus, E_{eqv}, can be approximated by an equivalent continuum formulation (Goodman *et al.*, 1968):

$$\frac{1}{E_{eqv}} = \frac{1}{E} + \frac{1}{k_n s} \qquad [6\text{-}2]$$

where E is the rock mass elastic modulus, k_n is the joint normal stiffness, and s is the joint spacing. Note that for these analyses, because the rock mass modulus already reflects the influence of in-situ joints, s corresponds to the coarse joint spacing in the model (24 metres).

6.5.2 Rock Joint Characterization

Discontinuities (joints) in these analyses are assigned either a bi-linear, elasto-plastic Coulomb slip law, or a non-linear strain softening law known as the continuously yielding (C-Y) joint model. The yield criteria for these laws are outlined in Section 5.3.3. The supposed error

in the C-Y joint model noted in Section 5.3.3 necessitated adopting a zero joint cohesion assumption in the analyses. The implications of this assumption are discussed in Section 6.7.3.

The rock joint model parameters used in the analyses are summarized in Table 6.2.

The bedding surfaces in the volcanic rocks are characterized as filled joints in these analyses. The strength and deformation behaviour of filled joints depend upon the type and thickness of the filling material (Goodman *et al.*, 1972, *in* Barton *et al.*, 1987; Bandis, 1990). In small-scale direct shear tests on brecciated intra-flow zones in layered basalts, Ruiz *et al.* (1970, *in* Barton *et al.*, 1987) report an effective friction angle and cohesion of 42 degrees and 242 kPa respectively. These values are considered an upper strength limit for these zones. Lu (1993) reports average friction angles from direct shear tests on tuffs of 35 and 30 degrees respectively for wet and dry samples. Residual angles and cohesions were not reported in these tests. Residual friction angles derived by Lu (1993) from uniaxial and triaxial tests vary between 17 and 20 degrees. Residual cohesion is assumed to be zero.

It was previously noted that rocks in the Cement Creek area are intensely folded. It is believed that a considerable amount of flexural slip has occurred on the intra-flow surfaces. Such slip can create shear localizations and aligned zones of fine-grained particles along the slip plane. The net effect is believed to reduce the peak mobilized shear strength along of the joint surface. For these reasons, a friction angle of 36 degrees was selected as a representative intermediate value. A residual friction angle for the sub-vertical joints is not used because shear displacement on these joints is within the elastic range in these analyses. Tensile strength is assumed to be zero on all joint surfaces.

UDEC was used to evaluate the monotonic shear stress/displacement behaviour of the linear and non-linear joint models using the values in Table 6.2. The evaluations were performed at constant applied normal stress. The linear joint model has a considerably greater peak shear strength than the non-linear model if an identical peak friction angle is used. It was decided to use an equivalent peak shear strength for the two joint models for the dynamic

analyses presented in Section 6.7. This required using a lower peak friction angle in the linear joint model, indicated in Table 6.2.. The shear stress/displacement behaviour of the adjusted joint models is illustrated on Figures 6.3 and 6.4. The linear model exhibits modest strain hardening behaviour in the plastic deformation zone. This behaviour is the result of normal closure on the joint surface under the ambient stresses, which produce a normal stress increment $\Delta\sigma_n = k_n \Delta u_n$, and hence a higher peak shear strength in accordance with the Coulomb friction law (Sec. 5.3.3). The peak strength increase is less than 0.4% over the range of displacements indicated on Figure 6.3, and is not considered a significant source of error in the analyses in Section 6.7. However, this behaviour may become a significant factor in analyses with relatively large strains.

Table 6.2. *Rock Joint Parameters Used in the UDEC Analyses*

Parameter	Sub-vertical joints	Intra-flow breccia zones	Viscous Boundary
Normal Stiffness (MPa/m)	1,000	1,000	1,000
Shear Stiffness (MPa/m)	400	100-400*	400
Peak Friction Angle (deg)	34	36 (29.5)**	36
Residual Friction Angle (deg)	N/A	18 (N/A)**	N/A
Cohesion (MPa)	0	0	0
Tensile Strength (MPa)	0	0	0

* The shear stiffness of most rock joints increases in response to increasing normal stress (Barton *et al.*, 1987). This effect is explicitly incorporated included in both the linear and non-linear analyses.

** Values in parentheses are for the bi-linear elasto-plastic joint model. All other values are common to both models.

6.6 Modelling Procedure

Dynamic simulations with UDEC consist of two distinct phases.

The first is a static phase that involves creation of the model, and simulation of the slope evolution as well as any external events that may have affected it. In these analyses, the model slopes are assumed to have been glacially excavated with an in-situ stress state of $K_0=0.5$. A sample UDEC input file included in Appendix 2 outlines the excavation procedure. The model is cycled to equilibrium in the post excavation state and is saved as a "base" model for the next stage of the simulation.

The second phase is a dynamic loading phase, in which digital strong motion input is applied to the base of the model and the free-field. This ensures that the far field conditions simulated by the free-field calculation have the same motion as the model domain. Earthquake strong motion is input as a stress or velocity boundary condition. The former is preferred because the velocity boundary condition tends to produce violent reactions in the model. Lorig (1991) makes use of velocity boundary input, but does not specify the boundary conditions used, or any assumptions regarding them.

Digital seismic data can usually be obtained as a velocity-time history, and is easily converted to a stress history by procedures outlined by Itasca (1992). The model is cycled until the seismic time history is ended. A period of quiescence after the dynamic loading phase may be included by simply appending an appropriate quantity of zeroes to the digital input file. Multiple strong motion records may be concatenated in sequence to simulate multiple earthquake loadings if desired.

6.7 Results of UDEC Modelling

6.7.1 Earthquake Data

No strong motion data are available for the Cement Creek area. The nearest strong motion accelerograph at Haines Junction, Yukon, some 140 km to the southwest, has never been triggered (Horner, 1991; *pers. comm.*). Digital strong motion records from a number of temporally separate earthquakes associated with the 1985 Nahanni, N.W.T. earthquake (Wetmiller *et al.*, 1988) were obtained from Pacific Geoscience Centre.

The earthquake record chosen for these analyses corresponds to a magnitude 4.6 event that occurred on November 9, 1985. The velocity time history is shown on Figure 6.5. Only the first three seconds of the earthquake record are used to reduce computation time; ground motions are very small in the remainder of the record, and do not contribute to slope deformation. Zeroes are appended to the end of the record to bring the total time to 4.0 seconds.

The velocity response of the UDEC model measured at location A on Figure 6.2 is shown on Figure 6.6. The response exhibits a modest amount of distortion when compared with the input signal, and peak response is approximately 14% less than the input record. These effects are attributed to joint slip on the bedding surfaces in the model as the shear wave propagates upward. Increasing the joint stiffness can improve the correspondence between input and response signals, but this can lead to unrealistic joint behaviour.

6.7.2 Deformation Response of the UDEC Models

The UDEC models were subjected to five consecutive loadings of the earthquake record described above. Only horizontal earthquake motions are input to these analyses. The results of these simulations is summarized in Figures 6.7 through 6.13.

Figure 6.7 illustrates total displacement vectors of the model elements in the simulation using the linear elasto-plastic joint displacement law. Both of the unconstrained layers at the top of the model have undergone shear displacement. Note that the displacement vectors in the top layer include the displacement increment of the bottom layer relative to the rest of the model domain. The vectors show generally increasing element displacement toward the toe of the model "landslide". Figure 6.8 illustrates this effect in greater detail. It depicts the total shear displacement at the bottom right hand corner of each quadrilateral element in the bottom layer. The horizontal coordinate of the corner's location is shown on the abscissa. It is clearly seen that the shear displacement is several times greater at the toe of the movement than at the crown.

Figure 6.9 is a detail view of the toe area of Figure 6.7. Time histories of shear displacement was monitored at the two contact locations noted. These histories are shown on Figure 6.10. With the exception of the first earthquake loading, the shear displacements induced by successive loading at each of the contacts are approximately equal. The greater displacement exhibited on the first pulse is believed to be related to the release of residual "locked in" shear stresses on the joint surface at the end of the static loading phase. It is not known if the "locked in" stresses are representative of in-situ conditions. The magnitude of the incremental displacement is different at each of the contacts, resulting in a widening of net displacement difference between the two contacts as the simulation progresses. The net displacement differences are manifest in the model as widening vertical gaps between the translating elements. This process is analogous to the formation of ground cracks observed near the toe of Cement Creek #1 Rock Slide. The gaps are also created up slope from the toe with smaller net increments of dilation with each successive earthquake event.

Figure 6.11 depicts total displacement vectors of the model using the non-linear strain softening joint displacement law. All of the elements below point "A" (indicated) are sliding down the basal slip plane, indicating general shear failure of the basal joint surfaces. All

elements above point "A" do not experience general shear failure at the end of the loading cycle, but have undergone irreversible plastic shear displacement. A detail of the toe area is shown on Figure 6.12.

Figure 6.13 shows the time history of shear displacements of the two contacts indicated on Figure 6.12. The progression of strain softening along the joint surface ultimately leading to shear failure is depicted. As with the linear joint model, the net difference in shear displacement between the contacts widens with successive earthquake load applications. The amount of difference increases rapidly as strain softening progresses. The third earthquake pulse causes general shear failure of contact 6172, as evidenced by the sloping displacement curve during the quiescent interval after the load interval. The fourth loading interval causes immediate large strains that are depicted by the nearly vertical displacement curve. Contact 5551 remains stable until the fifth loading interval, where it exhibits large strain behaviour similar to contact 6172. This simulation clearly demonstrate a possible mechanism for progressive, incremental slope failure. This type of movement has occurred at Cement Creek #1 Rock Slide. Plate 4.4 clearly shows a debris stream that emanated from the eastern portion of the toe and cascaded downward into Cement Creek canyon. Portions of the slide block above this area have remained stable.

6.7.3 Implications of Cohesionless Joints

The effect of using no joint cohesion may have an effect on the specific results reported here, but are not believed to substantively alter the general behaviour of the system. Including joint cohesion would have the effect of translating the curves in Figures 6.3 and 6.4 p the ordinate axis, without altering the shape of the curve. The result is that higher transient stresses during earthquake loading would be required to induce slope movement.

6.8 Summary

The data generated by these numerical simulations provides important verification of the role of seismicity as a landslide triggering mechanism for Neogene volcanic rocks in the Cement Creek area. Geomorphic features such as ground cracking and related landforms commonly referred to as sackungen (Hutchison, 1988) can be explained in terms of seismicity induced, non-critical slope deformation, although seismogenic deformations are not the only cause of such landforms.

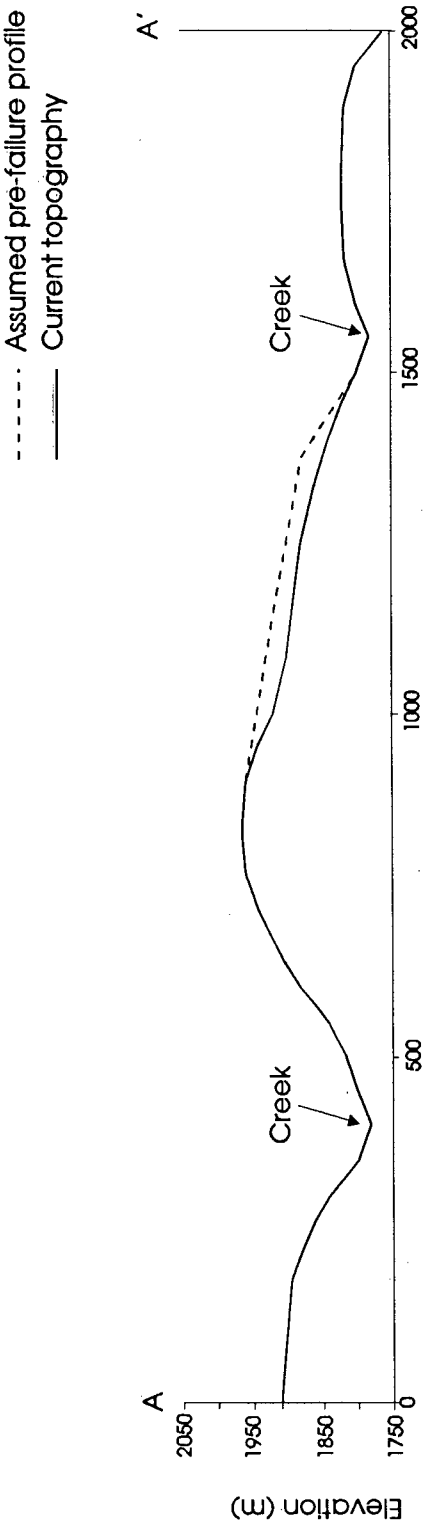

Figure 6.1. *Topographic profile A-A'*

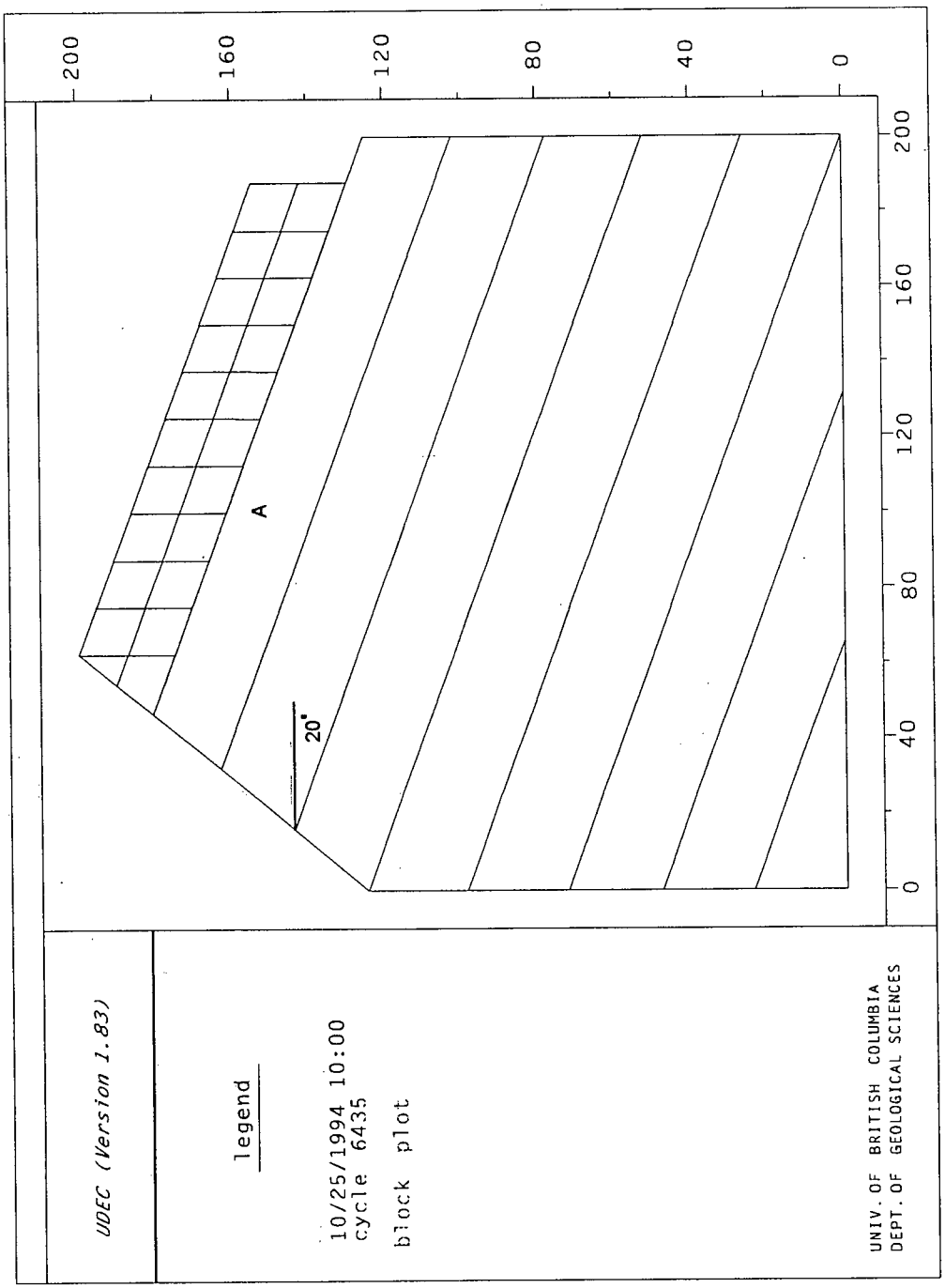

Figure 6.2. *The UDEC model. Dimensions are 200 m by 200m.*

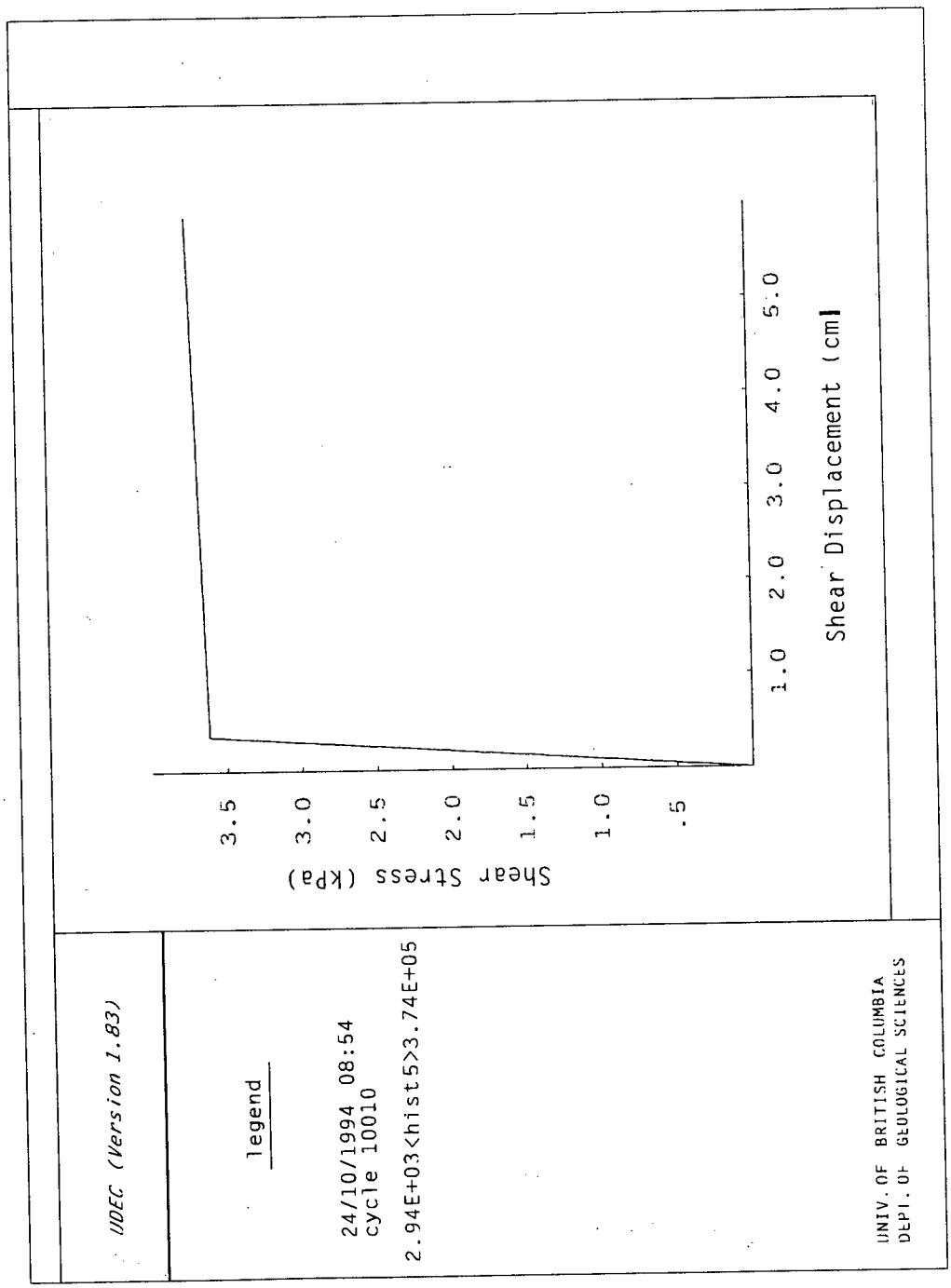

Figure 6.3. *Shear stess-displacement curve for the bi-linear elasto-plastic joint model.*

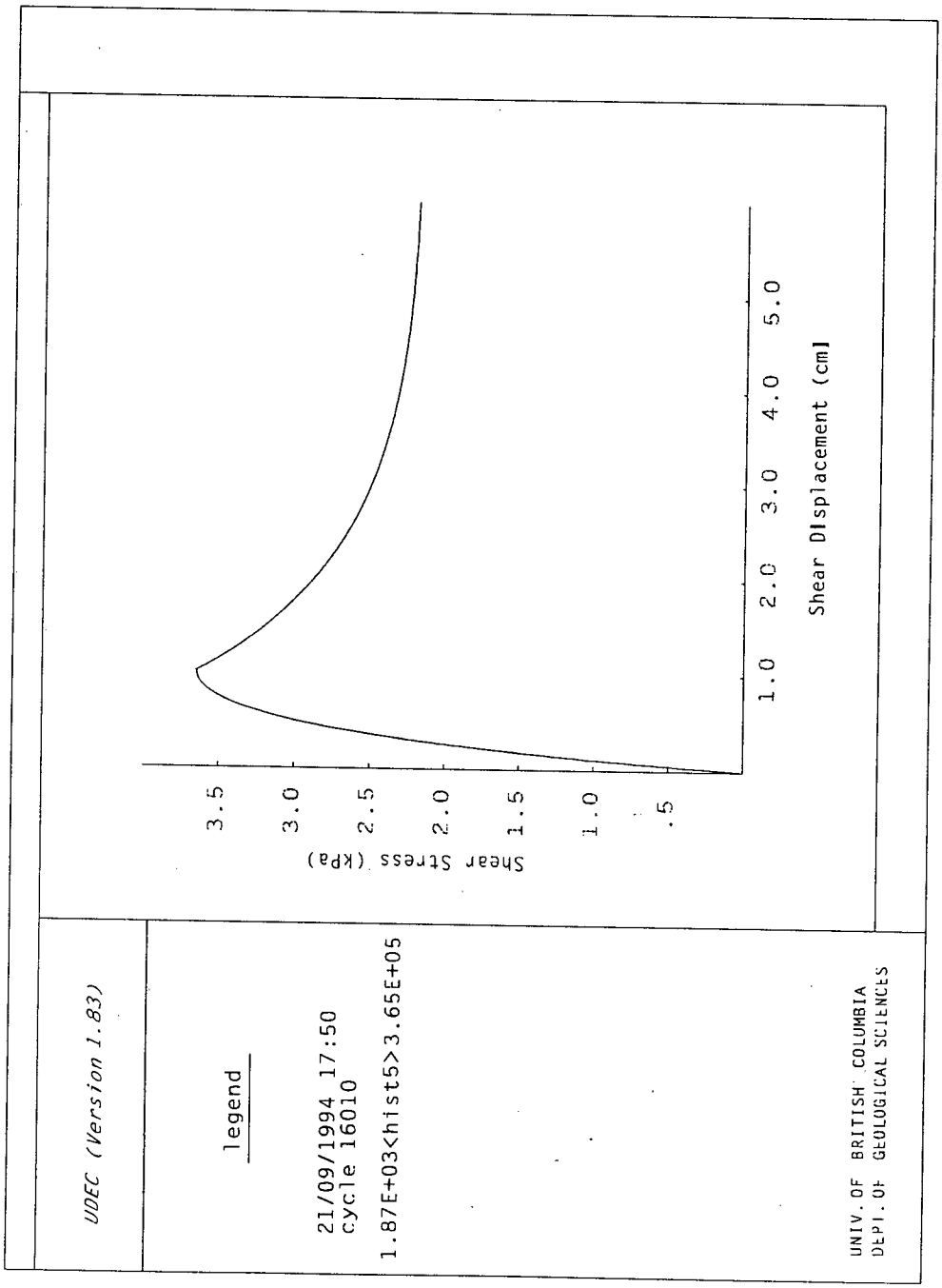

Figure 6.4. *Shear stess-displacement curve for the C-Y joint model.*

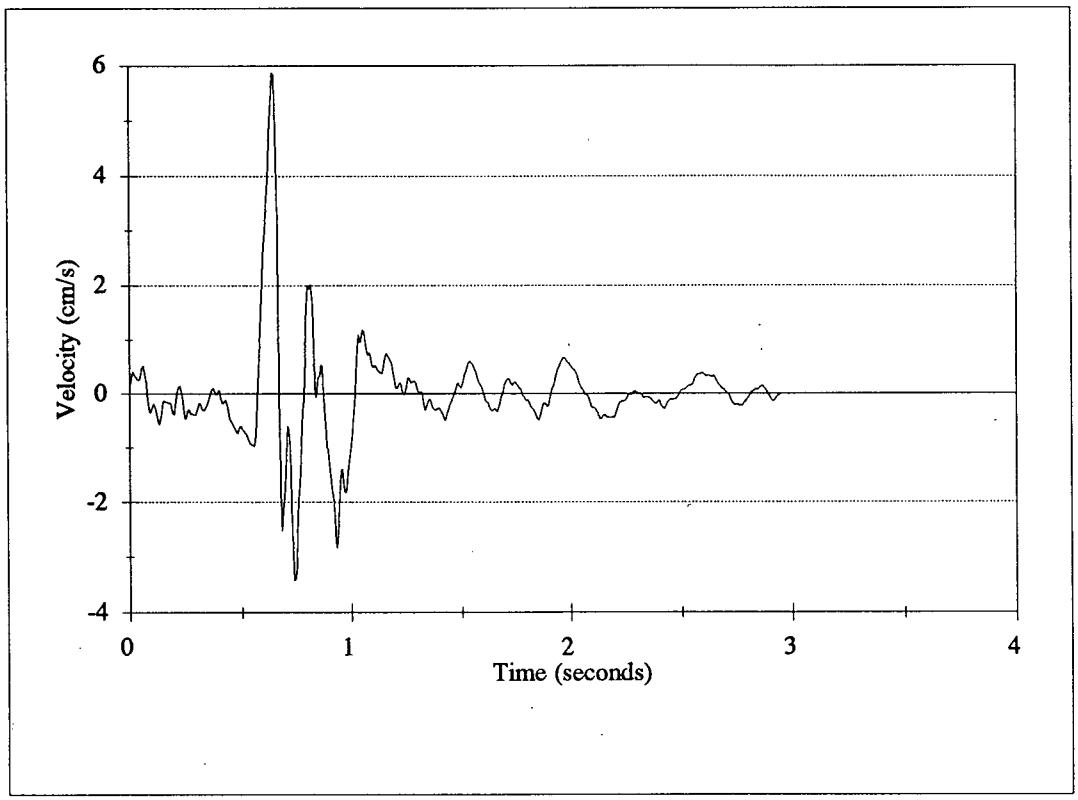

Figure 6.5. *Earthquake velocity input record.*

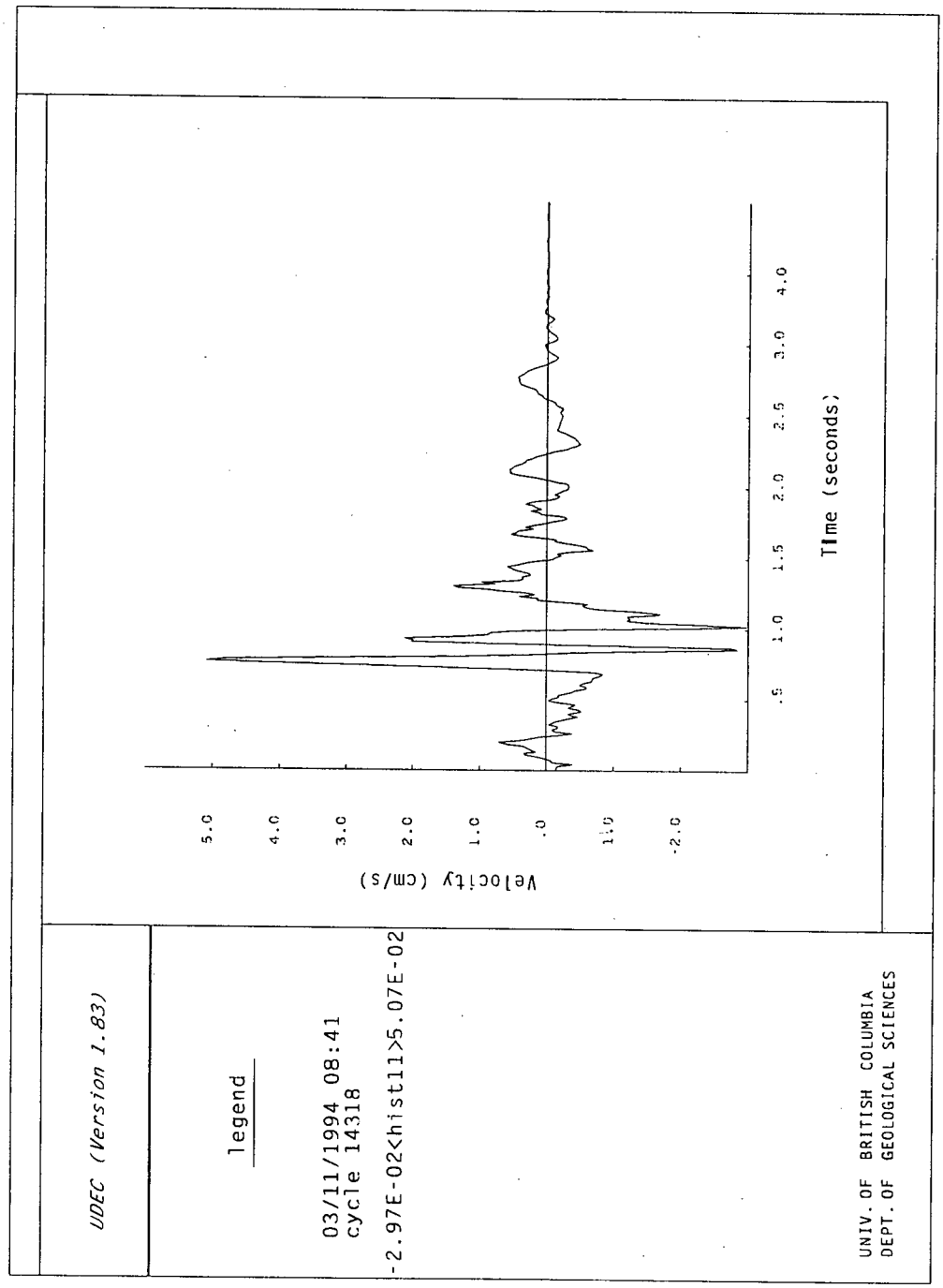

Figure 6.6. *UDEC model velocity response.*

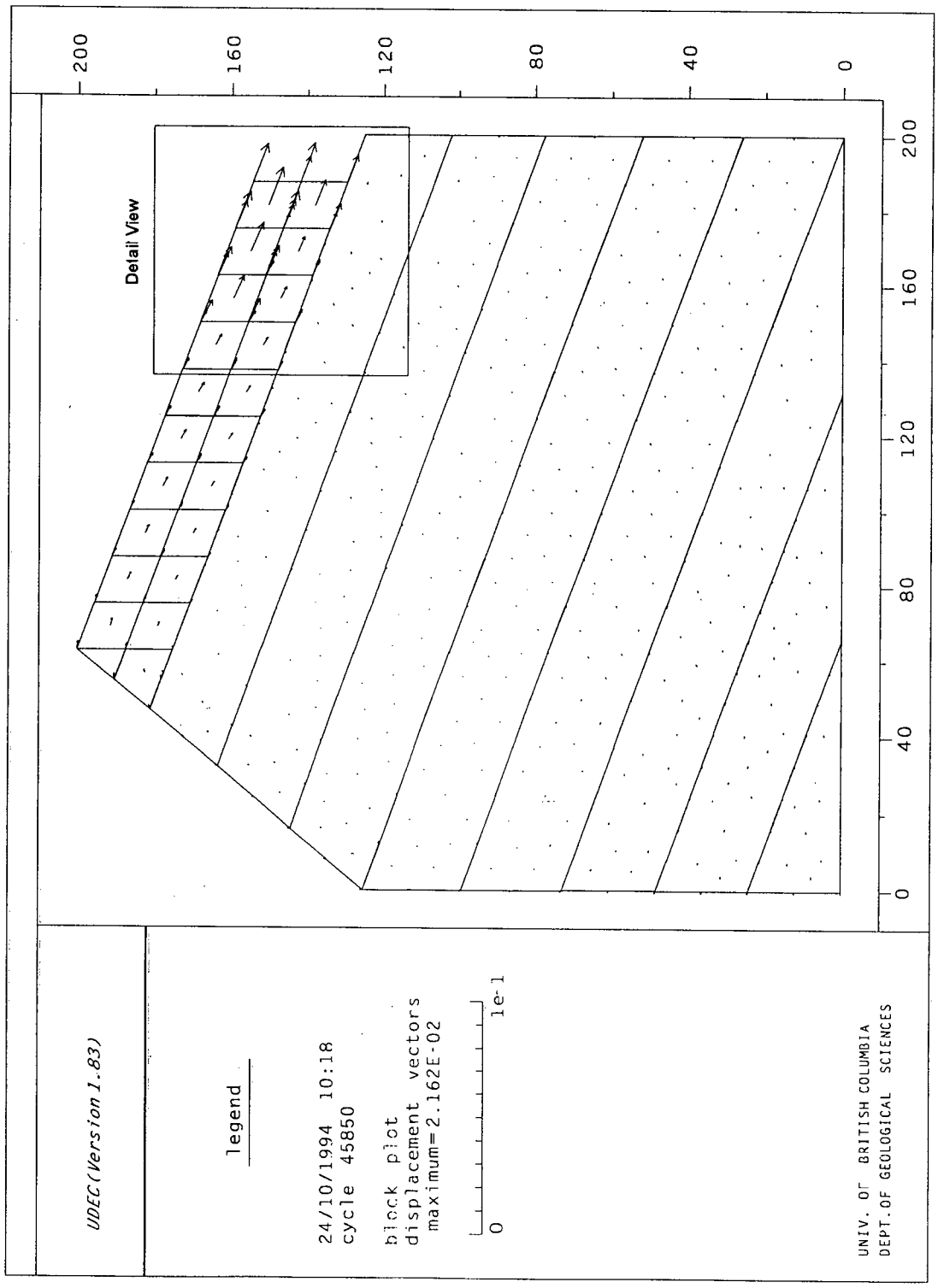

Figure 6.7 *Displacement vectors after 5 load cycles for the linear joint model.*

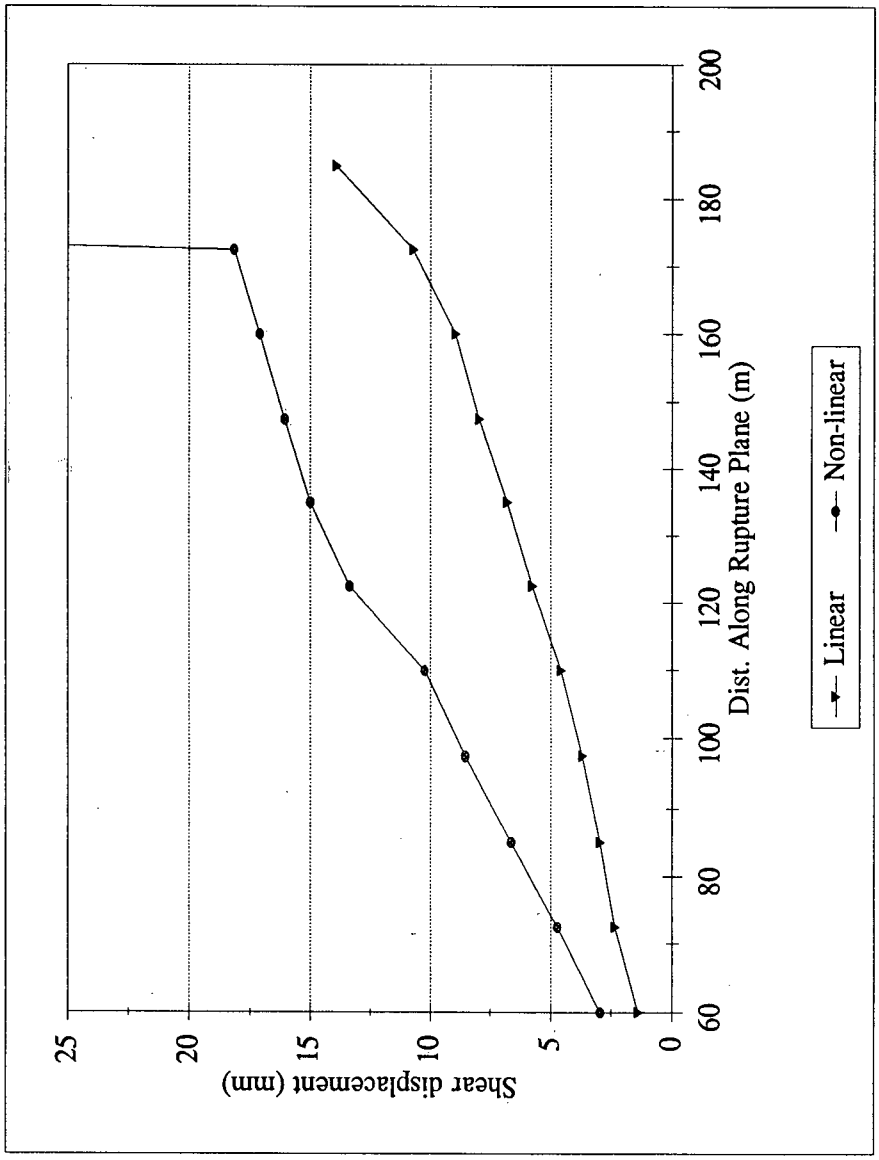

Figure 6.8. *Shear displacement along the basal slip surface after 4 load cycles.*

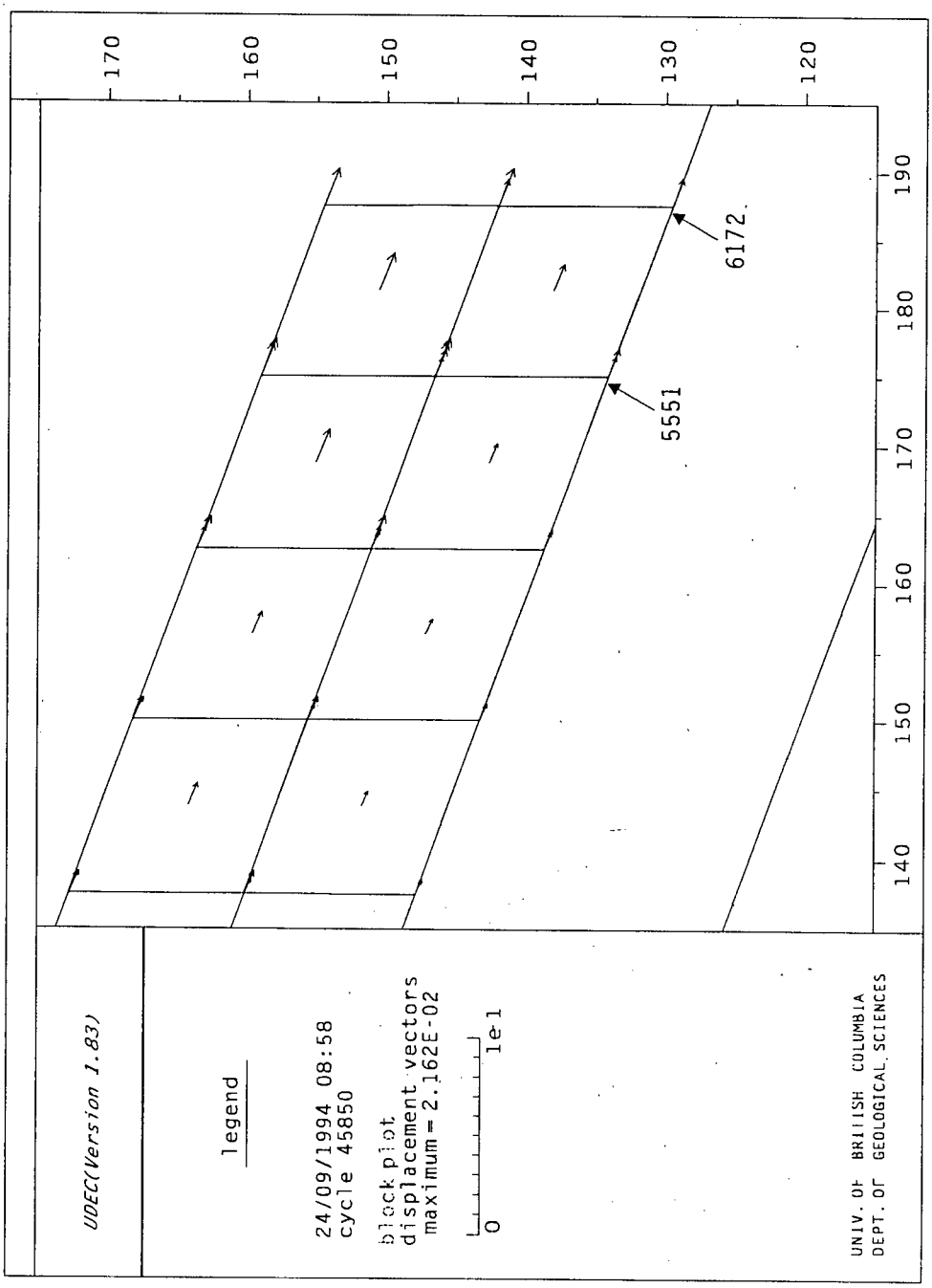

Figure 6.9. *Detail view from Figure 6.7.*

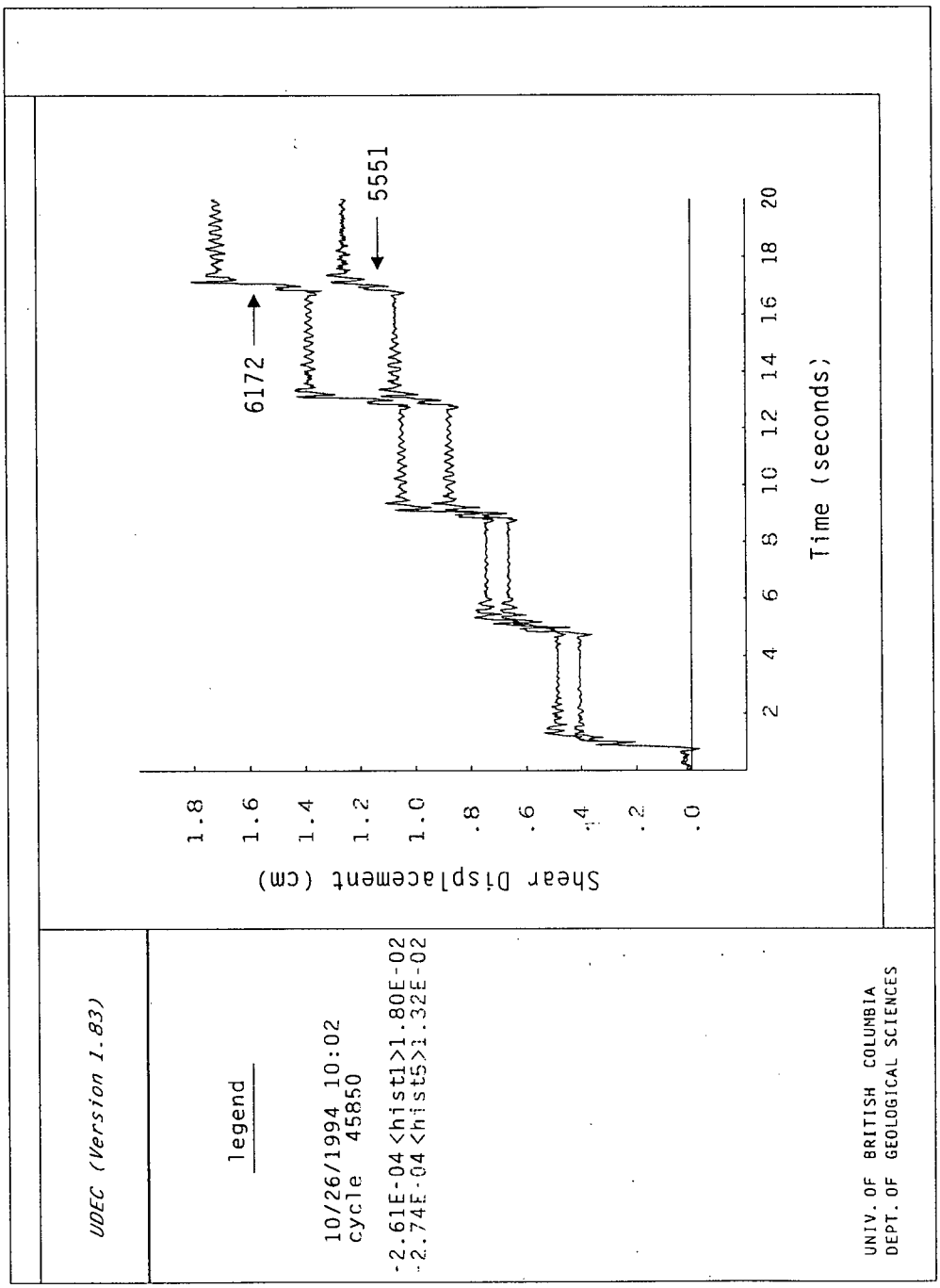

Figure 6.10. *Shear displacement on contacts 6172 and 5551 (linear joint model)*

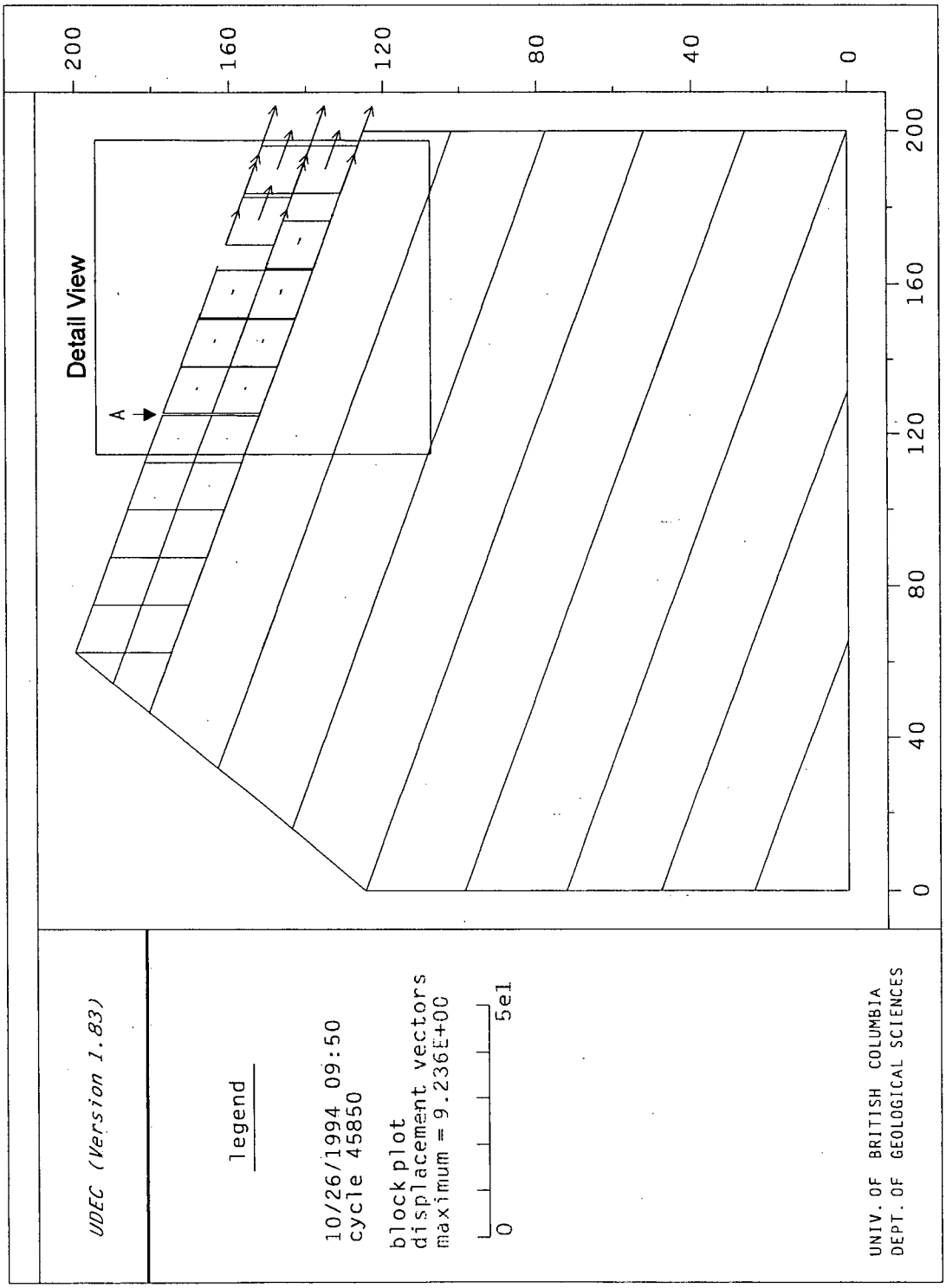

Figure 6.11 *Displacement vectors after 5 load cycles for the C-Y joint model.*

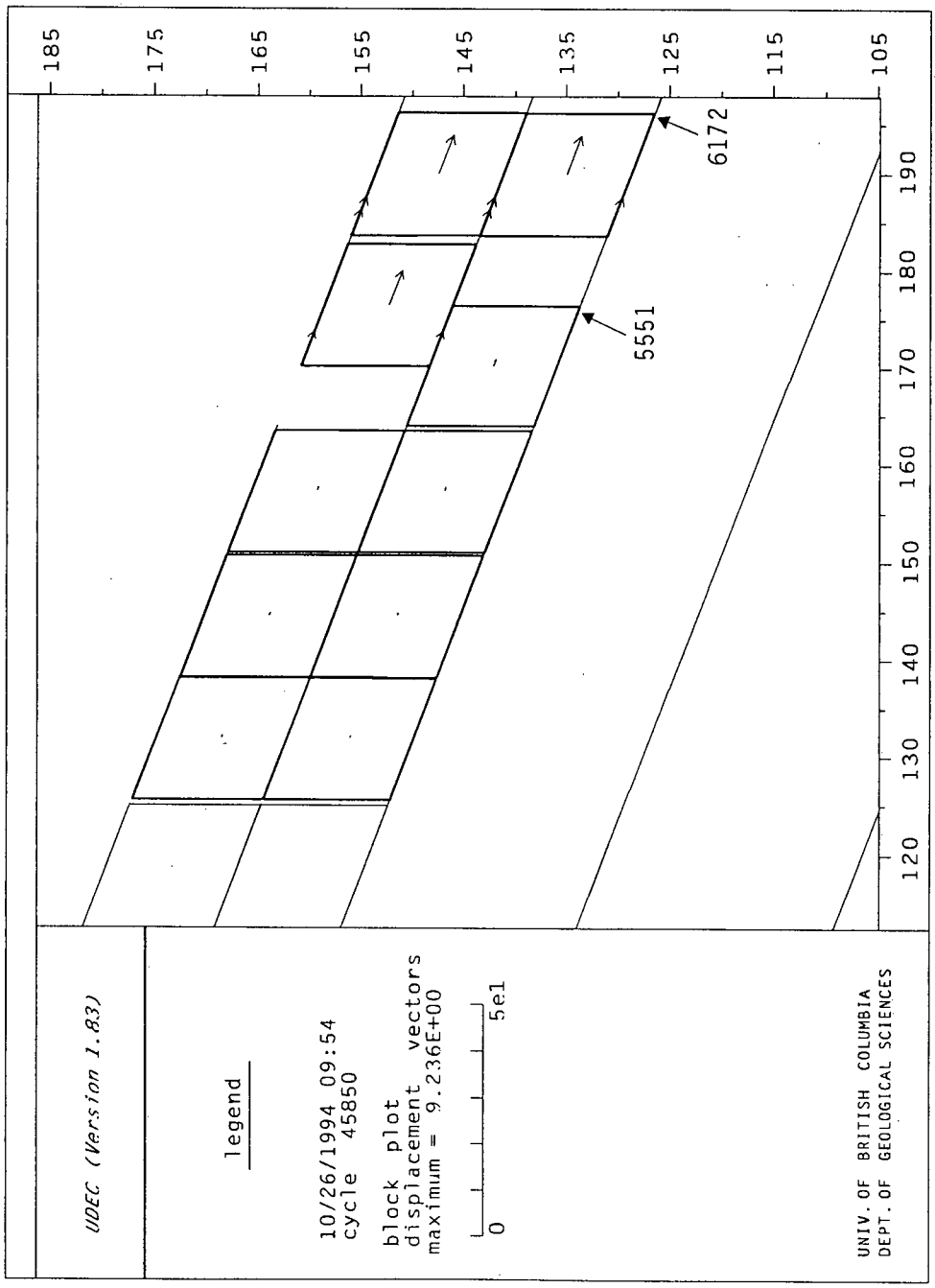

Figure 6.12. *Detail view from Figure 6.11.*

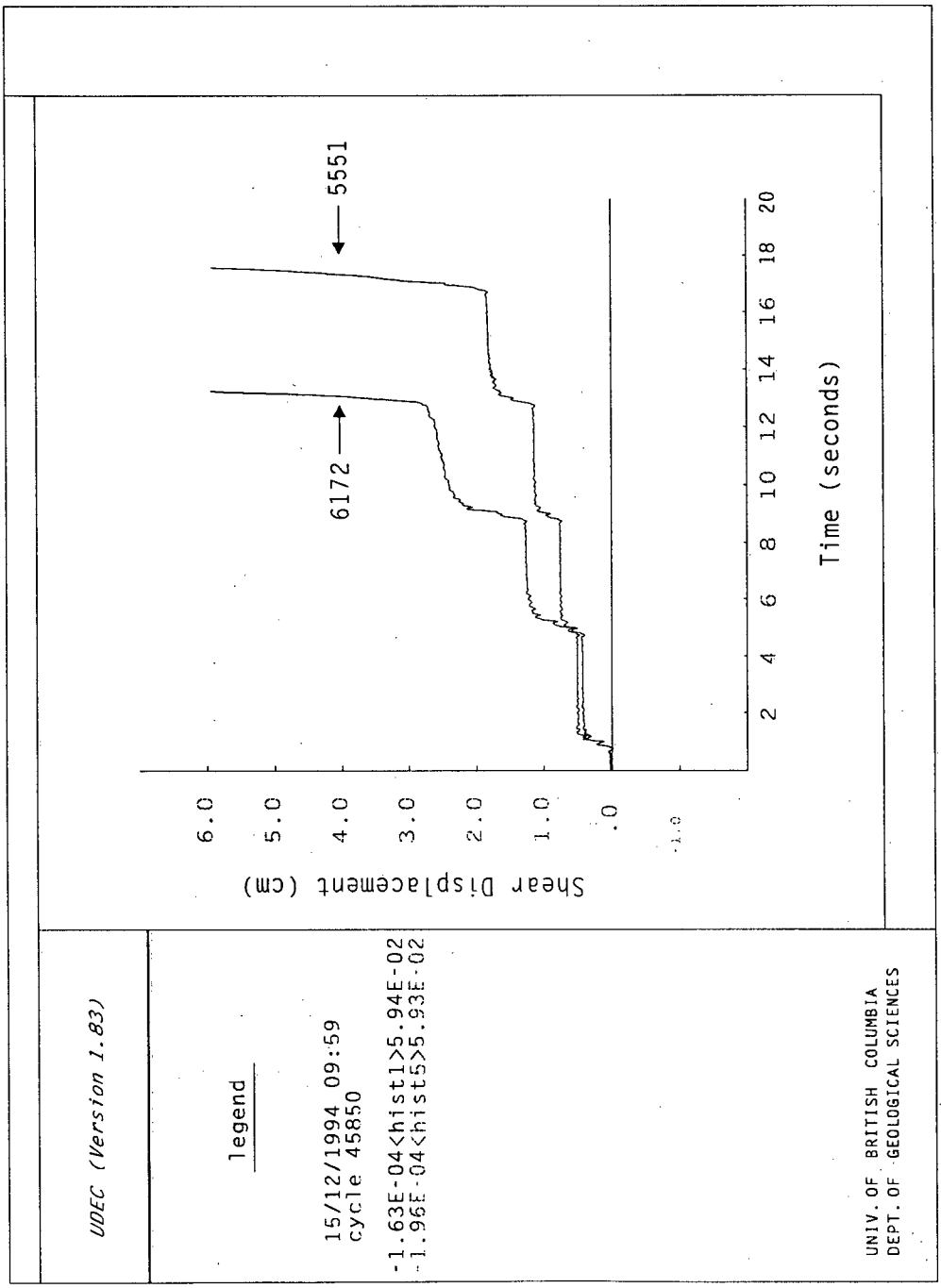

Figure 6.13. *Shear displacement on contacts 6172 and 5551 (C-Y joint model)*

CHAPTER 7

Conclusions

This research was undertaken to explore the relationship between large landslides and neotectonic processes in mountainous terrain. The focus of the study changes as data from the regional assessment is used to characterize a local, but generalized study of the role of seismicity as a slope deformation process.

The regional distribution of landslides in southwest Yukon correlates with several factors. Landslides are markedly more frequent in Neogene volcanic rocks (Wrangell Lavas) and in Permo-Pennsylvanian meta-sediments and meta-volcanics of Skolai Group. The higher number of landslides in these rocks can be attributed to the presence of pervasive structural discontinuities within them, and their high topographic position, which is accentuated by erosion and broad regional uplift. Landslides correlate well with zones of weakened rock adjacent to regional faults, and are comparatively more common near fault segments known to be seismically active. All of these factors impart a spatial bias to the landslide distribution.

Seismicity is particularly dense in the Cement Creek area. In addition to a high spatial density of landslides, the apparent temporal distribution departs from the expected regional slope exhaustion model. The geology, geomorphology, and landslides in this area were studied in relatively more detail during field reconnaissance in preparation for numerical studies of seismogenic slope deformation.

Program UDEC was selected for the dynamic numerical analyses, and limited verification testing was undertaken. UDEC simulations compare well with closed-form solutions for elasto-plastic shear displacement and vertical shear wave propagation in geometrically simple systems.

Results of generalized slope analyses with UDEC show a correlation between the observed geomorphic features associated with slope deformation in the Cement Creek area and comparatively low-magnitude seismic loading. The formation and pattern of ground cracking observed in the field can be explained by incremental slope displacement. Earthquake loading is shown to be a viable landslide triggering mechanism.

BIBLIOGRAPHY

Alheid, H.J., K.G. Hinzen, A. Honecker, & W. Sarfield 1988. Response of underground openings to earthquake and blasting loading. Proc. Sixth Int. Congress on Numerical Modelling in Geomechanics (Innsbruck 1988): G. Swoboda (ed.), pp. 1689-1696. Balkema: Rotterdam.

Bandis, S.C. 1990. Scale effects in the strength and deformability of rocks and rock joints. Scale Effects in Rock Masses: P. da Cunha (ed.), pp. 59-76. Balkema: Rotterdam: Brookfield.

Bandis, S.C., A.C. Lumsden, & N.R. Barton 1983. Fundamentals of rock joint deformation. International Journal of Rock Mechanics Mineral Science and Geomechanics Abstracts, Vol. 20, No. 6, pp. 249-268.

Bardet, J.-P., & R.F. Scott 1985. Seismic stability of fractured rock masses with the distinct element method. Proc. 26th US Symposium on Rock Mechanics, Rapid City, SD, June 1985, pp. 139-149.

Barton, N.R. 1990. Scale effects or sampling bias?. Scale Effects in Rock Masses, P. da Cunha (ed.), pp. 31-58. A.A. Balkema: Rotterdam: Brookfield.

Barton, N.R., & K. Bhaktar 1987. Description and modeling of rock joints for the hydrothermalmechanical design of nuclear waste units, Paper TR-418, Vol. 1. Terra Tek Engineering, Atomic Energy of Canada Ltd. 319 p.

Barton, N.R., & S.C. Bandis 1980. Some effects of scale on the shear strength of joints. Internatioal Journal of Rock Mechanics Mineral Sciences and Geomechanics Abstracts, Vol. 17, No. 1, pp. 69-73.

Bayrock, L.A., & T.H.F. Reimchem 1980. Surficial geology, Alberta Foothills and Rocky Mountains (6 maps). Alberta Research Council, Edmonton, Alberta.

Berg, H.C., D.L. Jones, & D.H. Richter 1972. Gravina-Nutzotin Belt - tectonic significance of an upper Mesozoic sedimentary and volcanic sequence in southern and southeastern Alaska. Professional Paper 800-D, U.S.G.S. Research 1972, pp. 1-24.

Bostock, H.S. 1948. Physiography of the Canadian Cordillera, with special reference to the area north of the fifty-fifth parallel. Geological Survey of Canada. Memoir 247, Department of Mines and Resources-Mines and Geology Branch: 106 p.

_____ 1952. Geology of northwest Shakwak Valley, Yukon Territory. Memoir 267, Geological Survey of Canada. Department of Mines and Technical Surveys. Queen's Printers: Ottawa: 54 p.

Brabb, E.E. 1984. Innovative approaches to landslide hazard and risk mapping. Proc. IV International Symposium on Landslides, Vol. 1, pp. 307-323. Toronto: Canada.

Brady, B., & J.V. Lemos 1988. Dynamic analysis of surface rock structures. *Reprint:* Proc. Secondo Ciclo di Conferenze di Meccanica e Ingegneria Delle Rocce, Torino, 1988. 11 p.

Burn, C.R. 1994. Permafrost, tectonics, and past and future regional climate change, Yukon and adjacent Northwest Territories. Canadian Journal of Earth Sciences, Vol. 31, No. 1, pp. 182-191.

Campbell, R.B., & C.J. Dodds 1975. Operation St. Elias, Yukon Territory. Geological Survey of Canada, Report of Activities Part A, Paper 75-1A, pp. 51-54..

_____ 1978. Operation St. Elias, Yukon Territory. Geological Survey of Canada, Current Research Part A, Paper 78-1A, pp. 35-41.

_____ 1979. Operation St. Elias, Yukon Territory. Geological Survey of Canada, Current Research Part A, Paper 79-1A, pp. 17-20..

Chase, C.G. 1978. Plate kinematics: the Americas, east Africa, and the rest of the world. Earth Planet. Sci. Let. No. 37, pp. 355-368.

Clague, J.J. 1979. The Denali Fault System in southwest Yukon Territory - a geologic hazard?. Geological Survey of Canada, Current Research Part A, Paper 79-1A, pp. 169-178.

_____ 1981. Landslides at the south end of Kluane Lake, Yukon Territory. Canadian Journal of Earth Sciences, Vol. 18, No. 5, pp. 959-971.

_____ 1982. The role of geomorphology in the identification and evaluation of natural hazards. Applied Geomorphology: R.J. Craig and J.L. Craft (eds.),pp. 17-43. George Allen and Unwin: New York.

Clough, R.W., & A.K. Chopra 1966. Earthquake stress analysis in earth dams. Journal of the Engineering Mechanics Division, ASCE, Vol. 92, No. EM2, Proc. Paper 4793, pp. 197-211.

Coates, D.R. 1977. Landslide perspectives. The Geological Society of America, Reviews in Engineering Geology, Vol. 3: D.R. Coates (ed.), pp. 3-28..

Crawford, A.M., & J.H. Curran 1982. The influence of rate- and displacement-dependent shear resistance on the response of rock slopes to seismic loads. International Journal of Rock Mechanics Mineral Science and Geomechaniccs Abstracts, Vol. 9, pp. 1-8. Pergamon: Great Britain.

Cruden, D.M. 1985. Rock slope movements in the Canadian Cordillera. Canadian Geotechnical Journal, Vol. 22, No. 4, pp. 528-540.

Cruden, D.M., & Z.Y. Lu 1992. The rockslide and debris flow from Mt. Cayley, B.C. in June 1984. Canadian Geotechnical Journal, Vol. 29, pp. 614-626.

Cruden, D.M., & T.M. Eaton 1987. Reconnaissance of rockslide hazards in Kananaskis country, Alberta. Canadian Geotechnical Journal Vol. 24, No. 3, pp. 414-429.

Cruden, D.M. & X.Q. Hu 1993. Exhaustion and steady-state models for predicting landslide hazards in the Canadian Rocky Mountains. Geomorphology, Vol. 8, No. 4, pp. 279-285.

da Cunha, P. 1990. Scale effects in rock mechanics. Scale Effects in Rock Masses: P. da Cunha (ed.), pp. 3-30. Balkema: Rotterdam: Brookfield.

Cundall, P.A. 1971. A computer model for simulating progressive large scale movements of blocky rock systems. Proc. of the Symposium of the International Society of Rock Mechanics, Vol. 1. Nancy; France.

_____ 1980. UDEC - a generalized distinct element program for modelling jointed rock. FInal Technical Report, European Research Office, U.S. Army: March, 1980.

_____ 1987. Distinct element models of rock and soil structure. Analytical and Computational Methods in Engineering Rock Mechanics: E.T. Brown (ed.), pp. 129-163. London: George Allen and Unwin.

Cundall, P.A., & M. Board 1988. A microcomputer program for modelling large-strain plasticity problems. Proc. Sixth International Congress on Numerical Methods in Geomechanics (Innsbruck 1988), G. Swoboda (ed.), pp. 2101-2108. Balkema: Rotterdam.

Cundall, P.A., & J.V. Lemos 1988. Numerical simulation of fault instabilities with the continuously-yielding joint model. Proc. of the 2nd International Symposium of Rockbursts and Seismicity in Mines, Minnesota, June 1988. 14 p.

Dafalias, Y.F., & L.R. Herrmann 1982. Bounding surface formulation of soil plasticity. Soil Mechanics - Transient and Cyclic Loads, Vol. 10, pp. 253-282. John Wiley and Sons: Chichester.

DeGraff, J.V., & P. Canuti 1988. Using isopleth mapping to evaluate landslide activity in relation to agricultural practises. Bulletin of the International Association of Engineering Geology, Vol. 38.

Denton, G.H., & R.L. Armstrong 1969. Miocene-Pliocene glaciations in southern Alaska. Geological Society of America Bulletin, Vol. 267, pp. 1121-1142.

Denton, G.H., & M. Stuiver 1967. Late Pleistocene glacial stratigraphy and chronology, northeastern St.. Elias Mountains, Yukon Territory, Canada. Geological Society of America Bulletin, Vol. 78, pp. 485-510.

Denton, G.H. 1974. Quaternary glaciation of the White River Valley, Alaska, with a regional synthesis for the northern St. Elias Mountains, Alaska and Yukon Territory. Geological Society of America Bulletin, Vol. 85, pp. 871-892.

Department of Energy, Mines and Resources 1978. Snag, Yukon Territory (115J & 115K), edition 2. Surveys and Mapping Branch: Ottawa.

_____ 1978. Mount St. Elias, Canada-United States of America (115B and 115C), edition 2. Surveys and Mapping Branch: Ottawa.

_____ 1983. Steele Creek, Yukon Territory (115G/5), edition 2. Surveys and Mapping Branch: Ottawa.

_____ 1987. Tempest Mountain, Yukon Territory (115F/8), edition 1. Surveys and Mapping Branch: Ottawa.

Department of Mines and Technical Surveys 1961. Kluane Lake, Yukon Territory (115G and 115F, E½), edition 1. Surveys and Mapping Branch: Ottawa.

_____ 1951. Dezadeash, Yukon Territory (115A). Topographic Survey: Ottawa.

Desai, C.S., & J.F. Abel 1972. Introduction to the finite element method: A numerical method for engineering analysis. Van Nostrand Reinhold Company: New York: Cincinatti: Chicago. 477 p.

Dezfulian, H., & H.B. Seed 1970. Seismic response of soil deposits underlain by sloping rock boundaries. Journal of the Soil Mechanics and Foundations Division, ASCE, Vol. 96, No. SM6, Proc. Paper 7659, pp.1893-1916.

Dodds, C.J. 1982*a*. S.W. Kluane Lake map area, Yukon Territory, 115 G&F (E½). Geological Survey of Canada, Open File 829.

_____ 1982*b*. Mt. St. Elias map area, Yukon Territory, 115 B&C. Geological Survey of Canada, Open File 830.

_____ 1982*c*. S.W. Dezadeash map area, Yukon Territory, 115 A. Geological Survey of Canada, Open File 831.

Eisbacher, G.H. 1975. Operation St. Elias, Yukon Territory: Dezadeash Group and Amphitheatre Formation. Geological Survey of Canada, Report of Activities Part A, Paper 75-1A, pp. 61-62.

_____ 1976. Sedimentology of the Dezadeash flysch and its implications for strike-slip faulting along the Denali Fault, Yukon Territory and Alaska. Canadian Journal of Earth Sciences, Vol. 13, pp. 1495-1513.

_____ 1978. Observations on the streaming mechanism of large rock slides, northern Cordillera. Geological Survey of Canada, Current Research Part A, Paper 78-1A, pp. 49-52.

_____ 1979. Cliff collapse and rock avalanches (sturzstroms) in the Mackenzie Mountains, Northwestern Canada. Canadian Geotechnical Journal, Vol. 16, No. 2, pp. 309-334.

Eisbacher, G.H., & S.L. Hopkins 1977. Mid-Cenozoic paleogeomorphology and tectonic setting of the St. Elias Mountains, Yukon Territory. Geological Survey of Canada, Report of Activities Part B, Paper 77-1B, pp. 319-335.

Environment Canada 1993. Canadian climate normals, 1961-1990. Vol. 3. Atmospheric Environment Service. Canada.

Erdmer, P. 1991. Metamorphic terrane east of Denali Fault between Kluane Lake and Kusawa Lake, Yukon Territory. Geological Survey of Canada, Current Research Part A, Paper 91-1A, pp. 37-42.

Evans, S.G., J.D. Aitken, R.J. Wetmiller, & R.B. Horner 1987. A rock avalanche triggered by the October 1985 North Nahanni Earthquake, District of Mackenzie, N.W.T. Canadian Journal of Earth Sciences, Vol. 24, No. 1, pp. 176-184.

Evans, S.G., & J.J. Clague 1988. Catastrophic rock avalanches in glacial environments. Landslides. Proc. of the Fifth International Symposium on Landslides, Vol. 2: C. Bonnard (ed.), pp. 1153-1158.

_____ 1989. Rain induced landslides in the Canadian Cordillera, July, 1988. Geoscience Canada, Vol. 16, No. 3, pp. 193-200.

Evans, S.G., J.J. Clague, G.J. Woodsworth, & O. Hungr 1989. The Pandemonium Creek rock avalanche, British Columbia. Canadian Geotechnical Journal, Vol. 26, No. 3, pp. 427-446.

Evans, S.G., & D.R. Lister 1983. The geomorphic effects of the July 1983 rainstorms in the southern Canadian Cordillera and their impact on transportation facilities. Geological Survey of Canada, Current Research Part B, Paper 84-1B, pp. 223-235.

Finn, W.D.L., M. Yogendrakumar, & N. Yoshida 1988. Dynamic nonlinear hysteretic effective stress analysis in geotechnical engineering. Proc. Sixth Int. Congress on Numerical Modelling in Geomechanics, Innsbruck, Austria: G. Swoboda (ed.). Balkema: Rotterdam.

Freeze, R.A. 1987. Modelling interrelationships between climate, hydrology and hydrogeology and the development of slopes. Slope stability: geotecnical enginering and geomorphology: M.G. Anderson and K.S. Richards (eds.), pp. 381-403. John Wiley and Sons Ltd.: Chichester.

French, H.M. 1985. Periglacial landforms and processes in the western Canadian arctic. Periglacial processes and landforms in Britain and Ireland, J. Boardman (ed.), pp. 27-43. Cambridge University Press: Cambridge.

Gardner, J.S. 1980. Frequency, magnitude, and spatial distribution of mountain rockfalls and rockslides in the Highwood Pass area, Alberta, Canada. Thresholds in Geomorphology: D.R. Coates and J.D. Vitek (eds.), pp. 267-295. George Allen & Unwin: London: Boston: Sydney.

Ghosh A., & W. Haupt 1989. Computation of the seismic stability of rock wedges. Rock Mechanics, Vol. 22, pp. 109-125. Springer-Verlag.

Goodman, R.E., F.E. Heuze, & Y. Ohnishi 1972. Research on strength-deformability-watre pressure relationship for faults in direct shear. University of California, Berkeley, Reports on ARPA contract.

Goodman, R.E., R.L. Taylor, & T.L. Brekke 1968. A model for the mechanics of jointed rock. Journal of the Soil Mechanics and Foundations Division, ASCE, No. SM3, pp. 637-658.

Hansen, A., & C.A.M. Franks 1991. Characterisation and mapping of earthquake triggered landslides for seismic zonation. Proc. EERI Fourth International Conference on Seismic Zonation, State-of-the-art-papers, pp. 149-195. Stanford, California

Heginbottom, J.A., & L.K. Radburn 1992. Permafrost and ground-ice conditions of northwestern Canada. Geological Survey of Canada, Map 1691*a*.

Hendron Jr., A.J., & F.D. Patton 1985. The Vaiont Slide, a geotechnical analysis based on new geologic observations of the failure surface, Vol. 1. Technical Report GL-85-5: U.S. Army Corps of Engineers: Washington, DC.

Heuze, F.E. 1980. Scale effects in the determination of rock mass strength and deformability. Rock Mechanics, Vol. 12, pp. 167-192. Springer-Verlag: Vienna: New York.

Hodge, R.A.L., & Freeze, R.A. 1977. Groundwater flow systems and slope stability. Canadian Geotechnical Journal, Vol. 14, No.4, pp. 466-476.

Horner, R.B. 1983. Seismicity in the St. Elias region of northwestern Canada and southeastern Alaska. Bulletin of the Seismological Society of America, Vol. 73, No. 4, pp. 1117-1137.

_____ 1988. Seismicity in the Glacier Bay region of southeast Alaska and adjacent areas of British Columbia. Proc. Second Glacier Bay Science Symposium, pp. 6-11. U.S. Dept. of the Interior, National Park Service: Alaska..

Hunt, R.E. 1986. Slope and embankment stability. Geotechncal Engineering Techniques and Practise, 729 p. McGraw Hill: USA.

Hutchison, J. 1988. TITLE MISSING. Proc. International Conference on Landslide Hazards, Lausanne, Switzerland, 1988.

Idriss, I.M., H. Bolton Seed, & N. Serff 1974. Seismic response by variable damping finite elements. Journal of the Geotechnical Engineering Division, ASCE, Vol. GT1, Proc. Paper 10284, pp. 1-13.

Itasca Consulting Group, Inc. 1992. UDEC: Universal Distinct Element Code. User's Manual, Version ICG 1.83, 601 p.

Kaliser, B.N., & R.W. Fleming 1986. The 1983 landslide dam at Thistle, Utah. Landslide Dams: Processes, Risk, and Mitigation: R.L. Schuster (ed.). Geotechnical Special Publication No. 3, ASCE, pp. 59-83. New York.

Keefer, D.K. 1984. Landslides caused by earthquakes. Geological Society of America Bulletin, Vol. 95, pp. 406-421.

Kindle, E. D. 1953. Dezadeash map area, Yukon Territory. Geological Survey of Canada, Memoir 268. Dept. of Mines and Technical Surveys. Queen's Printers: Ottawa: 68 p.

Kuhlmeyer, R.L., & J. Lysmer 1973. Finite element method accuracy for wave propogation problems. Journal of the Soil Mechanics and Foundations Division, ASCE, Vol. 99 SM-5, pp. 421-427.

Lama, R.D., & V.S. Vutukuri 1978*a*. Laboratory mechanical properties of rock. Handbook on Mechanical Properties of Rocks - Testing Techniques and Results. Series on Rock and Soil Mechanics, Vol. 2. Trans Tech Publications: Germany: 481 p.

_____ 1978*b*. In-Situ Testing of Rock. Handbook on Mechanical Properties of Rocks - Testing Techniques and Results. Series on Rock and Soil Mechanics, Vol. 3. Trans Tech Publications: Germany: 406 p.

_____ 1978*c*. Mechanical Behaviour of Jointed Rock. Handbook on Mechanical Properties of Rocks - Testing Techniques and Results. Series on Rock and Soil Mechanics, Vol. 4. Trans Tech Publications: Germany: 515 p.

Lanphere, M.A. 1978. Displacement history of the Denali Fault System, Alaska and Canada. Canadian Journal of Earth Sciences, Vol. 13, pp. 817-822.

Lemos, J.V., R.D. Hart, & P.A. Cundall 1985. A generalized distinct element program for modelling jointed rock mass. Proc. of the International Symposium on Fundamentals of Rock Joints (Bjorkliden): Stephansson (ed.), pp. 335-343. Centek.

Lisowski M., J.C. Savage, & R.O. Burford 1987. Strain accumulation across the Fairweather and Totschunda Faults, Alaska. Journal of Geophysical Research, Vol. 92, No. B11, pp. 11,552-11,560.

Lorig, L.J., R.D. Hart, & P.A. Cundall 1991. Slope stability analysis of jointed rock using the distinct element method. *Preprint:* Proc. of the Transportation Research Board, 70th Annual Meeting, January 1991. 32 p (with figures).

Lysmer, J., & R.L. Kuhlemeyer 1969. Finite dynamic model for infinite media. Journal of Engineering Mechanics, ASCE, Vol. 95 EM-4.

Lu, Z. 1993. Landslides and geotechnical properties of volcanic tuff on Mt. Cayley, British Columbia. Unpublished Ph.D. thesis, The University of Alberta, 263 p.

Mackevett Jr., E.M. 1978. Geological map of the McCarthy quadrangle, Alaska. Map I-1032, United States Geological Survey. Dept. of the Interior.

Miller, D.J. 1960. The Alaska earthquake of July 10, 1958: giant wave in Lituya Bay. Bulletin of the Seismological Society of America, Vol. 50, No. 2, pp. 253-266.

Minister, J.B., & T.H. Jordan 1978. Present-day plate motions. Journal of Geophysical Research, Vol. 92, pp. 5331-5334.

Mollard, J.D. 1977. Regional landslide types in Canada. Reviews in Engineering Geology, Vol. 3: D.R. Coates (ed.), pp 29-58. The Geological Society of America.

_____1988. First R.M. Hardy memorial lecture: fracture lineament research and applications on the western Canadian plains. Canadian Geotechnical Journal, Vol. 25, No. 4, pp. 749-767.

Monger, J.W.H. 1989. Overview of Cordilleran geology. Western Canada Sedimentary Basin, A Case History: B. Ricketts (ed.). Canadian Society of Petroleum Geologists: Calgary.

Muller, J.E. 1967. Kluane Lake map area, Yukon Territory. Geological Survey of Canada, Memoir 340. Department of Energy Mines and Resources Canada: 137 p.

Newmark, N.M. 1965. Effects of earhquakes on dams and embankments. Milestones in Soil Mechanics: The First Ten Rankine Lectures, pp. 109-130. The Institution of Civil Engineers: Thomas Telford Ltd..

Nilsen, T.H., & E.E. Brabb 1977. Slope-stability studies in the San Francisco Bay region, California. Reviews in Engineering Geology, Vol. 3: D.R. Coates (ed.), pp. 235-243. The Geological Society of America.

Otter, J.R.B., A.C. Cassell, & R.E. Hobbs 1966. Dynamic Relaxation. Proc. of the Institute of Civil Engineering, December, 1966, pp. 633-656.

Palmer, L. 1977. Large landslides of the Columbia River gorge, Oregon and Washington. Reviews in Engineering Geology, Vol. 3: D.R. Coates (ed.), pp. 69-84. The Geological Society of America.

Pasamehmetoglu, A.G., C. Karpuz, & T.Y. Irfan 1981. The weathering characteristics of Ankara andesites from the rock mechanics point of view. Proc. of the International Symposium on Weak Rock, Tokyo: K. Akai, M. Hayashi, and Y. Nishimatsu (eds.), pp. 185-190.

Perez, O.J., & K.H. Jacob 1980. Tectonic model and seismic potential of the eastern Gulf of Alaska and Yakataga seismic gap. Journal of Geophysical Research, Vol. 85, No. B12, pp. 7132-7150.

Piteau, D. 1977. Regional slope-stability controls and engineering geology of the Fraser Canyon, British Columbia. Reviews in Engineering Geology, Vol. 3, D.R. Coates (ed.), pp. 85-112. The Geological Society of America.

Plafker, G. 1968. Source areas of the Shattered Peak and Pyramid Peak landslides at Sherman Glacier. *Reprint:* The Great Alaska Earthquake of 1964, Vol. 3. National Academy of Sciences: Washington D.C.

_____ 1987. Regional geology and petroleum potential of the northern Gulf of Alaska continental margin. Earth Science Series Vol. 6, Geology and Resource Potential of the Continental Margin of Western North America and Adjacent Ocean Basins: D.W. Scholl, A. Grantz, & J.G. Vedder (eds.), pp. 229-268. Circum-Pacific Council for Energy and Mineral Resources.

Plafker, G., & G.E. Ericksen 1978. Nevados Huascaran avalanches, Peru. Rockslides and Avalanches, Vol. 1, Natural Phenomena: B. Voight (ed.), pp. 277-314. Elsevier Scientific Publishing Company: New York.

Plafker, G., T. Hudson, & D.H. Richter 1977. Preliminary Observations on late Cenozoic displacements along the Totschunda and Denali Fault systems. U.S.G.S. Circular 751-B: United States Geological Survey.

Plafker G., T. Hudson, T. Bruns, & M. Rubin 1978. Late Quaternary offsets along the Fairweather Fault and crustal plate interactions in Southern Alaska. Canadian Journal of Earth Sciences Vol. 15, No. 5, pp. 805-816.

Plafker, G., W.J. Nokleberg, & J.S. Lull 1989. Bedrock geology and tectonic evolution of the Wrangellia, Peninsular, and Chugach terranes along the trans-Alaska crustal transect in the Chugach Mountains and southern Copper River Basin, Alaska. Journal of Geophysical Research, Vol. 94, No. B4, pp. 4255-4295.

Polloni, G., M. Cerriani, S. Lauzi, S. Padovan, & G. Crosta 1991. Rainfall and soil slipping events in Valtellina. Landslides, Vol. 1: D.H. Bell (ed.), pp. 183-188. Balkema: Rotterdam.

Pritchard, M.A. 1989. Numerical modelling of large scale toppling. Unpublished M.A.Sc. thesis, University of British Columbia. 179 p.

Radbruch-Hall, D.H., R.B. Colton, W.E. Davies, I. Lucchita, B.A. Skipp, & D.J. Varnes 1982. Landslide overview map of the conterminous United States. Geological Survey Professional Paper 1183. United States Geological Survey. 25 p.

Rampton, V.N. 1971. Late pleistocene glaciations of the Snag-Klutlan area, Yukon Territory. Arctic, Vol. 24, No. 4, pp. 277-300.

_____ 1979*a*. Surficial geology and geomorphology, Burwash Creek, Yukon Territory. Map 6-1978, Geological Survey of Canada.

_____ 1979*b*. Surficial geology and geomorphology, Generc River, Yukon Territory. Map 7-1978, Geological Survey of Canada.

_____ 1979*c*. Surficial geology and geomorphology, Congdon Creek, Yukon Territory. Map 8-1978, Geological Survey of Canada.

_____ 1981. Surficial materials and landforms of Kluane National Park, Yukon Territory. Geological Survey of Canada, Paper 79-24. Energy Mines and Resources Canada. 37 p.

Ray, R.G. 1972. Aerial photographs in geologic interpretation and mapping. Geological Survey Professional Paper 373. United States Department of the Interior. 221 p.

Read, P.B. 1976. Operation St. Elias, Yukon Territory: pre-Cenozoic volcanic assemblages in the Kluane Ranges. Geological Survey of Canada, Report of Activities, Part A, Paper 76-1A, pp. 187-193.

Read, P.B., & J.W.H. Monger 1975. Operation St. Elias, Yukon Territory: the Mush Lake Group and Permo-Triassic rocks in the Kluane Ranges. Geological Survey of Canada, Report of Activities, Part A, Paper 75-1A, pp. 55-59.

Rib, H.T., & T. Liang 1978. Recognition and identification. Landslides: analysis and control: R.L. Schuster and J.K. Kryzek (eds.), pp. 34-80. Special Report 176, Transportation Research Board, National Research Council, National Academy of Sciences: Washington D.C.

Richter, D.H. 1976. Geological map of the Nabesna quadrangle, Alaska. Map I-932, United States Geological Survey. Dept. of the Interior.

Richter, D.H., & D.L. Jones 1973. Structure and stratigraphy of the eastern Alaska Range. Arctic Geology, Memoir 19, pp. 408-420. American Association of Petroleum Geologists.

Richter, D.H., & N.A. Matson, Jr. 1971. Quaternary faulting in the eastern Alaska Range. Geological Society of America Bulletin, Vol. 82, No. 6, pp. 1529-1540.

Ruiz, M.D., F.P. Camargo, N.F. Midea, & C.M. Nieble 1970. Some considerations regarding the shear strength of rock masses. Proc. International Symposium on Rock Mechanics, Madrid, pp. 159-169.

Savigny, K.W. *in press*. Engineering geology of large landslides in the lower Fraser River valley transportation corridor, southwestern Canadian Cordillera. Manuscript, accepted for publication. Canadian Geotechnical Journal: 35 p.

Scheidegger, A.E. 1973. On the prediction of the reach and velocity of catastrophic landslides. Rock Mechanics, Vol. 5, pp. 231-236. Springer-Verlag.

Shi, G.H., S., & R.E. Goodman 1989. Generalization of two-dimensional discontinuous deformation analysis for forward modelling. International Journal for Numerical and Analytical Methods in Geomechanics, Vol. 13, pp. 359-380.

Skulski, T., & D. Francis 1986. On the geology of the Tertiary Wrangell lavas in the St. Clare Province, St. Elias Mountains, Yukon. Yukon Geology, Vol. 1, pp. 161-170. Exploration and Geological Services Division Yukon: Indian and Northern Affairs Canada.

Souther, J.G. 1974. Cordilleran volcanic project. Geological Survey of Canada, Report of Activities, Part A, Paper 74-1A, pp. 39-41.

Starfield, A.M., & P.A. Cundall 1988. Towards a methodology for rock mechanics modelling. International Journal of Rock Mechanics Mineral Sciences and Geomechanics Abstracts, Vol 25, No. 3, pp. 99-106.

Taga Inc. 1989. TNMN (Version 1.13) Short Users Guide. 5p.

Tempelman-Kluit, D.J. 1974. Reconnaissance geology of Aishihik Lake, Snag and part of Stewart River map areas, west central Yukon. Geological Survey of Canada, Paper 73-41. Department of Energy, Mines and Resources: 97 p.

_____ 1976. The Yukon crystalline terrane: enigma in the Canadian Cordillera. Geological Society of America Bulletin, Vol. 87, pp. 1343-1357.

_____ 1980. Evolution of physiography and drainage in southern Yukon. Canadian Journal of Earth Sciences, Vol. 17, pp. 1189-1203.

Tempelman-Kluit, D.J., & R.K. Wanless 1975. Potassium-argon age determinations of metamorphic and plutonic rocks in Yukon crystalline terrane. Canadian Journal of Earth Sciences, Vol. 12, pp. 1895-1909.

Thurber Consultants Ltd. 1989. Kluane terrain hazard mapping study final report. Unpublished engineering report. Vancouver, B.C.: 25 p.

Valiappan, S., & K.K. Ang 1985. Dynamic analysis applied to rock mechanics problems. Proc. Fifth International Congress in Geomechanics, Nagoya, Japan: T. Kawamoto and Y. Ichikawa (eds.), pp. 119-132.

Varnes, D.J. 1978. Slope movement types and processes. Landslides: analysis and control: R.L. Schuster and J.K. Kryzek (eds.), pp. 11-33. Special Report 176, Transportation Research Board, National Research Council, National Academy of Sciences: Washington D.C.

Vita-Finzi, C. 1986. Recent earth movements - an introduction to neotectonics. Harcourt Brace Jovanovich, Publishers. Academic Press: London: Toronto.

Wahl, H.E., D.B. Fraser, R.C. Harvey, & J.B. Maxwell 1987. Climate of Yukon. Climatological Studies Number 40. Atmospheric Environment Service, Environment Canada. Supply and Services Canada. 323 p.

Wang, B., & V.K. Garga 1993. A numerical method for modelling large displacements of jointed rocks: I. Fundamentals. Canadian Geotechnical Journal, Vol. 30, No. 1, pp.96-108.

Weichert, D.H., R.B. Horner, P.S. Munro, R.J. Wetmiller, R.E. Baldwin, & M. Plouffe 1991. Nahanni, NWT, strong motion records: 1985-1989. Geological Survey of Canada, Open File 2415, 21 p. with encl.

Wetmiller, R.J., J.A. Drysdale, R.B. Horner, & M. Lamontagne 1989. Canadian earthquakes-1985-86. Geological Survey of Canada, Paper 88-14, Seismological Series No. 97. Supply and Services Canada: Ottawa: 25 p.

Wetmiller, R.J., & S.G. Evans 1989. Analysis of the earthquakes associated with the 1965 Hope landslide and their effects on slope stability at the site. Canadian Geotechnical Journal, Vol. 26, No. 3, pp. 484-490.

Wetmiller, R.J., R.B. Horner, H.S. Hasegawa, R.G. North, M. Lamontagne, D.H. Weichert, & S.G. Evans 1988. An analysis of the 1985 Nahanni earthquakes. Bulletin of the Seismological Society of America, Vol. 78, No. 2, pp. 590-616.

Wilson, E.L., & R.W. Clough 1962) Dynamic response by step-by-step- matrix analysis. Proc. Symposium on the Use of Computers in Civil Egineering, Lisbon. Paper No. 45, 14 p.

Wheeler, J.O., & P. McFeely 1987. Tectonic assemblage map of the Canadian Cordillera and adjacent parts of the United States of America. Geological Survey of Canada, Open File 1565. Dept. of Energy, Mines and Resources.

Whitehouse, I.E., & G.A Griffiths 1983. Frequency and hazard of large rock avalanches in the central southern Alps, New Zealand. Geology, Vol. 11, No. 6, pp. 331-334.

APPENDIX 1

YUKON LANDSLIDE INVENTORIES

LANDSLIDES OF THE KLUANE LAKE MAP AREA - NTS 115 F&G (E½)

Site Name	*#*	*Type*	*Location*	*Grid*	*Lithology*	*Comments*
Taylor Mountain		Rock Avalanche	140°38'W 61°58'N	1.2 O.1	Dezadeash Group	Steep, planar rupture surface is flanked by an intrusion; fresh looking colluvium has dammed tributary stream valley below the rupture surface; colluvium train has travelled down tributary stream valley into Miles Creek, deflecting it to the eastern side of the valley.
Tchawsahmon Lake		Landslide Zone	140°58'W 61°57'N	not shown	Dezadeash Group	Steep north-facing slope with no clear rupture surface; very modified colluvium is partially overlain by an alluvial fan, suggesting advanced age; steeply south dipping bedding may contribute to instability.
White River		Rock Avalanche(s)	140°37'W 61°55'N	1.3 N.2	Kluane Ranges Intrusions	Three closely spaced rock avalanches on a steep, south-facing slope have well-defined, concave rupture surfaces; longitudinal debris ridges remain on the highly modified colluvium surface; much of the colluvium has been removed by White River.
Rabbit Creek		Rock Avalanche	140°53'W 61°52'N	not shown	Station Creek Formation	Planar rupture surface extends to top of scarp slope; intersected by strong lineaments parallel to steeply west-dipping bedding; probable fault contact at base; hummocky, subdued colluvium has filled an abandoned meltwater channel at the base of the slope.
Hazel Creek		Rock Block Slide	140°28'W 61°52'N	2.5 N.0	Undivided Paleozoic metamorphic complex	Head scarp of largely intact slide block intersects an intrusive contact on its western edge; small creek at the toe of the slide has been deflected; appears to be fresh movement at the toe.

LANDSLIDES OF THE KLUANE LAKE MAP AREA - NTS 115 F&G (E½)

Site Name	*#*	*Type*	*Location*	*Grid*	*Lithology*	*Comments*
Mount Brooke	1	Rock Slump	140°41'W 61°32'N	0.8 H.7	Wrangell Lavas (St. Clare Province)	Large rock slump with well-defined head scarp appears to have diverted the stream at its toe; parallel furrows on the slump surface suggest internal deformation; moderately south dipping bedding may define the basal surface.
	2	Rock Block Slide	140°41'W 61°32'N	0.8 H.7	Wrangell Lavas (St. Clare Province)	Virtually undeformed rock block has deflected the stream at its toe; the sharply defined sliding surface is approximately perpendicular to moderately south dipping bedding.
	3	Rock Avalanche	140°41'W 61°31'N	0.8 H.3	Wrangell Lavas (St. Clare Province)	Relatively small rock avalanche originates on a south-facing scarp slope; fresh, hummocky looking colluvium has run down stream valley for nearly one kilometre; south dipping bedding probably contributes to this failure.
	4	Rock Avalanche	140°41'W 61°30'N	0.8 H.2	Wrangell Lavas (St. Clare Province)	Highly mobile rock avalanche has detached from ridge crest and run down a south-facing slope; the colluvium surface is hummocky but subdued; south dipping bedding probably contributes to this failure.
Count Creek	1	Rock Slide	140°30'W 61°30'N	2.3 H.4	Wrangell Lavas (St. Clare Province)	Large rock slide with toe extending into Count Creek; axis of anticline passes through centre of slide; colluvium has hummocky, subdued appearance.
	2	Rock Slide	140°30'W 61°29'N	not shown	Wrangell Lavas (St. Clare Province)	Planar rupture surface is approximately perpendicular to bedding on bedrock spur; colluvium has subdued appearance; fresh slumping at toe.

LANDSLIDES OF THE KLUANE LAKE MAP AREA - NTS 115 F&G (E½)

Site Name	*#*	*Type*	*Location*	*Grid*	*Lithology*	*Comments*
Tepee Lake		Rock Slide	140°14'W 61°33'N	4.1 I.4	Wrangell Lavas (St. Clare Province)	Large rock slide located on scarp-edge of Wolverine Plateau; south dipping bedding is dislocated by north-facing rupture surface; well modified colluvium has a subdued appearance and has run out into Tepee Lake.
Lynx Creek		Rock Avalanche	139°56'W 61°34'N	6.3 I.6	Undivided Paleozoic metamorphic complex	Possibly several coalescing avalanches; source area has indistinct boundaries and is intersected by several lineaments; appearance of remaining colluvium suggests it may have failed into a body of water.
Donjek River	1	Rock Avalanche(s)	139°50'W 61°33'N	7.0 I.0	Undivided Paleozoic metamorphic complex	Possibly several coalescing rock avalanches at this site; prominent cracking at ridge crown parallel to the head scarp; the colluvium exhibits longitudinal debris ridges in the distal area; the slide debris appears highly modified.
	2	Landslide Zone	139°28'W 61°04'N	10.0 B.0	Undivided Wrangell Lavas	Extensive area of slope instability along creek with hummocky colluvium at base of slope; no clear failure mode.
Wolverine Creek	1	Rock Slide	140°07'W 61°32'N	4.8 H.8	Wrangell Lavas (St. Clare Province)	Source area extends to top of slope; uniform rupture surface may be a bedding plane; colluvium appears fresh and has blocked tributary of Wolverine Creek; a sag pond is visible in mid-slope.
	2	Rock Block Slide	140°05'W 61°32'N	5.1 H.8	Wrangell Lavas (St. Clare Province)	Rock block appears with a prominent back scarp appears undeformed; toe of slide has deflected Wolverine Creek to the west.

LANDSLIDES OF THE KLUANE LAKE MAP AREA - NTS 115 F&G (E½)

Site Name	*#*	*Type*	*Location*	*Grid*	*Lithology*	*Comments*
	3	Rock Slide	140°07'W 61°30'N	5.0 H.5	Wrangell Lavas (St. Clare Province)	Source area is a bowl-shaped scar that may extend to the ridge top; the colluvium is extensively modified.
	4	Rock Slide	140°10'W 61°31'N	4.4 H.8	Wrangell Lavas (St. Clare Province)	Small rock slide on tributary of Wolverine Creek; planar rupture surface may be controlled by bedding.
	5	Rock Slump	140°12'W 61°33'N	4.2 I.1	Wrangell Lavas (St. Clare Province)	Rupture surface is intersected by two lineaments, but there is no clear control on the slide; the colluvium has deflected the stream at its toe; the slip surface may be bedding.
	6	Rock Slide	140°12'W 61°32'N	not shown	Wrangell Lavas (St. Clare Province)	Source area extends to ridge top; rupture surface appears biplanar; colluvium is subdued.
	7	Rock Slide	140°02'W 61°34'N	not shown	Undivided Permo-Triassic Volcanics	Very modified colluvium forms large bulge at slope base; source area is indistinct as slope is very eroded.
Wolverine Plateau	1	Rock Slide	139°53'W 61°28'N	6.5 G.9	Wrangell Lavas (St. Clare Province)	Rock slide located on north limb of northwest trending syncline; rupture surface may be shallowly southwest dipping bedding; intersected by lineament.
	2	Rock Slide	139°53'W 61°30'N	6.5 H.3	Wrangell Lavas (St. Clare Province)	Rock slide is located on scarp rim of Wolverine Plateau facing Donjek River; the rupture surface dislocates southwest dipping bedding; the subdued appearing colluvium forms a bulge in the valley profile.

LANDSLIDES OF THE KLUANE LAKE MAP AREA - NTS 115 F&G (E½)

Site Name	*#*	*Type*	*Location*	*Grid*	*Lithology*	*Comments*
	3	Rock Slide	139°55'W 61°32'N	6.2 H.8	Wrangell Lavas (St. Clare Province)	As Wolverine Plateau #2.
	4	Rock Slide	139°56'W 61°31'N	6.1 H.7	Wrangell Lavas (St. Clare Province)	Rock slide originates from scarp slope perpendicular to southwest dipping bedding; colluvium is very subdued.
	5	Rock Avalanche	140°02'W 61°31'N	5.4 H.5	Wrangell Lavas (St. Clare Province)	Wide area of slope instability appears to be the result of several slope movements; prominent slope top cracking is clearly visible, suggesting additional failures are incipient; colluvium is highly modified.
	6	Rock Slide	139°59'W 61°28'N	not shown	Wrangell Lavas (St. Clare Province)	Source area near top of arrete ridge; colluvium blankets the slope, but has been eroded away at the valley bottom.
	7	Rock Slide	139°57'W 61°31'N	not shown	Wrangell Lavas (St. Clare Province)	Source area in weathered, concave scar near top of slope; colluvium very modified
	8	Rock Slump	139°56'W 61°31'N	not shown	Wrangell Lavas (St. Clare Province)	Slump is well efined by bowl-shaped back scarp; all highly modified.
Quill Creek		Rock Slide	139°26'W 61°28'N	9.7 H.0	Hasen Creek Formation	Steep, planar south-facing rupture surface; debris has deflected tributary of Quill Creek; located in complexly folded and faulted area.

LANDSLIDES OF THE KLUANE LAKE MAP AREA - NTS 115 F&G (E½)

Site Name	*#*	*Type*	*Location*	*Grid*	*Lithology*	*Comments*
St. Clare Creek	1	Rock Slide	140°19'W 61°28'N	3.5 H.0	Wrangell Lavas (St. Clare Province)	Suspected large landslide on the north limb of a west trending anticline; rupture surface is possibly bedding controlled; very modified colluvium extends down slope into St. Clare Creek; intersected by weak north-trending lineament.
	2	Landslide Zone	140°25'W 61°25'N	not shown	Wrangell Lavas (St. Clare Province)	Both slopes of small valley centred on northwest trending syncline are unstable; very clear bedding control on rupture surfaces; colluvium is very modified and is dissected by small streams.
	3	Rock Slump	140°22'W 61°23'N	3.1 F.3	Wrangell Lavas (St. Clare Province)	Suspected very large slump in tightly folded rocks; prominent antislope scarps sub-parallel to headscarp; direction of movement is roughly perpendicular to bedding in west trending anticline; smaller slides at toe of slump are aggravated by fluvial erosion.
	4	Rock Slump	140°09'W 61°22'N	4.5 F.3	Wrangell Lavas (St. Clare Province)	Small slump in tightly folded rocks has pushed out into tributary of St. Clare Creek; small graben is developing below the head scarp; small scale active sliding at toe.
	5	Rock Slump (?)	140°12'W 61°22'N	4.3 F.3	Wrangell Lavas (St. Clare Province)	Suspected slump in steep valley slope, deflecting stream at its toe; small scarp is developing near the crown.
	6	Rock Slide	140°14'W 61°22'N	4.0 F.3	Wrangell Lavas (St. Clare Province)	Slide near valley bottom has well-defined back scarp; intersected by a strong lineament; toe is pushing out into St. Clare Creek.

LANDSLIDES OF THE KLUANE LAKE MAP AREA - NTS 115 F&G (E½)

Site Name	*#*	*Type*	*Location*	*Grid*	*Lithology*	*Comments*
Cement Creek	1	Rock Slide	139°53'W 61°24'N	6.5 F.8	Wrangell Lavas (St. Clare Province)	Slide is situated near centre of northwest trending syncline; rupture surface appears to be a bedding plane; prominent arcuate backscarp and several medial cracks; colluvium has partially dammed Cement Creek; studied by Power (1988); field checked.
	2	Rock Slide	139°56'W 61°24'N	6.3 F.8	Wrangell Lavas (St. Clare Province)	Strong lineament in headscarp of slide coincides with fault; rocks are highly altered and sheared; headscarp is retrogressing and the toe is actively slumping into stream; bedding in headscarp is subparallel to failure plane; field checked.
	3	Rock Slide	139°57'W 61°24'N	6.3 F.8	Wrangell Lavas (St. Clare Province)	Suspected slide may have originated in a cirque; bedding dips south into valley; colluvium surface is subdued and well vegetated; localized slumping occurring near the toe; field checked.
	4	Rock Slide	139°59'W 61°23'N	5.8 F.6	Wrangell Lavas (St. Clare Province)	Several landslides have occurred at this site; rupture is localized along south dipping bedding; well modified colluvium deflecting Cement Creek from a large, ancient event; recent instability is occurring on the western edge and near the head scarp; rocks at the head of the rupture surface are highly altered; field checked.
	5	Rock Slide	139°58'W 61°23'N	6.0 F.5	Wrangell Lavas (St. Clare Province)	Small rockslide near bottom of valley slope has run out onto valley floor.

LANDSLIDES OF THE KLUANE LAKE MAP AREA - NTS 115 F&G (E½)

Site Name	*#*	*Type*	*Location*	*Grid*	*Lithology*	*Comments*
	6	Rock Slide	140°00'W 61°22'N	5.8 F.4	Wrangell Lavas (St. Clare Province)	Large slide on steep sided tributary valley; rupture surface may be bedding in a north dipping homocline; colluvium has deflected small stream at toe.
	7	Rock Slide	139°48'W 61°23'N	7.1 F.8	Wrangell Lavas (St. Clare Province)	Debris lobe of the slide has deflected small creek; intersected by linears related to Cement Creek Fault.
Steele Creek	1	Rock Slide	139°58'W 61°18'N	not shown	Wrangell Lavas (St. Clare Province)	Source area appears to be concave scar in valley slope; colluvium is hummocky but eroded.
	2	Rock Slide	139°54'W 61°19'N	6.1 E.7	Wrangell Lavas (St. Clare Province)	The slide originates on a steep slope well above the valley bottom; the colluvium appears hummocky and fresh; close to the trace of Duke River Fault.
	3	Rock Slump	139°52'W 61°19'N	6.3 E.8	Wrangell Lavas (St. Clare Province)	Source area is concave scar in upper slope, and may extend down into under laying sediments; proximal to the trace of Duke River Fault.
	4	Rock Slide	139°50'W 61°20'N	not shown	Wrangell Lavas (St. Clare Province)	A group of rupture scars at several elevations coalesce in what may have been a cirque; no colluvium is discernible.
	5	Rock Slide	139°49'W 61°18'N	6.5 E.7	Undivided Upper Paleozoic sediments	A concave scar near the valley floor appears to be the source area; the colluvium is very modified; a vertical southwest trending foliation may coincide with the rupture surface; close to the trace of Duke River Fault.

LANDSLIDES OF THE KLUANE LAKE MAP AREA - NTS 115 F&G (E½)

Site Name	*#*	*Type*	*Location*	*Grid*	*Lithology*	*Comments*
	6	Rock Slide	139°48'W 61°18'N	6.6 E.8	Undivided Upper Paleozoic sediments	See Steele Creek #5.
Wade Creek		Rock Slump	139°37'W 61°24'N	8.4 F.9	Amphitheatre Formation	Slump has created bulge in slope profile below head scarp.
Wade Mountain		Rock Avalanche	139°37'W 61°22'N	8.4 F.2	Station Creek Formation	Large landslide (Possible landslide zone) of probable advanced age; source area on knife-edged ridge is close to fault contact.
Granite Creek		Rock Slide	139°22'W 61°18'N	10.2 E.6	Amphitheatre Formation	Rock slide has pushed out into Granite Creek; intersected by strong lineaments related to the Wade Mountain fault zone; rupture surface may be controlled by southwest dipping bedding.
Halfbreed Creek	1	Rock Slide	139°05'W 61°15'N	12.3 E.0	Undivided Wrangell Lavas	Large slide bracketed by an extension of the Wade Mountain fault zone in the north and a possible splay of the Duke River Fault to the south; bedding dips moderately to the southwest; colluvium has pushed out into tributary of Halfbreed Creek.
	2	Rock Slide	139°04'W 61°13'N	12.5 D.4	Undivided Wrangell Lavas	Small slide proximal to a Wrangell intrusion; basement rocks are very deformed.
Duke River		Rock Slide	139°05'W 61°12'N	12.3 D.3	Undivided Wrangell Lavas	Suspected large rockslide; colluvium is very subdued and modified, suggesting an advanced age; possible rock glaciers at this site.

LANDSLIDES OF THE KLUANE LAKE MAP AREA - NTS 115 F&G (E½)

Site Name	*#*	*Type*	*Location*	*Grid*	*Lithology*	*Comments*
Bighorn Creek		Rock Avalanche	139°17'W 61°12'N	10.8 D.0	Undivided Wrangell Lavas	Large rock avalanche originating in over steepened cirque in Neogene volcanics; large rock blocks in head area have translated on a basal rupture surface; colluvium has very fresh appearance; the slide is bounded by a strong fault lineament on the west side; field checked.
Landmark Mountain		Rock Slide	139°14'W 61°10'N	not shown	Donjek Greywacke	Steep, west dipping rupture surface is perpendicular to southwest dipping foliation; colluvium has subdued appearance and has been eroded by a stream.
Congdon Creek		Rock Avalanche	138°38'W 61°09'N	15.8 C.5	Station Creek Formation	Large rock avalanche has translated onto the Congdon Creek alluvial fan; appears to have an anomalously long run out; steeply east dipping bedding and foliation may coincide with the rupture surface; colluvium exhibits longitudinal and contorted debris ridges and molards in the distal zone.
Nines Creek		Rock Block Slide	138°46'W 61°07'N	14.6 C.1	Undivided Wrangell Lavas	Large block of rock has translated on smooth, planar rupture surface into Nines Creek with minimal distortion; toe is actively deflecting Nines Creek to east side of valley; strong lineament intersecting the slide coincides with a mapped fault; field checked.
Grizzly Creek	1	Rock Slump	139°04'W 61°10'N	12.2 C.8	Undivided Wrangell Lavas	Suspected slump defined by prominent arcuate scarp; direction of movement is perpendicular to moderately southwest dipping bedding.

LANDSLIDES OF THE KLUANE LAKE MAP AREA - NTS 115 F&G (E½)

Site Name	*#*	*Type*	*Location*	*Grid*	*Lithology*	*Comments*
	2	Rock Slide	139°07'W 61°09'N	12.0 C.5	Undivided Wrangell Lavas	Rockslide has deflected stream to south side of valley; colluvium has uneven, hummocky surface; intersected by several strong lineaments; rupture surface is parallel to moderately southwest dipping bedding.
	3	Rock Avalanche	139°11'W 61°09'N	11.7 C.5	Donjek Greywacke	Source area extends to ridge crest; colluvium is hummocky and appears fresh; near-vertical south-southwest dipping foliation is subparallel to the rupture surface.
	4	Landslide Zone	139°11'W 61°08'N	11.7 C.3	Donjek Greywacke	Several rockslides originating from headwall of unoccupied cirque; two strong lineament intersect in the cirque; appearance of colluvium suggests individual slides have different ages.
Fisher Creek	1	Landslide Zone	138°40'W 61°04'N	15.1 B.3	Hasen Creek Formation	Extensive area rockfall and slumping on steep eastern valley slope; colluvium is hummocky and somewhat modified; strong lineament intersects the source area.
	2	Rock Slump	138°41'W 61°03'N	15.1 B.3	Hasen Creek Formation	Slump has a well defined arcuate headscarp; the toe is pushing into creek.
	3	Landslide Zone	138°41'W 61°03'N	15.1 B.2	Amphitheatre Formation	Several coalescing slumps on western wall of stream valley; the stream appears to follow a mapped fault (Dodds, 1982a).
	4	Rock Slump	138°40'W 61°02'N	not shown	Hasen Creek Formation	Slump appears to be very old; bowl-shaped back scarp is very weathered, but similar in form to Fisher Creek #2; slump colluvium has been truncated by stream and does not appear to be moving.

LANDSLIDES OF THE KLUANE LAKE MAP AREA - NTS 115 F&G (E½)

Site Name	*#*	*Type*	*Location*	*Grid*	*Lithology*	*Comments*
	5	Rock Slide	138°39'W 61°02'N	not shown	Nikolai Greenstone	Source area of slide extends to ridge crest; colluvium has been eroded away at the toe by Fisher Creek.
Sheep Creek		Rock Slump	138°35'W 61°01'N	15.9 A.5	Nikolai Greenstone	Large slump with well defined arcuate head scarp has pushed out into Sheep Creek; renewed slumping on southern portion of the slump mass; lineament intersecting the head scarp area.
Sheep Mountain		Rock Avalanche	138°32'W 61°02'N	16.5 A.8	Nikolai Greenstone	Source area is in highly deformed rocks; debris train has run funnelled down steep chute into Kluane Lake; some fresh rock debris in chute suggests continuing instability; studied by Clague (1981); field checked.
Slims River		Rock Slide	138°37'W 61°00'N	15.9 A.2	Nikolai Greenstone, Chitistone Limestone	Slide is bounded by a strong fault lineament; located near centre of a south plunging syncline; colluvium has run out onto the Bullion Creek alluvial fan.

LANDSLIDES OF THE MT. ST. ELIAS AND DEZADEASH MAP AREAS - NTS 115 B&C

Site Name	*#*	*Type*	*Location*	*Grid*	*Lithology*	*Comments*
Kimberly Creek		Rock Slump	138°02'W 60°52'N	2.8 M.3	Dezadeash Group	Sharp linears parallel to steeply west dipping bedding and east dipping foliation define the head scarp; the trace of Denali fault is at the toe of the slump.
Hoodoo Mountain		Rock Slump	138°12'W °42'N 60	1.5 K.2	Wrangell Lavas (Alsek Province)	Large, possibly retrogressive rock slump with well defined head scarp; renewed movement near the toe of the slump.
Telluride Creek		Rock Slide	138°17'W 60°54'N	1.0 N.1	Dezadeash Group	Suspected rockslide appears to originate from concave scar in upper slope; source area is coincident with the trace of Duke River Fault; no distinct accumulation of colluvium downslope.
Chalcedony Mountain	1	Rock Slide (?)	138°08'W 60°42'N	2.0 K.2	Wrangell Lavas (Alsek Province)	Suspected rock slide; colluvium appears very modified.
	2	Rock Slide (?)	138°12'W 60°40'N	1.5 J.8	Wrangell Lavas (Alsek Province)	Suspected large rock slide with prominent head scarp.
	3	Rock Slide	138°09'W 60°38'N	2.1 J.9	Wrangell Lavas (Alsek Province)	Large landslide may have originated in cirque on scarp-edged plateau; colluvium is very subdued and is locally unstable.
Lower Cottonwood Creek	1	Rock Avalanche	137°33'W 60°27'N	6.0 G.4	Station Creek Formation	Rock avalanche originated in concave depression near crest of slope; lacking a defined colluvium accumulation.

LANDSLIDES OF THE MT. ST. ELIAS AND DEZADEASH MAP AREAS - NTS 115 B&C

Site Name	*#*	*Type*	*Location*	*Grid*	*Lithology*	*Comments*
	2	Rock Avalanche	137°32'W 60°25'N	6.3 G.0	Station Creek Formation	Colluvium from failure has run up opposite wall of valley; may have been deposited in a glacial lake; strong southwest dipping foliation may have contributed to failure; field checked.
	3	Rock Avalanche	137°32'W 60°24'N	6.4 F.9	Station Creek Formation	Relatively small zone of unstable rock; foliation is causing local toppling at this site; field checked.
Kathleen Lake		Rock Slide	137°28'W 60°30'N	6.6 H.5	Dezadeash Group	Suspected large rock slide with source area near the top of a glacially over steepened valley wall; very subdued, gently rolling colluvium forms a bulge in the slope profile; backscarp is bounded by a strong linear.
Upper Cottonwood Creek	1	Rock Slide	137°28'W 60°27'N	6.7 G.5	Nikolai Greenstone, Chitistone Limestone	Relatively small slide with smooth, gently curved basal plane; situated on north limb of northwest plunging anticline; very close to the trace of Denali Fault.
	2	Rock Slump	137°28'W 60°26'N	6.7 G.3	Hasen Creek Formation	Trace of Denali Fault is coincident with the back scarp; situated on north limb of northwest plunging anticline; rocks are heavily altered; colluvium is hummocky and well modified.
Virgin Creek		Rock Topple	137°26'W 60°23'N	7.1 F.5	Nikolai Greenstone	Massive topple situated on south limb of northwest plunging anticline, approx. one km from Denali Fault; backscarp is intersected by a strong linear; strong steeply northeast dipping trending foliation probably a factor.
Upper Victoria Creek	1	Rock Avalanche (?)	137°28'W 60°25'N	6.8 G.0	Hasen Creek Formation	Relatively small slide situated on south limb of northwest plunging anticline; antislope scarps and cracks immediately north; colluvium is hummocky.

LANDSLIDES OF THE MT. ST. ELIAS AND DEZADEASH MAP AREAS - NTS 115 B&C

Site Name	*#*	*Type*	*Location*	*Grid*	*Lithology*	*Comments*
	2	Rock Slump (?)	137°23'W 60°24'N	7.6 F.8	Dezadeash Group	Suspected large rock slump intersected by several lineaments, some of which are parallel to the back scarp; trace of Denali Fault at toe; bedrock along the fault trace has an unstable appearance; there is no apparent translation into the creek.
Shorty Creek	1	Rock Slump	137°13'W 60°25'N	8.7 G.0	Dezadeash Group	Two coalescing slumps in highly deformed bedrock; no apparent movement into creek at the toe.
	2	Rock Slide	137°15'W 60°23'N	8.5 F.7	Amphitheatre Formation	Large slide with northeast dipping, smooth, planar rupture surface; rupture surface is intersected by a strong lineament parallel to it; colluvium is very hummocky with local ponding; very close to intrusive contact.
Alder Creek		Rock Avalanche	137°10'W 60°22'N	9.0 F.3	Dezadeash Group	Avalanche originated near crest of over steepened valley wall; concave, smooth rupture surface; colluvium may have altered shoreline of small lake.
Shaft Creek		Rock Avalanche	137°36'W 60°22'N	5.9 F.1	Undivided Wrangell Lavas (?)	Colluvium may have translated into a body of water; colluvium surface is rolling and well modified.
Mush Creek		Rock Slump	137°23'W 60°11'N	7.2 C.4	Station Creek Formation	Multiple retrogressive slump of surficial debris is moving into tributary of Mush Creek; coincident with trace of Duke River Fault.

LANDSLIDES OF THE MT. ST. ELIAS AND DEZADEASH MAP AREAS - NTS 115 B&C

Site Name	*#*	*Type*	*Location*	*Grid*	*Lithology*	*Comments*
Tatshenshini River		Landslide Zone	137°10'W 60°07'N	9.1 B.2	Kluane Ranges Intrusions	Widespread cracking and apparent vertical displacements of mountain top of over 40 m; large accumulation of hummocky colluvium at base of over steepened slope suggests widespread instability; colluvium appears to overlay Holocene (?) glacial deposits.
Pirate Creek		Rock Avalanche	137°05'W 60°03'N	1.0 A.5	Kluane Ranges Intrusions	Colluvium appears to have anomalously long run out distance and a well defined extent; possibly a multiple event originating from several possible source areas on the mountain side; molards are readily visible in the distal area.
Takhanne River		Rock Avalanche	136°51W '60°08'N	11.3 B.9	Nisling Intrusions (?)	Source area is near top of valley slope; rock is heavily cracked and there may be several incipient landslides; colluvium is blocky in upper slope and has been largely eroded in river channel.

APPENDIX 2

EXAMPLE UDEC INPUT FILE

```
* CEMENT (n1) UDEC 1.83
* Static modelling phase with excavation
*
new
* Set defaults
set jcondf 8
set clemin 2
set deg on
set grav 0.0 -9.81
head
CEM(n1)
*
* Set material properties
* Rock mass material & sub-vertical joints (1) E=16.0 GPa; v=0.25
prop mat 1  d=2600  k=10.667e9  g=6.40e9  fr=45  coh=2.0e6  ten=2.0e5 &
jkn=1.0e9  jks=4.0e8  jfr=34  jco=0.0  jte=0.0
* Interflow material (2) C-Y joint model
prop mat 2  jkn=1.0e9  jks=2275  jen=0.0  jes=1.0  jr=0.015 &
jif=36  jfr=18  minjks=1e8  maxjks=4e8
* Viscous boundaries (3) E=9.0 GPa; v=0.16
prop mat 3  d=2600  k=4.69e9  g=3.81e9 &
jkn=1.0e9  jks=4.0e8  jfr=36  jco=0.0  jte=0.0
*
* Generate initial geometry
ro 0.10
bl 0,0 0,200 200,200 200,0
cr 62.5,200 200,150
cr 0,125 62.5,200
cr 0,210 200,137.5
del bl 86
del bl 388
del bl 243
Create bedding planes and vertical cracks
cr 0,198 200,125
cr 0,175 200,102
cr 0,150 200,77.5
```

```
cr 0,125 200,52
cr 0,99 200,26
cr 0,72.5 200,0
cr 0,48 200,-25
cr 0,24 200,-49
jdel
cr 62.5,200 62.5,175
cr 75,195.5 75,170.5
cr 87.5,191 87.5,166
cr 100,186.5 100,161.5
cr 112.5,182 112.5,157
cr 125,177.5 125,152.5
cr 137.5,173 137.5,148
cr 150,168.5 150,143
cr 162.5,164 162.5,138
cr 175,159.5 175,132.5
cr 187.5,155 187.5,129
jdel
del bl 6620
del bl 6297
*
* Generate finite-difference mesh in blocks
gen edge 14
*
* Assign material properties to model
ch mat 1 con 1 jmat 2 jcon 8
ch ang 88 92 jmat 1 jcon 8
*
* Set boundary conditions
bo mat 3
bo cor 37 63 xvis yvis ff
bo cor 24 266 xvis yvis ff
bo cor 63 24 xvis yvis yvel 0
*
* Free field lateral boundaries - 20 nodes
ff gen 0 125 20
```

```
ff 0 125 mat 1 con 1
ff xvel 0 yvel 0
*
* Set damping & insitu stress (K0=0.5)
damp auto
insitu str -2.5506e6 0 -5.1012e6 ygr 1.2753e4 0 2.5506e4 &
szz -2.5506e6 zgr 0 1.2753e4
*
* Excavate model with time-varying external stress condition
tab 1 0,1 2.5,1 5,0 7,0
bo cor 266 37 str -2.5506e6 0 -5.1012e6 ygr 1.2753e4 0 2.5506e4 hi tab 1
*
* Cycle initial state to equilibrium
cy t 5
* Release external stress on top boundary; cycle to equilibrium; save model
bo cor 266 37 xfr yfr
cy t 2
sav n1.mod
*
*******************************************************************************
* CEMENT (n1) UDEC 1.83
* Dynamic model run example
*
new
r n1.mod
head
CEM (n1) - N12(T5)
*
* Reset global variables & assign monitoring points
reset hist disp rot jdisp time
his ncyc 25 type 1 &
sdis(6172) ndis(6172) sstr(6172) nstr(6172) &
sdis(5551) ndis(5551) sstr(5551) nstr(5551) &
sdis(100,150) ydis(100,150) xvel(100,150) yvel(100,150) &
xdis(100,162) ydis(100,162) xvel(100,162) yvel(100,162) &
xacc(100,150)
```

```
*
* Damping: 1% @ 12.0 Hz stiffness proportional for dynamic analysis
damp .01 12 stiff
*
* Boundary Conditions
* Read digital earthquake record
bo hread 1 c:\udec\n12t5.der
bo cor 37 63 xvis yvis ff
bo cor 24 266 xvis yvis ff
* Transient stress boundary on bottom of model and free-field
bo cor 63 24 str 0 -4.0e4 0 xhis 1
bo cor 63 24 xvis yvis yvel 0
bo xhis 1
ff sxy -4.0e4 xvis yvis yvel 0
*
* Cycle and save state
cy t 4
sav 12t.n1
cy t 4
sav 12t2.n1
cy t 4
sav 12t3.n1
cy t 4
sav 12t4.n1
cy t 4
sav 12t5.n1
*
return
*****
```